

**EXPLORING THE INTERACTIONS OF THERAPEUTIC  
PHYTOCHEMICALS, FLAVOKAWAIN B, PINOSTROBIN  
AND 6-SHOGAOL WITH HUMAN SERUM ALBUMIN:  
SPECTROSCOPIC AND MOLECULAR DOCKING  
INVESTIGATIONS**

**SHEVIN RIZAL BIN FERAZ**

**FACULTY OF SCIENCE  
UNIVERSITY OF MALAYA  
KUALA LUMPUR**

**2015**

**EXPLORING THE INTERACTIONS OF  
THERAPEUTIC PHYTOCHEMICALS, FLAVOKAWAIN  
B, PINOSTROBIN AND 6-SHOGAOL WITH HUMAN  
SERUM ALBUMIN: SPECTROSCOPIC AND  
MOLECULAR DOCKING INVESTIGATIONS**

**SHEVIN RIZAL BIN FERAZ**

**THESIS SUBMITTED IN FULFILLMENT OF THE  
REQUIREMENTS FOR THE DEGREE OF DOCTOR OF  
PHILOSOPHY**

**INSTITUTE OF BIOLOGICAL SCIENCES  
FACULTY OF SCIENCE  
UNIVERSITY OF MALAYA  
KUALA LUMPUR**

**2015**

**UNIVERSITY OF MALAYA**  
**ORIGINAL LITERARY WORK DECLARATION**

Name of Candidate: Shevin Rizal bin Feroz

Registration/Matric No: SHC 130026

Name of Degree: Doctor of Philosophy (Ph.D.)

Title of Thesis ("this Work"): Exploring the interactions of therapeutic phytochemicals, flavokawain B, pinostrobin and 6-shogaol with human serum albumin: Spectroscopic and molecular docking investigations

Field of Study: Biochemistry

I do solemnly and sincerely declare that:

- (1) I am the sole author/writer of this Work;
- (2) This Work is original;
- (3) Any use of any work in which copyright exists was done by way of fair dealing and for permitted purposes and any excerpt or extract from, or reference to or reproduction of any copyright work has been disclosed expressly and sufficiently and the title of the Work and its authorship have been acknowledged in this Work;
- (4) I do not have any actual knowledge nor do I ought reasonably to know that the making of this work constitutes an infringement of any copyright work;
- (5) I hereby assign all and every rights in the copyright to this Work to the University of Malaya ("UM"), who henceforth shall be owner of the copyright in this Work and that any reproduction or use in any form or by any means whatsoever is prohibited without the written consent of UM having been first had and obtained;
- (6) I am fully aware that if in the course of making this Work I have infringed any copyright whether intentionally or otherwise, I may be subject to legal action or any other action as may be determined by UM.

Candidate's Signature

Date:

Subscribed and solemnly declared before,

Witness's Signature

Date:

Name: Prof. Dr. Saad Tayyab

Designation: Supervisor

Witness's Signature

Date:

Name: Dr. Saharuddin bin Mohamad

Designation: Co-Supervisor

## ABSTRACT

The rhizomes of the plants of Zingiberaceae family are rich sources of bioactive phytochemicals and therefore, are major targets for discovering new phytomedicines. Three of these phytochemicals, namely, flavokawain B (FB), pinostrobin (PS) and 6-shogaol (6S) have shown various therapeutic properties including antioxidant, anticarcinogenic, anti-inflammatory and antimicrobial activities. The interactions of these compounds with the main *in vivo* drug carrier, human serum albumin (HSA) were investigated using a multitude of spectroscopic methods, supported by molecular docking studies. Significant quenching of HSA fluorescence intensity was observed upon titration of the protein with these compounds. Analysis of the fluorescence data revealed the involvement of static quenching phenomena in these interactions, thus suggesting the formation of ligand–HSA complexes. The association constants,  $K_a$  of these ligand–HSA systems were found to lie in the range,  $0.63\text{--}1.03 \times 10^5 \text{ M}^{-1}$  at  $25 \text{ }^\circ\text{C}$ , characteristic of moderate affinity binding. Thermodynamic analysis of the binding data showed that the binding reactions were accompanied by negative enthalpy ( $-\Delta H$ ) and positive entropy ( $+\Delta S$ ) changes, which were indicative of the involvement of hydrophobic and van der Waals forces along with hydrogen bonds in the complex formation. This was corroborated by molecular docking results depicting the formation of hydrogen bonds and identification of hydrophobic residues in the vicinity of the docked ligands. Synchronous and three-dimensional fluorescence data suggested significant change in the microenvironment around Tyr and Trp residues of HSA upon binding to these compounds. Far-UV circular dichroism results indicated relatively higher thermal stability of the protein in the presence of these ligands. Competitive drug displacement experiments along with docking simulation results suggested a clear binding preference of FB and PS for Sudlow's site I (subdomain IIA) of HSA, while 6S was able to bind favourably to Sudlow's site I as well as with Sudlow's site II (subdomain IIIA).

## ABSTRAK

Rizom tumbuhan yang berasal daripada keluarga Zingiberaceae adalah kaya dengan pelbagai molekul bioaktif dan merupakan sumber yang penting untuk mencari molekul fitokimia baru. Tiga daripadanya, flavokawain B (FB), pinostrobin (PS) dan 6-shogaol (6S) telah terbukti memiliki pelbagai ciri-ciri terapeutik termasuk aktiviti antikosida, antikarsinogenik, antiinflamasi dan antimikrobial. Interaksi molekul-molekul ini dengan protein pengangku utama di dalam tubuh, albumin serum manusia (HSA) telah diselidik menggunakan pelbagai kaedah spektroskopik dan disokong oleh kajian dok molekular. Pelindapkejutan intensiti fluorens HSA yang signifikan telah diperhati apabila protein tersebut dititrat dengan molekul-molekul ini. Analisis data fluorens menunjukkan penglibatan fenomena pelindapkejutan statik di dalam interaksi diatas, dengan itu menunjukkan bahawa berlaku formasi kompleks ligan-HSA. Nilai konstan kesatuan,  $K_a$  bagi sistem ligan-HSA tersebut ditemui berada diantara  $0.63-1.03 \times 10^5 \text{ M}^{-1}$  pada  $25^\circ\text{C}$ , dan merupakan suatu ciri kekuatan pengikatan yang sederhana. Analisis termodinamik pula menunjukkan bahawa reaksi pengikatan ini diikuti dengan perubahan nilai entalpi negatif ( $-\Delta H$ ) dan entropi yang positif ( $+\Delta S$ ). Ini menunjukkan penglibatan daya hidrofobik dan van der Waals serta ikatan hidrogen di dalam formasi kompleks. Ini juga disokong oleh hasil eksperimen dok molekular yang memberi gambaran formasi ikatan hidrogen dan identifikasi residu hidrofobik sekitar ligan yang telah didok kepada HSA. Data fluorens sinkronus dan tiga-dimensi menunjukkan perubahan yang signifikan kepada persekitaran mikro sekeliling residu Tyr dan Trp HSA apabila berinteraksi dengan molekul-molekul ini. Hasil kajian dikroisma bulatan UV-jauh menunjukkan peningkatan relatif stabiliti terma protein dengan kehadiran ligan-ligan tersebut. Keputusan eksperimen anjakan dadah kompetitif serta simulasi dok menunjukkan bahawa FB dan PS jelas mempunyai keutamaan untuk berikat dengan tapak Sudlow I (subdomain IIA)

HSA, manakala 6S berupaya untuk berikat secara baik dengan tapak Sudlow I serta tapak Sudlow II (subdomain IIA) HSA.

University of Malaya

## ACKNOWLEDGMENTS

I extend my heartfelt gratitude towards my principal supervisor, Professor Saad Tayyab whose encouragement, guidance and support have been the major element in the undertaking and completion of this project. I express my utmost appreciation to my co-supervisor, Dr. Saharuddin Mohamad whose kind advice and invaluable input have been instrumental throughout the duration of this study. It has been a pleasure to work under them and the experience is one that I am ever grateful for.

My special thanks go to Professor Datin Sri Nurestri Abdul Malek and members of her research group especially, Dr. Hong Sok Lai and Dr. Lee Guan Sern for graciously providing the compounds used in this project.

I will fail in my duties if I forget to thank Dr. Zazali Alias, Coordinator of the Biochemistry Programme, Associate Professor Rosli Ramli, Head, Institute of Biological Sciences and Professor Zanariah Abdullah, Dean, Faculty of Science, University of Malaya as well as their predecessors, Associate Professor Habsah Abdul Kadir, Professor Rosli Hashim and Professor Dato' Sofian Azirun, respectively, for providing a favorable environment for research.

I am most grateful to Wong Yin How whose company I shall cherish forever. This journey would never be the same if not for his constant advice, assistance and camaraderie throughout our years in the University of Malaya. I also express my sincere thanks to friends and colleagues, in particular Adyani Azizah Abd Halim and Mohammed Suleiman Zaroog for their constant help, patience and support.

The work presented in this thesis was carried out in the laboratories of the Institute of Biological Sciences, University of Malaya, and in addition to my supervisors, I wish to thank the staff of the Institute. Financial support from the University of Malaya in the form of the University of Malaya Fellowship Scheme and the University of Malaya Postgraduate Research Fund are also greatly acknowledged.

My deepest gratitude goes to my beloved family their continuous support, encouragement, patience and prayers.

Shevin Rizal Feroz

December 2015

University of Malaya

# CONTENTS

	<b>Page</b>
<b>ABSTRACT</b>	iii
<b>ABSTRAK</b>	iv
<b>ACKNOWLEDGEMENTS</b>	vi
<b>CONTENTS</b>	viii
<b>LIST OF FIGURES</b>	xii
<b>LIST OF TABLES</b>	xxi
<b>LIST OF ABBREVIATIONS / SYMBOLS</b>	xxiii
<b>1. INTRODUCTION</b>	1
<b>1.1. Natural products as medicines</b>	1
<b>1.2. Phytochemicals from the Zingiberaceae family</b>	6
<i>1.2.1. Flavokawain B</i>	7
<i>1.2.2. Pinostrobin</i>	9
<i>1.2.3. 6-Shogaol</i>	12
<b>1.3. Transport of therapeutic ligands through blood plasma</b>	15
<i>1.3.1. Physicochemical properties of HSA</i>	15
<i>1.3.2. Structural organization of HSA</i>	17
<i>1.3.2.1. Amino acid composition and primary structure</i>	17
<i>1.3.2.2. Three-dimensional structure</i>	21
<i>1.3.3. Genetics, synthesis and distribution of HSA</i>	24
<i>1.3.4. Functions of HSA</i>	26
<i>1.3.5. Ligand binding sites of HSA</i>	27
<i>1.3.5.1. Site I</i>	30
<i>1.3.5.2. Site II</i>	32
<i>1.3.5.3. Additional binding sites</i>	33
<b>1.3.6. Clinical implications of ligand binding to HSA</b>	34

<b>2. MATERIALS AND METHODS</b>	38
<b>2.1. Materials</b>	38
<b>2.1.1. Protein and bioactive compounds</b>	38
<b>2.1.2. Reagents used in drug displacement studies</b>	38
<b>2.1.3. Miscellaneous</b>	38
<b>2.2. Methods</b>	39
<b>2.2.1. pH measurements</b>	39
<b>2.2.2. Analytical procedures</b>	39
2.2.2.1. Preparation of protein solution	39
2.2.2.2. Preparation of ligand solutions	39
<b>2.2.3. Spectral measurements</b>	40
2.2.3.1. Absorption spectroscopy	40
2.2.3.2. Fluorescence spectroscopy	40
2.2.3.3. Circular dichroism spectroscopy	41
<b>2.2.4. Ligand–HSA interaction studies</b>	41
2.2.4.1. Fluorescence quenching titration	41
2.2.4.2. Spectrofluorimetric analysis	42
I. Inner filter effect correction	42
II. Quenching and binding parameters	42
III. Thermodynamic parameters	43
<b>2.2.5. Thermal stability studies</b>	44
<b>2.2.6. Competitive drug displacement studies</b>	44
2.2.6.1. Flavokawain B–HSA system	44
2.2.6.2. Pinostrobin–HSA system	45
2.2.6.3. 6-Shogaol–HSA system	46
<b>2.2.7. Molecular docking studies</b>	46
<b>2.2.8. Statistical analysis</b>	47

<b>3. RESULTS AND DISCUSSION</b>	50
<b>3.1. Flavokawain B–human serum albumin interaction</b>	50
3.1.1. <i>Quenching of HSA fluorescence and binding characteristics</i>	50
3.1.2. <i>Thermodynamic parameters and binding forces</i>	57
3.1.3. <i>Microenvironmental alterations around HSA fluorophores</i>	60
3.1.3.1. <i>Synchronous fluorescence spectra</i>	60
3.1.3.2. <i>Three-dimensional fluorescence spectra</i>	63
3.1.4. <i>FB-induced thermal stabilization of HSA</i>	68
3.1.5. <i>Binding site specificity of FB on HSA</i>	72
3.1.6. <i>Molecular docking</i>	74
<b>3.2. Pinostrobin–human serum albumin interaction</b>	84
3.2.1. <i>Quenching of HSA fluorescence and binding characteristics</i>	84
3.2.2. <i>Thermodynamic parameters and binding forces</i>	88
3.2.3. <i>Microenvironmental alterations around HSA fluorophores</i>	92
3.2.3.1. <i>Synchronous fluorescence spectra</i>	92
3.2.3.2. <i>Three-dimensional fluorescence spectra</i>	95
3.2.4. <i>PS-induced thermal stabilization of HSA</i>	99
3.2.5. <i>Binding site specificity of PS on HSA</i>	101
3.2.6. <i>Molecular docking</i>	107
<b>3.3. 6-Shogaol–human serum albumin interaction</b>	117
3.3.1. <i>Quenching of HSA fluorescence and binding characteristics</i>	117
3.3.2. <i>Thermodynamic parameters and binding forces</i>	121
3.3.3. <i>Microenvironmental alterations around HSA fluorophores</i>	125
3.3.3.1. <i>Three-dimensional fluorescence spectra</i>	126

3.3.4. <i>6S-induced thermal stabilization of HSA</i>	126
3.3.5. <i>Binding site specificity of 6S on HSA</i>	129
3.3.6. <i>Molecular docking</i>	140
<b>4. CONCLUSIONS</b>	149
<b>5. REFERENCES</b>	151
<b>LIST OF PUBLICATIONS / PRESENTATIONS</b>	169
<b>BIOGRAPHY</b>	180

University of Malaya

## LIST OF FIGURES

	<b>Page</b>
<b>Figure 1.1.</b> Chemical structure (A) and ball-and-stick model (B) of flavokawain B.	8
<b>Figure 1.2.</b> Chemical structure (A) and ball-and-stick model (B) of pinostrobin.	11
<b>Figure 1.3.</b> Chemical structure (A) and ball-and-stick model (B) of 6-shogaol.	13
<b>Figure 1.4.</b> Primary structure of HSA.	20
<b>Figure 1.5.</b> Three-dimensional structure of HSA.	22
<b>Figure 1.6.</b> Helices and disulfide bridges of HSA.	23
<b>Figure 1.7.</b> Map of the HSA gene.	25
<b>Figure 1.8.</b> Ligand binding sites of HSA.	31
<b>Figure 3.1.</b> Fluorescence spectra of HSA in the absence and the presence of increasing FB concentrations, obtained in 10 mM Tris-HCl buffer, pH 7.4 at 25 °C upon excitation at 280 nm.	51
<b>Figure 3.2.</b> Stern-Volmer plots for the fluorescence quenching data of the FB-HSA system at three different temperatures.	53
<b>Figure 3.3.</b> Modified Stern-Volmer plots for the fluorescence quenching data of the FB-HSA system at three different temperatures.	56

- Figure 3.4.** van't Hoff plot for the interaction between FB and HSA. 58
- Figure 3.5.** Synchronous fluorescence spectra of HSA in the absence and the presence of increasing FB concentrations at 25 °C, obtained in 10 mM Tris-HCl buffer, pH 7.4, using  $\Delta\lambda$  of 15 nm. 61
- Figure 3.6.** Synchronous fluorescence spectra of HSA in the absence and the presence of increasing FB concentrations at 25 °C, obtained in 10 mM Tris-HCl buffer, pH 7.4, using  $\Delta\lambda$  of 60 nm. 62
- Figure 3.7.** Three-dimensional fluorescence spectra and corresponding contour map of HSA, obtained in 10 mM Tris-HCl buffer, pH 7.4 at 25 °C. 64
- Figure 3.8.** Three-dimensional fluorescence spectra and corresponding contour map of FB–HSA (2:1) complex, obtained in 10 mM Tris-HCl buffer, pH 7.4 at 25 °C. 65
- Figure 3.9.** Three-dimensional fluorescence spectra and corresponding contour map of FB–HSA (4:1) complex, obtained in 10 mM Tris-HCl buffer, pH 7.4 at 25 °C. 66
- Figure 3.10.** Thermal denaturation and renaturation curves of HSA and FB–HSA (4:1) complex, as studied by  $CD_{222\text{ nm}}$  measurements in the temperature range, 25–100 °C in 10 mM Tris-HCl buffer, pH 7.4. 69

- Figure 3.11.** Thermal denaturation and renaturation curves of HSA and FB–HSA (4:1) complex, as studied by CD<sub>222 nm</sub> measurements in the temperature range, 25–80 °C in 10 mM Tris-HCl buffer, pH 7.4. 71
- Figure 3.12.** Displacing effect of FB on the visible CD spectrum of BR–HSA (1:1) complex at 25 °C. 73
- Figure 3.13.** Displacing effect of FB on the fluorescence spectrum of WFN–HSA (1:1) complex at 25 °C. 75
- Figure 3.14.** Plots showing the decrease in the relative CD value at 458 nm of BR–HSA complex (A) and the relative fluorescence intensity at 383 nm of WFN–HSA complex (B) with increasing FB concentrations. 76
- Figure 3.15.** Fluorescence spectra of (A) HSA and (B) FB–HSA (3:1) complex in the absence and the presence of increasing DZP concentrations, obtained in 10 mM Tris-HCl buffer, pH 7.4 at 25 °C upon excitation at 280 nm. 77
- Figure 3.16.** Plots showing the decrease in the relative fluorescence intensity at 337 nm of HSA and FB–HSA complex (3:1) with increasing DZP concentrations. 78
- Figure 3.17.** Cluster analysis of the docking of FB to Sudlow’s sites I (A) and II (B) of HSA crystal structure (1BM0). 80

- Figure 3.18.** Binding orientation of the lowest docking energy conformation of FB (ball and stick rendered) in Sudlow's site I (subdomain IIA) of HSA (1BM0). 81
- Figure 3.19.** Fluorescence spectra of HSA in the absence and the presence of increasing PS concentrations, obtained in 10 mM Tris-HCl buffer, pH 7.4 at 25 °C upon excitation at 280 nm. 85
- Figure 3.20.** Stern-Volmer plots for the fluorescence quenching data of the PS-HSA system at four different temperatures. 86
- Figure 3.21.** Double logarithmic plots of  $\log (F_0 - F) / F$  versus  $\log [1 / ([L_T] - (F_0 - F)[P_T] / F_0)]$  for the fluorescence quenching data of the PS-HSA system at four different temperatures. 89
- Figure 3.22.** van't Hoff plot for the interaction between PS and HSA. 90
- Figure 3.23.** Synchronous fluorescence spectra of HSA in the absence and the presence of increasing PS concentrations at 25 °C, obtained in 10 mM Tris-HCl buffer, pH 7.4, using  $\Delta\lambda$  of 15 nm. 93
- Figure 3.24.** Synchronous fluorescence spectra of HSA in the absence and the presence of increasing PS concentrations at 25 °C, obtained in 10 mM Tris-HCl buffer, pH 7.4, using  $\Delta\lambda$  of 60 nm. 94

- Figure 3.25.** Three-dimensional fluorescence spectra and corresponding contour maps of (A) HSA and (B) PS–HSA (1:1) complex, obtained in 10 mM Tris-HCl buffer, pH 7.4 at 25 °C. 96
- Figure 3.26.** Three-dimensional fluorescence spectra and corresponding contour maps of (A) PS–HSA (2:1) complex and (B) PS–HSA (3:1) complex, obtained in 10 mM Tris-HCl buffer, pH 7.4 at 25 °C. 97
- Figure 3.27.** Thermal denaturation and renaturation curves of HSA and PS–HSA (5:1) complex, as studied by CD<sub>222 nm</sub> measurements in the temperature range, 25–100 °C (A) and 25–80 °C (B) in 10 mM Tris-HCl buffer, pH 7.4. 100
- Figure 3.28.** Displacing effect of PS on the visible CD spectrum of BR–HSA (1:1) complex at 25 °C. 102
- Figure 3.29.** Displacing effect of PS on the fluorescence spectrum of WFN–HSA (1:1) complex at 25 °C. 104
- Figure 3.30.** Plots showing the decrease in the relative CD value at 458 nm of BR–HSA complex (A) and the relative fluorescence intensity at 383 nm of WFN–HSA complex (B) with increasing PS concentrations. 105
- Figure 3.31.** Displacing effect of PS on the CD spectrum of DZP–HSA (2:1) complex at 25 °C. 106

- Figure 3.32.** Displacing effect of PS on the CD spectrum of KTN–HSA (2:1) complex at 25 °C. 108
- Figure 3.33.** Plots showing the decrease in the relative CD value at 259 nm of DZP–HSA complex (A) and the relative CD value at 340 nm of KTN–HSA complex (B) with increasing PS concentrations. 109
- Figure 3.34.** Cluster analysis of the docking of PS to Sudlow’s sites I (A) and II (B) of HSA crystal structure (1BM0). 111
- Figure 3.35.** Cluster analysis of the docking of PS to Sudlow’s sites I (A) and II (B) of HSA crystal structure (2BXD). 112
- Figure 3.36.** Cluster analysis of the docking of PS to Sudlow’s sites I (A) and II (B) of HSA crystal structure (2BXF). 113
- Figure 3.37.** Binding orientation of the lowest docking energy conformation of PS (ball and stick rendered) in Sudlow’s site I (subdomain IIA) of HSA (1BM0). 114
- Figure 3.38.** Fluorescence spectra of HSA in the absence and the presence of increasing 6S concentrations, obtained in 10 mM sodium phosphate buffer, pH 7.4 at 25 °C upon excitation at 295 nm. 118
- Figure 3.39.** Stern-Volmer plots for the fluorescence quenching data of the 6S–HSA system at four different temperatures. 119

- Figure 3.40.** Double logarithmic plots of  $\log (F_0 - F) / F$  versus  $\log [1 / ([L_T] - (F_0 - F)[P_T] / F_0)]$  for the fluorescence quenching data of the 6S–HSA system at four different temperatures. 122
- Figure 3.41.** van't Hoff plot for the interaction between 6S and HSA. 123
- Figure 3.42.** Three-dimensional fluorescence spectra and corresponding contour maps of (A) HSA, (B) 6S–HSA (2:1) complex and (C) 6S–HSA (4:1) complex, obtained in 10 mM sodium phosphate buffer, pH 7.4 at 25 °C. 127
- Figure 3.43.** Thermal denaturation and renaturation curves of HSA and 6S–HSA (4:1) complex, as studied by  $CD_{222\text{ nm}}$  measurements in the temperature range, 25–100 °C (A) and 25–80 °C (B) in 10 mM sodium phosphate buffer, pH 7.4. 130
- Figure 3.44.** Fluorescence spectra of (A) HSA and (B) 6S–HSA (5:1) complex in the absence and the presence of increasing PBZ concentrations, obtained in 10 mM sodium phosphate buffer, pH 7.4 at 25 °C upon excitation at 295 nm. 131
- Figure 3.45.** Plots showing the decrease in the relative fluorescence intensity at 338 nm of HSA and 6S–HSA (5:1) complex with increasing PBZ concentrations. 132
- Figure 3.46.** Fluorescence spectra of (A) HSA and (B) PBZ–HSA (5:1) complex in the absence and the presence of increasing 6S concentrations, obtained in 10 mM sodium phosphate buffer, pH 7.4 at 25 °C upon excitation at 295 nm. 134

- Figure 3.47.** Plots showing the decrease in the relative fluorescence intensity at 338 nm of HSA and PBZ–HSA (5:1) complex with increasing 6S concentrations. 135
- Figure 3.48.** Fluorescence spectra of (A) HSA and (B) 6S–HSA (5:1) complex in the absence and the presence of increasing KTN concentrations, obtained in 10 mM sodium phosphate buffer, pH 7.4 at 25 °C upon excitation at 295 nm. 136
- Figure 3.49.** Plots showing the decrease in the relative fluorescence intensity at 338 nm of HSA and 6S–HSA (5:1) complex with increasing KTN concentrations. 137
- Figure 3.50.** Fluorescence spectra of (A) HSA and (B) KTN–HSA (5:1) complex in the absence and the presence of increasing 6S concentrations, obtained in 10 mM sodium phosphate buffer, pH 7.4 at 25 °C upon excitation at 295 nm. 138
- Figure 3.51.** Plots showing the decrease in the relative fluorescence intensity at 338 nm of HSA and KTN–HSA (5:1) complex with increasing 6S concentrations. 139
- Figure 3.52.** Cluster analysis of the docking of 6S to Sudlow’s sites I (A) and II (B) of HSA crystal structure (1BM0). 141
- Figure 3.53.** Cluster analysis of the docking of 6S to Sudlow’s sites I (A) and II (B) of HSA crystal structure (2BXD). 142

- Figure 3.54.** Cluster analysis of the docking of 6S to Sudlow's sites I (A) and II (B) of HSA crystal structure (2BXF). 143
- Figure 3.55.** Binding orientation of the lowest docking energy conformation of 6S (ball and stick rendered) in Sudlow's site I (subdomain IIA) of HSA (1BM0). 145
- Figure 3.56.** Binding orientation of the lowest docking energy conformation of 6S (ball and stick rendered) in Sudlow's site II (subdomain IIIA) of HSA (1BM0). 146

University of Malaysia

## LIST OF TABLES

	<b>Page</b>
<b>Table 1.1.</b> Important drugs derived from plants, their medicinal uses and sources.	3
<b>Table 1.2.</b> Physicochemical properties of HSA.	16
<b>Table 1.3.</b> Amino acid composition of HSA.	18
<b>Table 1.4.</b> Binding of drugs to sites I and II of HSA.	28
<b>Table 3.1.</b> Quenching and binding parameters for the interaction of FB with HSA, obtained from fluorescence quenching titration experiments at different temperatures, pH 7.4.	54
<b>Table 3.2.</b> Thermodynamic parameters for the interaction of FB with HSA, obtained from fluorescence quenching titration experiments at different temperatures, pH 7.4.	59
<b>Table 3.3.</b> Three-dimensional fluorescence spectral characteristics of HSA and FB–HSA complexes at pH 7.4, 25 °C.	67
<b>Table 3.4.</b> Distance of the predicted hydrogen bonds formed between interacting atoms of the amino acid residues of HSA (site I) and FB.	82
<b>Table 3.5.</b> Quenching and binding parameters for the interaction of PS with HSA, obtained from fluorescence quenching titration experiments at different temperatures, pH 7.4.	87

<b>Table 3.6.</b>	Thermodynamic parameters for the interaction of PS with HSA, obtained from fluorescence quenching titration experiments at different temperatures, pH 7.4.	91
<b>Table 3.7.</b>	Three-dimensional fluorescence spectral characteristics of HSA and PS–HSA complexes at pH 7.4, 25 °C.	98
<b>Table 3.8.</b>	Distance of the predicted hydrogen bonds formed between interacting atoms of the amino acid residues of HSA (site I) and PS.	116
<b>Table 3.9.</b>	Quenching and binding parameters for the interaction of 6S with HSA, obtained from fluorescence quenching titration experiments at different temperatures, pH 7.4.	120
<b>Table 3.10.</b>	Thermodynamic parameters for the interaction of 6S with HSA, obtained from fluorescence quenching titration experiments at different temperatures, pH 7.4.	124
<b>Table 3.11.</b>	Three-dimensional fluorescence spectral characteristics of HSA and 6S–HSA complexes at pH 7.4, 25 °C.	128
<b>Table 3.12.</b>	Distance of the predicted hydrogen bonds formed between interacting atoms of the amino acid residues of HSA and 6S.	147

## LIST OF ABBREVIATIONS / SYMBOLS

Ala	Alanine
ANOVA	Analysis of variance
Arg	Arginine
Asn	Asparagine
Asp	Aspartic acid
ATP	Adenosine triphosphate
BR	Bilirubin
BSA	Bovine serum albumin
CD	Circular dichroism
cGMP	Cyclic guanosine monophosphate
cm	Centimeter
CNS	Central nervous system
COX	Cyclooxygenase
Cys	Cysteine
3-D	Three-dimensional
Da	Dalton
dL	Deciliter
DZP	Diazepam
EDTA	Ethylenediaminetetraacetic acid
ER	Endoplasmic reticulum
ESA	Equine serum albumin
FB	Flavokawain B
g	Gram

Gln	Glutamine
Glu	Glutamic acid
Gly	Glycine
h	Hour
HCl	Hydrochloric acid
His	Histidine
HSA	Human serum albumin
HSV-1	Herpes simplex virus-1
IC <sub>50</sub>	Half maximal inhibitory concentration
Ile	Isoleucine
$K_a$	Association/binding constant
kb	Kilobase
$K_{SV}$	Stern-Volmer constant
KTN	Ketoprofen
$k_q$	Bimolecular quenching constant
Leu	Leucine
LPS	Lipopolysaccharide
Lys	Lysine
M	Molar
MALDI-TOF	Matrix assisted laser desorption/ionization-time of flight
Met	Methionine
mg	Milligram
min	Minute
mL	Milliliter
mm	Millimeter

mM	Millimolar
NaOH	Sodium hydroxide
NF- $\kappa$ B	Nuclear factor-kappa B
nm	Nanometer
NO	Nitric oxide
PBZ	Phenylbutazone
PDB	Protein Data Bank
PGE <sub>2</sub>	Prostaglandin E2
Phe	Phenylalanine
PKC	Protein kinase C
PS	Pinostrobin
6S	6-Shogaol
s	Second
S	Svedberg unit
Ser	Serine
Thr	Threonine
TNF- $\alpha$	Tumor necrosis factor-alpha
Tris	Tris(hydroxymethyl)aminomethane
Trp	Tryptophan
Tyr	Tyrosine
UV	Ultraviolet
Val	Valine
WFN	Warfarin
Å	Angstrom
$\Delta G$	Gibbs free energy change

$\Delta H$	Enthalpy change
$\Delta S$	Entropy change
$\Delta\lambda$	Wavelength difference
$\varepsilon$	Extinction coefficient
$\lambda_{em}$	Emission wavelength
$\lambda_{ex}$	Excitation wavelength
$\mu\text{m}$	Micrometer
$\mu\text{M}$	Micromolar

University of Malaya



*Chapter 1*

---

# INTRODUCTION

---



# 1. INTRODUCTION

## 1.1. Natural products as medicines

The therapeutic properties of natural products, particularly those derived from plant sources, have been known to mankind since the advent of the human civilization. Due to the diverse biological activities and medicinal potentials of these plant products, almost all major civilizations have accumulated a vast body of knowledge on their use (Ji et al., 2009). One of the oldest medical texts discovered originated from ancient Mesopotamia (c. 2600 BC) and describes approximately 1,000 plant species and plant-derived substances, such as the oils of *Cedrus* species (cedar), the resin of *Commiphora myrrha* (myrrh) and the juice of *Papaver somniferum* (poppy seed), all of which are still in use today for their curative properties (Newman et al., 2000). The Egyptian Ebers Papyrus, dating around 1550 BC, contains about 800 complex prescriptions and more than 700 natural agents such as *Aloe vera* (aloe), *Boswellia carteri* (frankincense) and the oil of *Ricinus communis* (castor) (Newman et al., 2000). Natural product-based medicines also flourished in the Orient. *Charaka Samhita*, the first treatise devoted to the concepts and practice of Indian Ayurveda, was written around 900 BC and contains details on 341 plant-derived medicines (Dev, 1999). Further East, traditional Chinese medicine is also famous for the use of natural products. The earliest Chinese medicine book, *Wu Shi Er Bing Fang (Prescriptions for Fifty Two Diseases)* was compiled around 350 BC and lists 247 natural drugs and about 150 combinatorial drug formulae, along with practical advice regarding the properties, efficacies and synergies of natural medicines (Ji et al., 2009). In the ancient Western world, the Greeks and the Romans contributed immensely to the development of medicines from natural sources. While Hippocrates (c. 400 BC), the famous Greek physician documented over 400 plants for therapeutic use (Castiglioni, 1985), the natural scientist, Theophrastus (c. 300 BC) discussed the medicinal properties of herbs and the possibility of changing their characteristics through cultivation (Newman

et al., 2000). In the first century, the Roman physician, Pedanius Dioscorides wrote what is arguably the most influential early European manual of medicinal plants, *De Materia Medica (On Medical Material)*, which described the dosage and efficacy of about 600 plant-derived medicines and laid the foundations of pharmacology in Europe (Wermuth, 2003).

Despite the wide use of plant products for medicinal applications, the identity of the chemicals that produced the desired therapeutic effects remained all but unknown until the beginning of the nineteenth century. However, some early physicians such as Galen did suggest that various natural products contained different compounds that would each affect the human body differently (Griggs, 1997). Modern chemistry has ushered in a new era for the study and use of natural products by providing tools to purify various compounds and to determine their structures. In 1804, the German pharmacist Friedrich Wilhelm Sertürner isolated morphine from opium and it became the first pure naturally-derived medicine (Schmitz, 1985). Subsequently, many pharmaceutical companies began to prefer purified natural products as ingredients to make new drugs, rather than crude extracts. The elucidation of the molecular structures of many natural products allowed chemists to synthesize them, rather than isolating them from natural sources, which significantly reduced the cost of drug production (Ji et al., 2009). Since then, a large number of natural compounds have been identified and synthesized in the laboratory. It is estimated that about 60% of the drugs that are currently available in the market and many of which are commonly prescribed, are either directly or indirectly derived from plant products (Newman, 2008). A few examples of these drugs together with their therapeutic properties are listed in Table 1.1.

There has been a renewed interest in natural product research in recent times due to the relative lack of success of alternative drug discovery methods to deliver promising lead compounds in many key therapeutic areas such as immunosuppression, anti-infective

**Table 1.1.** Important drugs derived from plants, their medicinal uses and sources.\*

<b>Drug</b>	<b>Medicinal use</b>	<b>Plant source</b>
Acetyldigoxin	Cardiac stimulant	<i>Digitalis lanata</i>
Adoniside	Cardiac stimulant	<i>Adonis vernalis</i>
Ajmalicine	Antihypertensive	<i>Rauwolfia serpentina</i>
Anisodamine	Anticholinergic	<i>Anisodus tanguticus</i>
Asiaticoside	Vulnerary	<i>Centella asiatica</i>
Atropine	Anticholinergic	<i>Atropa belladonna</i>
Berberine	Anti-dysentery	<i>Berberis vulgaris</i>
Bergenin	Antitussive	<i>Ardisia japonica</i>
Caffeine	CNS stimulant	<i>Coffea arabica</i>
Cocaine	Anesthetic	<i>Erythroxylum coca</i>
Codeine	Analgesic	<i>Papaver somniferum</i>
Colchicine	Antigout, anticancer	<i>Colchicum autumnale</i>
Convallatoxin	Cardiac stimulant	<i>Convallaria majalis</i>
Curcumin	Choleretic	<i>Curcuma longa</i>
Cynarin	Choleretic	<i>Cynara scolymus</i>
Deserpidine	Antihypertensive	<i>Rauwolfia canescens</i>
Deslanoside	Cardiac stimulant	<i>Digitalis lanata</i>
Digitalin	Cardiac stimulant	<i>Digitalis purpurea</i>
Digitoxin	Cardiac stimulant	<i>Digitalis purpurea</i>
Digoxin	Cardiac stimulant	<i>Digitalis lanata</i>

**Table 1.1.** continued

---

Emetine	Amoebicide, emetic	<i>Cephaelis ipecacuanha</i>
Ephedrine	Sympathomimetic	<i>Ephedra sinica</i>
Etoposide	Anticancer	<i>Podophyllum peltatum</i>
Gitalin	Cardiac stimulant	<i>Digitalis purpurea</i>
Glaucaroubin	Amoebicide	<i>Simarouba glauca</i>
Hemsleyadin	Anti-dysentery	<i>Helmsleya amabilis</i>
Hydrastine	Hemostatic	<i>Hydrastis canadensis</i>
Hyoscamine	Cardiac stimulant	<i>Hyoscamus niger</i>
Khellin	Bronchodilator	<i>Ammi visnaga</i>
Lanatoside	Cardiac stimulant	<i>Digitalis lanata</i>
Lobeline	Respiratory stimulant	<i>Lobelia inflata</i>
Monocrotaline	Anticancer	<i>Crotolaria sessiliflora</i>
Morphine	Analgesic	<i>Papaver somniferum</i>
Neoandrographolide	Anti-dysentery	<i>Andrographis paniculata</i>
Noscapine	Antitussive	<i>Papaver somniferum</i>
Ouabain	Cardiac stimulant	<i>Strophanthus gratus</i>
Papaverine	Musculotropic relaxant	<i>Papaver somniferum</i>
Picrotoxin	Analeptic	<i>Anamirta cocculus</i>
Pilocarpine	Parasympathomimetic	<i>Pilocarpus jaborandi</i>
Protoveratrine	Antihypertensive	<i>Veratrum album</i>
Pseudoephedrine	Sympathomimetic	<i>Ephedra sinica</i>

---

**Table 1.1.** continued

---

Quinine	Antimalaric	<i>Cinchona ledgeriana</i>
Rescinnamine	Antihypertensive	<i>Rauwolfia serpentina</i>
Reserpine	Antihypertensive	<i>Rauwolfia serpentina</i>
Rhomitoxine	Antihypertensive	<i>Rhododendron molle</i>
Rorifone	Antitussive	<i>Rorippa indica</i>
Rotundine	Analgesic	<i>Stephania sinica</i>
Salicin	Analgesic	<i>Salix alba</i>
Scillarin	Cardiac stimulant	<i>Urginea maritima</i>
Scopolamine	Anesthetic	<i>Datura metel</i>
Silymarin	Antihepatotoxic	<i>Silybum marianum</i>
Taxol	Anticancer	<i>Taxus brevifolia</i>
Teniposide	Anticancer	<i>Podophyllum peltatum</i>
Tetrahydrocannabinol	Analgesic	<i>Cannabis sativa</i>
Tetrahydropalmatine	Analgesic	<i>Corydalis ambigua</i>
Theobromine	Diuretic, bronchodilator	<i>Theobroma cacao</i>
Theophylline	Diuretic, bronchodilator	<i>Camellia sinensis</i>
Valepotriates	Anesthetic	<i>Valeriana officinalis</i>
Vincamine	Vasodilator	<i>Vinca minor</i>
Vincristine	Anticancer	<i>Catharanthus roseus</i>
Xanthotoxin	Antipsoriasis	<i>Ammi majus</i>

---

\* Compiled from Butler (2005); Fabricant & Farnsworth (2001) and Lahlou (2013).

and metabolic diseases (Lahlou, 2013). Research on natural products however, continues to explore a variety of lead structures, which may be used as templates for the development of new drugs by the pharmaceutical industry (Koehn & Carter, 2005). These molecules represent the wide structural diversity of natural products and demonstrate their lasting significance in modern drug discovery efforts. In this regard, plants of the Zingiberaceae family have attracted much attention due to their contribution in the development of not only new drugs, but also functional food products and dietary supplements which exhibit high potential in the prevention of various diseases (Hartati et al., 2014; Murakami et al., 2008).

## **1.2. Phytochemicals from the Zingiberaceae family**

The ginger family, Zingiberaceae, is a monocotyledonous family belonging to the order Zingiberales. The family comprises of around 53 genera with a total of about 1,300 species. The family is essentially tropical in distribution, with few species present in the temperate climate. It is richly represented in the Indo-Malesian flora, covering the region from India to New Guinea (Chen et al., 2008; Kress et al., 2002). Many plants from this family have a long history of therapeutic use in traditional medicine and have been the subject of substantial pharmacological and clinical investigations over the last few decades. The rhizomes of these plants have traditionally been used in the treatment of a great variety of ailments including dyspepsia, colic, nausea, vomiting, cold and flu, migraine as well as muscular and rheumatic disorders (Bode & Dong, 2011; Chen et al., 2008). They are considered to be a rich source of bioactive compounds of different classes and thus, are the major targets for discovering new phytomedicines. Various classes of Zingiber constituents with therapeutic potential include flavonoids, alkaloids, tannins, terpenoids and phenolic acids (Chan et al., 2011; Kumar et al., 2011; Pancharoen et al., 2000). Among the large number of compounds of pharmacological significance isolated

from these rhizomes, three of them, i.e., flavokawain B (FB), pinostrobin (PS) and 6-shogaol (6S) were chosen as the subjects of the present investigation.

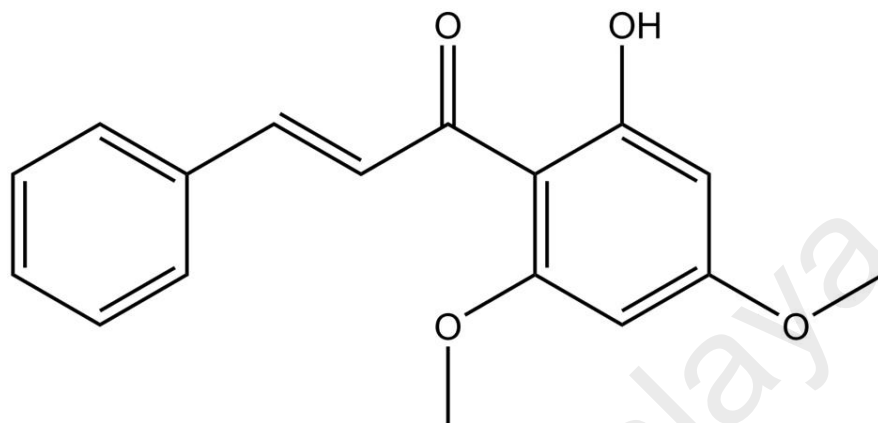
### **1.2.1. Flavokawain B**

Flavokawain B [(2E)-1-(2-hydroxy-4,6-dimethoxyphenyl)-3-phenylprop-2-en-1-one] is a member of the chalcone family of flavonoids, with a basic molecular structure of two aromatic rings, linked by an unsaturated three carbon bridge (Figure 1.1). FB was first identified in the roots of the plant, *Piper methysticum*, commonly known as kava-kava in the Pacific islands (hence the origin of its name) (Sauer & Hansel, 1967). Later investigations have discovered the presence of FB in several other plants, particularly from the genus *Alpinia* (Kuo et al., 2010; Lin et al., 2009; Malek et al., 2011).

Several reports have attributed a variety of beneficial therapeutic properties to FB, which include anti-inflammatory, anticancer and antinociceptive activities. The inhibitory effects of FB on the activities of different cyclooxygenases such as COX-1 and COX-2, the major enzymes involved in the inflammatory response were first reported by Wu et al. (2002). In a later investigation, FB was also found to inhibit the production of pro-inflammatory mediators such as nitric oxide (NO), tumor necrosis factor-alpha (TNF- $\alpha$ ) and prostaglandin E2 (PGE<sub>2</sub>) in lipopolysaccharide (LPS)-stimulated macrophages (Lin et al., 2009). This anti-inflammatory effect was shown to be mediated by down-regulation of inducible nitric oxide synthase and COX-2 expression via the suppression of nuclear factor-kappa B (NF- $\kappa$ B) (Lin et al., 2009).

In a recent study, FB has been shown to possess potent inhibitory activity against various osteosarcoma cell lines, viz. 143B, SaOS-2, MG-63 and U2OS (Ji et al., 2013). The apoptotic effect of FB on these cells involved the activation of caspases-3/7, -8 and -9, which were responsible for the down-regulation of the inhibitory apoptotic markers, including Bcl-2 and survivin and up-regulation of the apoptotic proteins, Bax, Puma and Fas (Ji et al., 2013). In addition, FB also induced G2/M phase cell cycle arrest, as revealed

**A**



**B**

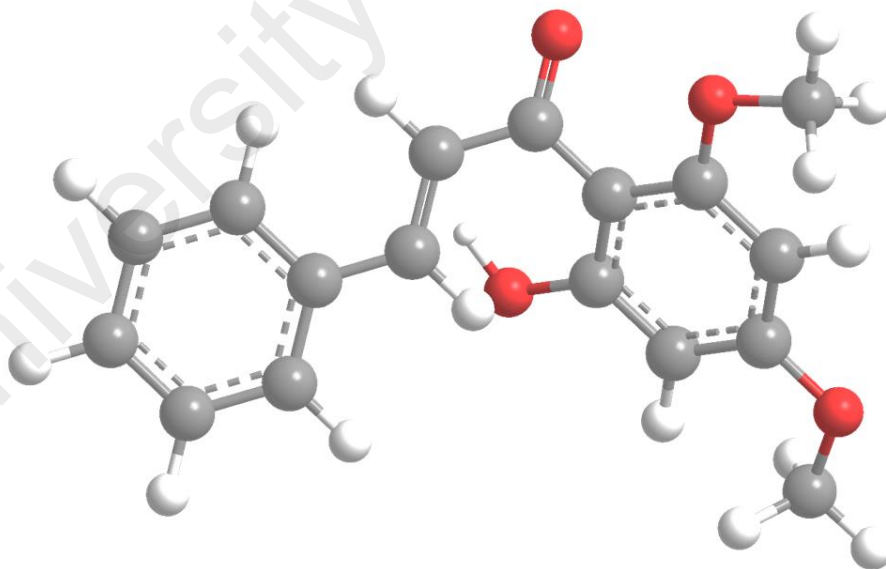


**Figure 1.1.** Chemical structure (A) and ball-and-stick model (B) of flavokawain B.

by the reduced levels of cyclin B1, cdc2 and cdc25c and increased Myt1 level (Ji et al., 2013). Furthermore, FB treatment showed less toxicity in normal bone marrow cells compared to conventional chemotherapeutic drugs (Ji et al., 2013). Similar molecular mechanisms of anticancer action of FB were also reported in oral carcinoma cell lines, ACC-2 (Zhao et al., 2011) and HSC-3 (Hseu et al., 2012); synovial sarcoma cell lines, SYO-1 and HS-SY-2 (Sakai et al., 2012); uterine leiomyosarcoma cell line, SK-LMS-1; endometrial adenocarcinoma cell line, ECC-1 (Eskander et al., 2012); prostate cancer cell lines, DU145 and PC-3 (Tang et al., 2010); lung cancer cell line, H460 (An et al., 2012) and colon cancer cell line, HCT116 (Kuo et al., 2010). Apart from *in vitro* models, antitumor activity of FB has also been demonstrated under *in vivo* system, using animal models. For example, in nude mice transplanted with DU145 cells, FB exhibited significant reduction in the tumor growth without any signs of necrosis or growth irregularities (Tang et al., 2010). FB treatment also inhibited growth of patient-derived mice xenografts of human squamous (Lin et al., 2012) and prostate (Li et al., 2012) cancer cell lines.

FB also produced pronounced antinociceptive effect against chemical and thermal models of pain in mice, exhibiting both peripheral and central analgesic activities (Mohamad et al., 2010). It was suggested that this antinociceptive action involved activation of the NO-cGMP-PKC-ATP-sensitive K<sup>+</sup> channel pathway (Mohamad et al., 2011).

### **1.2.2. Pinostrobin**

Pinostrobin [(2S)-5-hydroxy-7-methoxy-2-phenyl-2,3-dihydrochromen-4-one] is a natural flavanone, found in different Zingiberaceae plant species including the genera *Boesenbergia* (Abdelwahab et al., 2011; Fahey & Stephenson, 2002), *Alpinia* (Mohamad et al., 2004), *Renealmia* (Gomez-Betancur et al., 2014) and *Kaempferia* (Yenjai & Wanich, 2010). Being a member of the flavonoid class of secondary metabolites, PS

structural features (Figure 1.2) bear a close resemblance to FB. However, in contrast to FB which is a chalcone, the three carbon chain connecting the aromatic rings of PS is closed to form an oxacyclohexane (tetrahydropyran) ring.

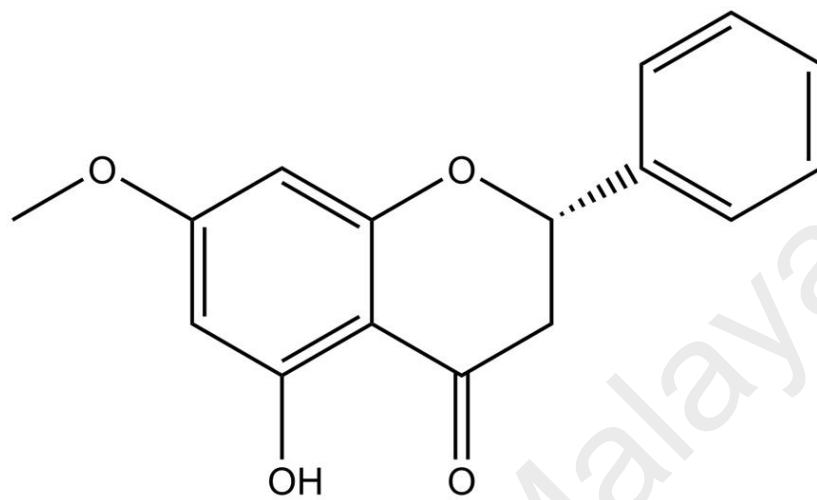
Like many other flavonoids, PS has been found to exhibit inhibitory activity against different cancer cell types. Studies on human breast cancer cell line, MCF-7 led Le Bail and coworkers (2000) to conclude that PS possessed characteristics of an ideal anticancer compound. In addition, PS was also shown to induce a remarkable apoptotic response in both Jurkat and HL60 leukemic cells (Smolarz et al., 2006). Similar apoptotic results were also obtained with SK-BR-3, PC-3 and COLO 320DM cancer cell lines using PS and its derivatives (Poerwono et al., 2010). Furthermore, PS has also been described as a potent inducer of mammalian phase-2 chemoprotective and antioxidant enzymes in hepatoma cells (Fahey & Stephenson, 2002).

Interestingly, PS has also displayed antiviral activity against herpes simplex virus-1 (HSV-1) under both *in vitro* and *in vivo* conditions (Wu et al., 2011). PS treatment inhibited the replication process and induced changes in the morphology and size of HSV-1. Moreover, oral administration of PS to HSV-1 infected mice was found to significantly retard the development of lesions compared to untreated mice.

An investigation on the protective properties of PS against  $\beta$ -amyloid-induced neurotoxicity in PC12 cells revealed that PS inhibited oxidative stress and intracellular calcium influx, stabilized mitochondrial functions and reduced neuronal apoptosis (Xian et al., 2012). These observations indicated promising activity of PS against Alzheimer's disease through the attenuation of  $\beta$ -amyloid-induced toxicity.

The anti-ulcerogenic effect of PS was recently demonstrated through its cytoprotective action in ulcer-induced rats, as evidenced by the reduction in the ulcer area and mucosal content upon PS treatment. In addition, submucosal edema and leukocytes infiltration were also significantly reduced in PS-treated rats (Abdelwahab et al. 2011). In another

**A**



**B**

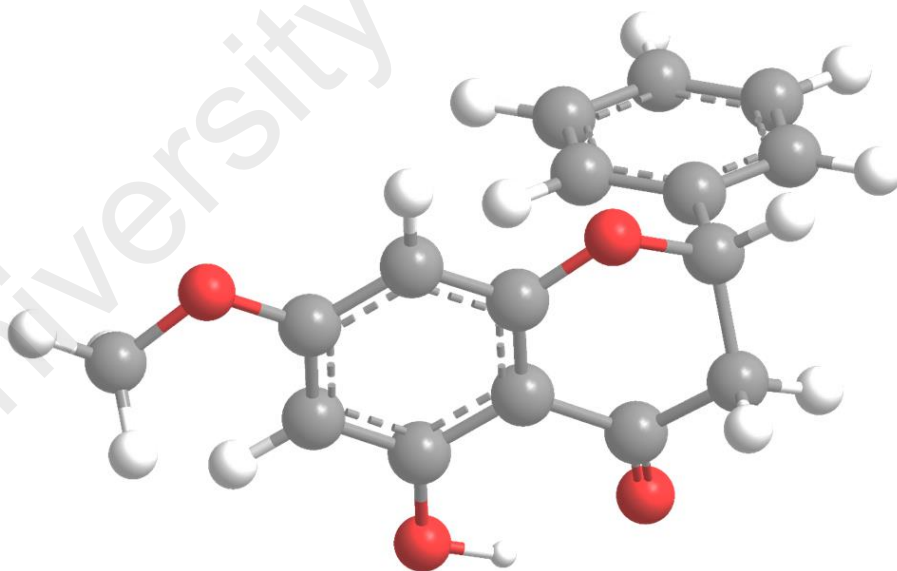


**Figure 1.2.** Chemical structure (A) and ball-and-stick model (B) of pinostrobin.

study, PS was also found to exhibit antimicrobial activity against several different isolates of *Helicobacter pylori* (Bhamarapravati et al., 2006), the bacterium commonly associated with peptic ulcer and other gastrointestinal disorders.

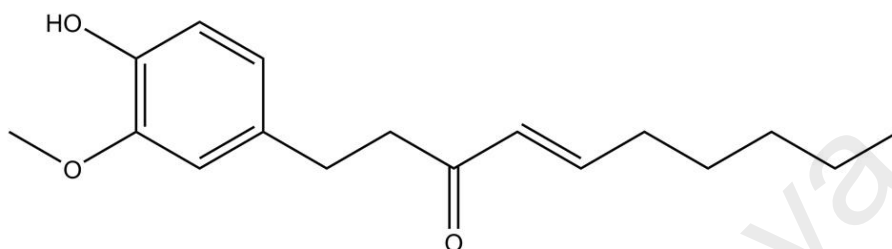
Additionally, PS-induced inhibition of cyclooxygenase enzyme pathway (Wu et al., 2002) as well as topical inflammation in rats (Tuchinda et al., 2002) have also indicated its potential as an anti-inflammatory agent.

### **1.2.3. 6-Shogaol**

Among the plants of the Zingiberaceae family, the common ginger (*Zingiber officinale*) is one of the most studied plants for its medicinal value. Due to its prevalence in the diet, investigations on its molecular constituents have led to the discovery of at least 115 compounds of different classes (Bode & Dong, 2011). Gingerols and their dehydration products, shogaols represent the two major classes of bioactive compounds found in fresh and dried gingers, respectively. 6-Shogaol [(4E)-1-(4-hydroxy-3-methoxyphenyl)dec-4-en-3-one] being named after *shoga*, the Japanese word for ginger, represents the main component of dried ginger (Bode & Dong, 2011; Jolad et al., 2005; Zick et al., 2008). The molecular structure of 6S (Figure 1.3) was first elucidated in 1927 by a Japanese group working on the characterization of compounds isolated from ginger (Connell, 1969).

Reports highlighting significantly higher anticancer efficacy of shogaols, particularly 6S, compared to gingerols generated greater interest in this class of ginger constituents. This was exemplified by the report suggesting significant inhibition of the growth of A-2780 ovarian cancer cells in the presence of 6S, while 6-, 8- and 10-gingerols produced little or no effect (Rhode et al., 2007). In another report, 6S has shown stronger growth-inhibitory effects on A-549 human lung cancer cells, SK-OV-3 human ovarian cancer cells, SKMEL-2 human skin cancer cells and HCT-15 human colon cancer cells than 4-, 6-, 8- and 10-gingerols (Kim et al., 2008). Furthermore, 6-, 8- and 10-shogaols exhibited

**A**



**B**

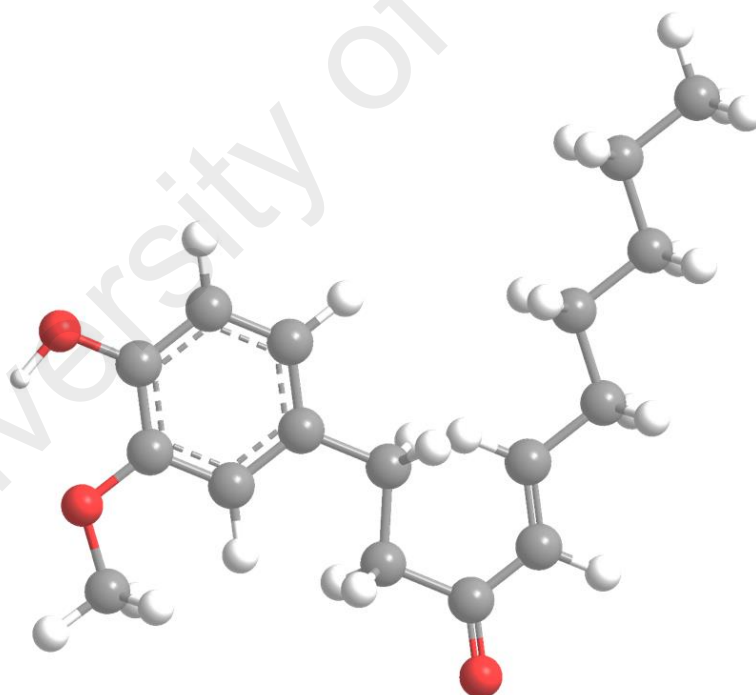


**Figure 1.3.** Chemical structure (A) and ball-and-stick model (B) of 6-shogaol.

higher antiproliferative potency than 6-, 8- and 10-gingerols against H-1299 human lung cancer cells, with an IC<sub>50</sub> values of 8 μM for 6S and 150 μM for 6-gingerol (Sang et al., 2009). Several investigations involving animal models have also shown antitumor activity of 6S based on its growth-inhibitory effects on lymphatic (Liu et al., 2013), prostate (Saha et al., 2014), lung and breast (Hsu et al., 2015) cancers.

Although research on the bioactivity of 6S has been focused primarily on its anticancer potential, a number of reports have also explored its other pharmacological effects. Ha et al. (2012) reported 6S as an effective therapeutic agent for treating neurodegenerative diseases due to its modulatory effects against neuroinflammation. They showed that 6S suppressed microglial activation induced by LPS both in primary cortical neuron-glia culture and *in vivo* neuroinflammatory model. Moreover, 6S exhibited significant neuroprotective effects *in vivo* in transient global ischemia via inhibition of microglia (Ha et al., 2012). The anti-inflammatory and antioxidant properties of 6S were also evident from several other investigations, which revealed that the compound inhibited production of various inflammatory mediators and showed significant free radical scavenging action (Dugasani et al., 2010; Guo et al., 2014; Lantz et al., 2007; Tokuhara et al., 2013). Furthermore, the potency of 6S as an anti-inflammatory and antioxidant agent has been attributed to the presence of the  $\alpha$ ,  $\beta$ -unsaturated ketone moiety in its structure (Dugasani et al., 2010).

In addition, it has been recently demonstrated that 6S protects vein endothelial cells against oxidized low-density lipoprotein (oxLDL)-induced endothelial injuries by inhibiting the lectin-like oxLDL receptor-1 signaling pathway, thus highlighting its potential in the prevention of vascular diseases (Wang et al., 2013). It is also interesting to note that 6S was reported to possess antipyretic and analgesic effects, on top of inhibition of spontaneous motor activity (Suekawa et al., 1984).

### **1.3. Transport of therapeutic ligands through blood plasma**

The interaction between a pharmacologically active molecule and plasma proteins can greatly influence its distribution, delivery as well as elimination from the body (Li & Hagerman, 2013). Such interactions also exert profound effects on the therapeutic efficacy and toxicity of the compound (Olson & Christ, 1996). The ligand–protein complex acts primarily as a transport system to carry small molecules to their target sites. This is especially important for compounds that exhibit poor solubility in aqueous environment, which is true for most phytochemicals. Protein binding slows the movement of free drug from the plasma into tissues by decreasing the concentration gradient (Vallner, 1977). Furthermore, it also serves as a depot of free drug to replace those molecules removed from the target site, thus ensuring a longer duration of their pharmacological action (Bertucci & Domenici, 2002). Additionally, protein-bound drugs are protected from rapid metabolism by the body’s detoxification system (Lindup & Orme, 1981). Among all the plasma proteins available for drug binding, human serum albumin (HSA) is of paramount significance due to its relative abundance and ability to bind reversibly a large number of molecules of varying structural features. The following sections describe structural and molecular properties of HSA.

#### **1.3.1. Physicochemical properties of HSA**

The major physicochemical properties of HSA are listed in Table 1.2. A value of 66,438 Da for the molecular mass of HSA, as calculated from its amino acid composition (Minghetti et al., 1986), agreed well with the value of 66,479 Da, obtained using matrix-assisted laser desorption/ionization-time of flight (MALDI-TOF) mass spectrometry (Dockal et al., 1999). X-ray crystallographic study revealed the structure of HSA approximately as an equilateral triangle with sides of 80 Å and a depth of 30 Å (He & Carter, 1992). The axial ratio was predicted to be 3:1 based on frequency dispersion of the dielectric constant (Scheider et al., 1976). The radius of gyration was determined as

**Table 1.2.** Physicochemical properties of HSA.

Property	Value	Reference
Molecular mass		
• Amino acid composition	66,438 Da	Minghetti et al., 1986
• MALDI-TOF	66,479 Da	Dockal et al., 1999
Overall dimension	80 × 80 × 30 Å	He & Carter, 1992
Axial ratio	3:1	Scheider et al., 1976
Radius of gyration	26.7 Å	Carter & Ho, 1994
Sedimentation coefficient, $S_{20,w}$	4.5 S	Oncley et al., 1947
Diffusion coefficient, $D_{20,w}$	$6.1 \times 10^{-7} \text{ cm}^2 \text{ s}^{-1}$	Oncley et al., 1947
Partial specific volume, $\bar{v}$	$0.733 \text{ cm}^3 \text{ g}^{-1}$	Hunter, 1966
Frictional ratio	1.28:1	Oncley et al., 1947
Intrinsic viscosity, $\eta$	$0.046 \text{ dL g}^{-1}$	Hunter, 1966
Isoelectric point		
• Native	4.7	Peters, 1996
• Defatted	5.8	Gianazza et al., 1984
Isoionic point	5.16	Hughes, 1954
$\alpha$ -helix	67%	Carter & Ho, 1994
$\beta$ -form	10%	Carter & Ho, 1994
Net charge per molecule		
• at pH 7.4	-19	Tanford, 1950
• Amino acid sequence	-15	Peters, 1996
$\epsilon_{1 \text{ cm}}^{1\%}$ at 280 nm	5.3	Wallevik, 1973

26.7 Å (Carter & Ho, 1994), which was similar to the rotational hydrodynamic radius value of 26.4 Å, measured by light scattering and electron spin resonance (Cannistraro & Sacchetti, 1986). Hydrodynamic parameters such as sedimentation coefficient and diffusion coefficient were found to be 4.5 S (Oncley et al., 1947) and  $6.1 \times 10^{-7} \text{ cm}^2 \text{ s}^{-1}$  (Oncley et al., 1947), respectively. The partial specific volume was determined to be  $0.733 \text{ cm}^3 \text{ g}^{-1}$  (Hunter, 1966), similar to the value reported for other globular proteins. The values of frictional ratio and intrinsic viscosity of HSA also reflected its globular conformation, being 1.28:1 (Oncley et al., 1947) and  $0.046 \text{ dL g}^{-1}$  (Hunter, 1966), respectively. A low isoelectric point of 4.7 (Peters, 1996) revealed the acidic nature of native HSA, which increased to 5.8 in the fatty acid free form (Gianazza et al., 1984). The isoionic point of the protein was determined as 5.16 (Hughes, 1954). The structure of HSA is predominantly  $\alpha$ -helical (67%), while the remaining residues are arranged in  $\beta$ -form (10%) as well as extended or flexible regions (23%) between subdomains (Carter & Ho, 1994). At physiological pH, the net charge of HSA is  $-19$  (Tanford, 1950), which is slightly higher than the calculated value of  $-15$  (Peters, 1996) from its amino acid sequence. The high negative charge of the protein contributes to its high solubility in aqueous environment. A specific extinction coefficient value at 280 nm of 5.3 (Wallevik, 1973) can be attributed to the presence of the aromatic amino acids, Trp and Tyr in the HSA molecule.

### **1.3.2. Structural organization of HSA**

#### *1.3.2.1. Amino acid composition and primary structure*

Human serum albumin is a negatively charged, unglycosylated single chain polypeptide of 585 amino acid residues. Its amino acid composition is shown in Table 1.3. HSA contains a single Trp residue, while the contents of Met (6), Gly (12) and Ile (8) residues are also atypically low. On the other hand, HSA has an abundance of Cys

**Table 1.3.** Amino acid composition of HSA. \*

Amino acid	No. of residues
Alanine	62
Arginine	24
Asparagine	17
Aspartic acid	36
Cysteine	35
Glutamic acid	62
Glutamine	20
Glycine	12
Histidine	16
Isoleucine	8
Leucine	61
Lysine	59
Methionine	6
Phenylalanine	31
Proline	24
Serine	24
Threonine	28
Tryptophan	1
Tyrosine	18
Valine	41
<b>Total</b>	<b>585</b>
Calculated molecular mass	66,438 Da
Average residue mass	113.57 Da

\* Adapted from Peters (1996)

(35), Leu (61) as well as the charged amino acid residues, Asp (36), Glu (62), Lys (59) and Arg (24).

As illustrated in Figure 1.4, the 585 amino acid residues of HSA form nine loops, which are arranged into a distinct pattern centered around eight sequential Cys-Cys pairs. The repetition of these loops as triplets of long-short-long loops, allows them to group into three homologous domains, encompassing the residues 1–195 (domain I), 196–383 (domain II) and 384–585 (domain III) in the amino acid sequence. The first two loops within each domain, viz. loops 1-2, 4-5 and 7-8 are grouped together to constitute subdomains IA, IIA and IIIA, respectively; while loops 3, 6 and 9 form subdomains IB, IIB and IIIB, respectively. HSA contains 17 disulfide bridges involving all but one of its Cys residues (Cys-34). The unique arrangement of these disulfide links offers flexibility as well as resistance to extreme conditions to the protein molecule. The loops can associate together to form a globular structure and yet can separate from each other reversibly under denaturing conditions (Peters, 1996).

The three domains of HSA show structural similarities with some degree of sequence conservation, leading to 18–25% sequence homology, which is highest among long loops 3, 6, and 9 (Peters, 1996). The distribution of net charge shows a gradient along the molecule; with domain I possessing the highest net negative charge (–9), followed by domain II (–8) while domain III is nearly neutral (+2) (Peters, 1996).

High degree of sequence homology has been noticed among albumins from different species. About 76% sequence homology was found between 3 pairs of mammalian albumins, viz. HSA and bovine serum albumin (BSA); HSA and equine serum albumin (ESA); ESA and rabbit serum albumin, while BSA and ESA showed 73% sequence homology (He & Carter, 1992; Ho et al., 1993; Peters, 1996). Approximately 50% residues are found conserved in all known albumin sequences (Carter & Ho, 1994).

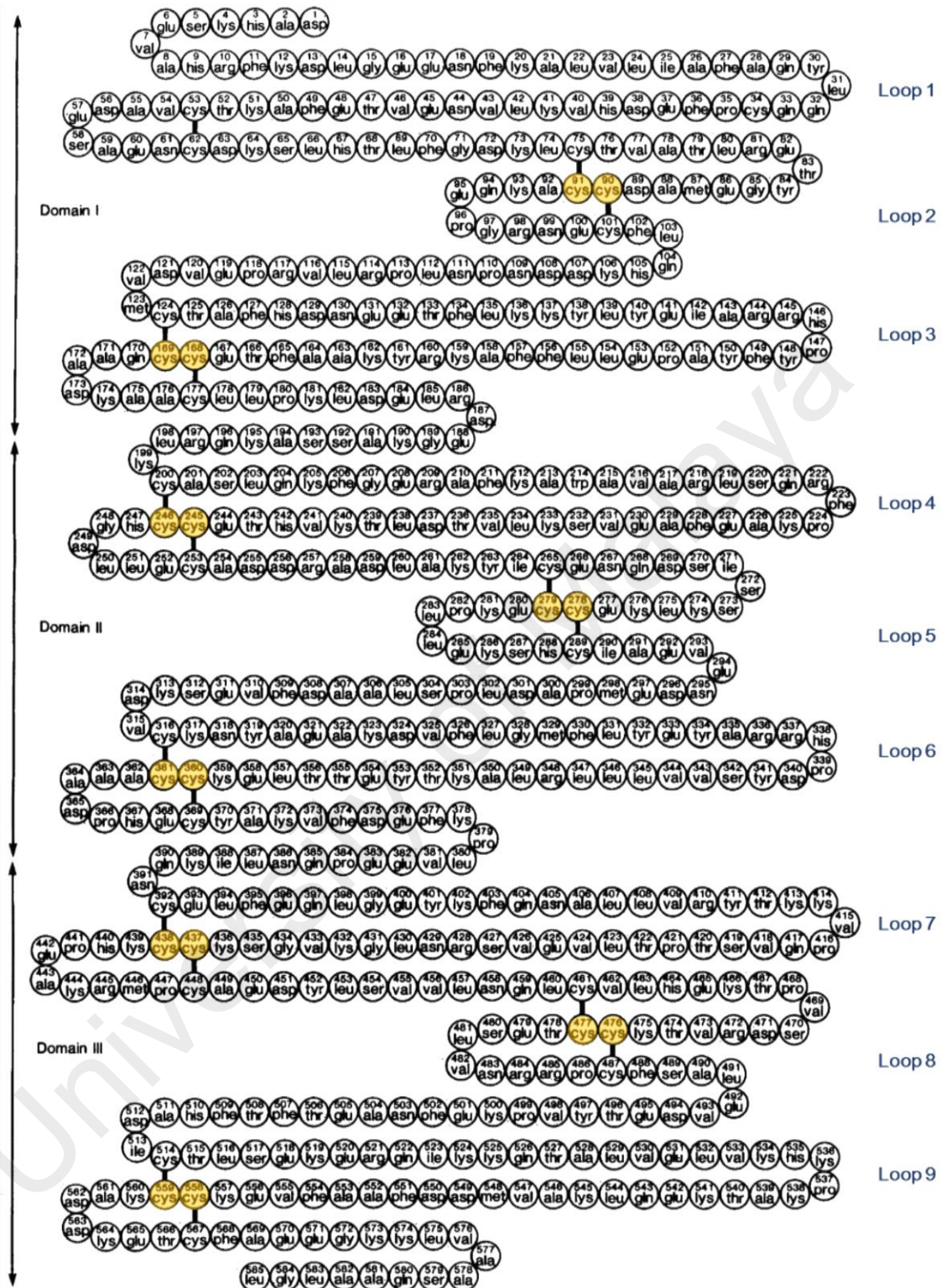


**Figure 1.4.** Primary structure of HSA, arranged into three domains, each containing one short and two long loops. The sequential Cys pairs are highlighted in yellow. (Adapted from Dugaiczky et al., 1982).

### 1.3.2.2. Three-dimensional structure

The crystal structure of HSA reveals the molecular shape resembling an equilateral triangle with sides of about 80 Å and a depth of 30 Å (Figure 1.5). This is popularly known as the heart-shaped structure of HSA, in contrast to a cigar-shaped molecule, suggested earlier based on hydrodynamic data (Peters, 1996). Under neutral pH conditions, HSA has an axial ratio of 2.66:1 (He & Carter, 1992), which was in agreement with the value of 3:1, predicted from earlier physical data (Scheider et al., 1976). The two subdomains, A and B, in each domain are composed of six and four  $\alpha$ -helices, respectively and share a common motif, where helices h1–h4 in subdomain A are identical to those (h1–h4) in subdomain B (Figure 1.6). However, subdomain A contains two additional short helices, h5 and h6, that are antiparallel to each other. The two subdomains assemble through hydrophobic helix packing interactions, involving mainly a-h2, a-h3 and b-h2 helices. Additionally, they are also linked by a flexible extension of amino acid residues, consisting of Lys-106–Glu-119, Glu-292–Val-315 and Glu-492–Ala-511 in domains I, II and III, respectively. Domains I–II and II–III are connected through extensions of Ib–h4–IIa-h1 and Iib-h4–IIIa-h1, respectively; creating the two longest helices in HSA (Carter & Ho, 1994). Thus, the actual number of helices in HSA is 28 instead of 30.

Although the three domains of HSA are topologically similar, their global assembly is rather asymmetric. Domain I is orientated perpendicular to domain II, forming a T-shaped configuration. Conversely, there is a 45° angle shift between domains II and III, forming a Y-shaped configuration (Figure 1.5). It is this arrangement of the domains that gives albumin its characteristic heart-shaped structure. Domain II interacts with domain I (the interface region between subdomains IA and IB), as well as with domain III through hydrogen bond and hydrophobic interactions. On the other hand, formation of a large channel involving subdomains IB, IIIA and IIIB, does not allow contact between domains

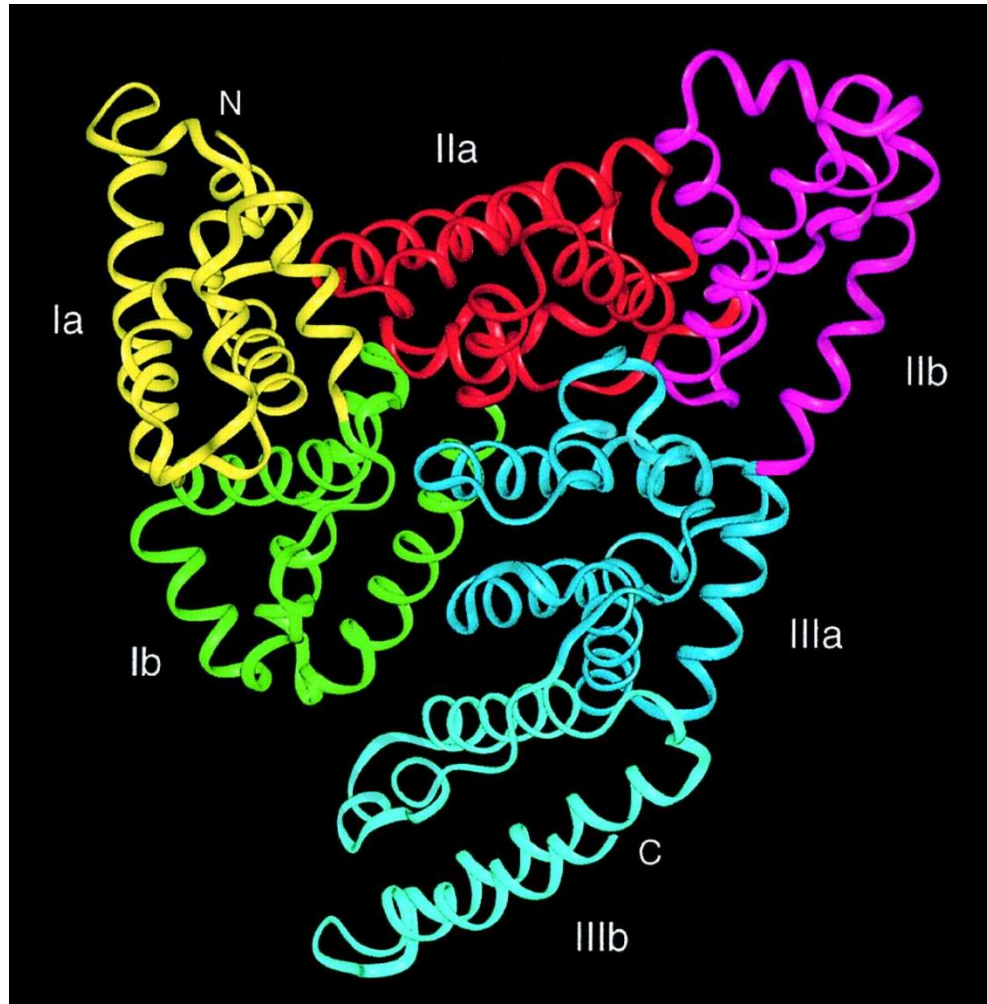


**Figure 1.5.** Three-dimensional structure of HSA. Each subdomain is marked with a different color as follows: IA, yellow; IB, green; IIA, red; IIB, magenta; IIIA, blue; and IIIB, cyan. The N- and C-termini are marked as N and C, respectively. (Adapted from Sugio et al., 1999).

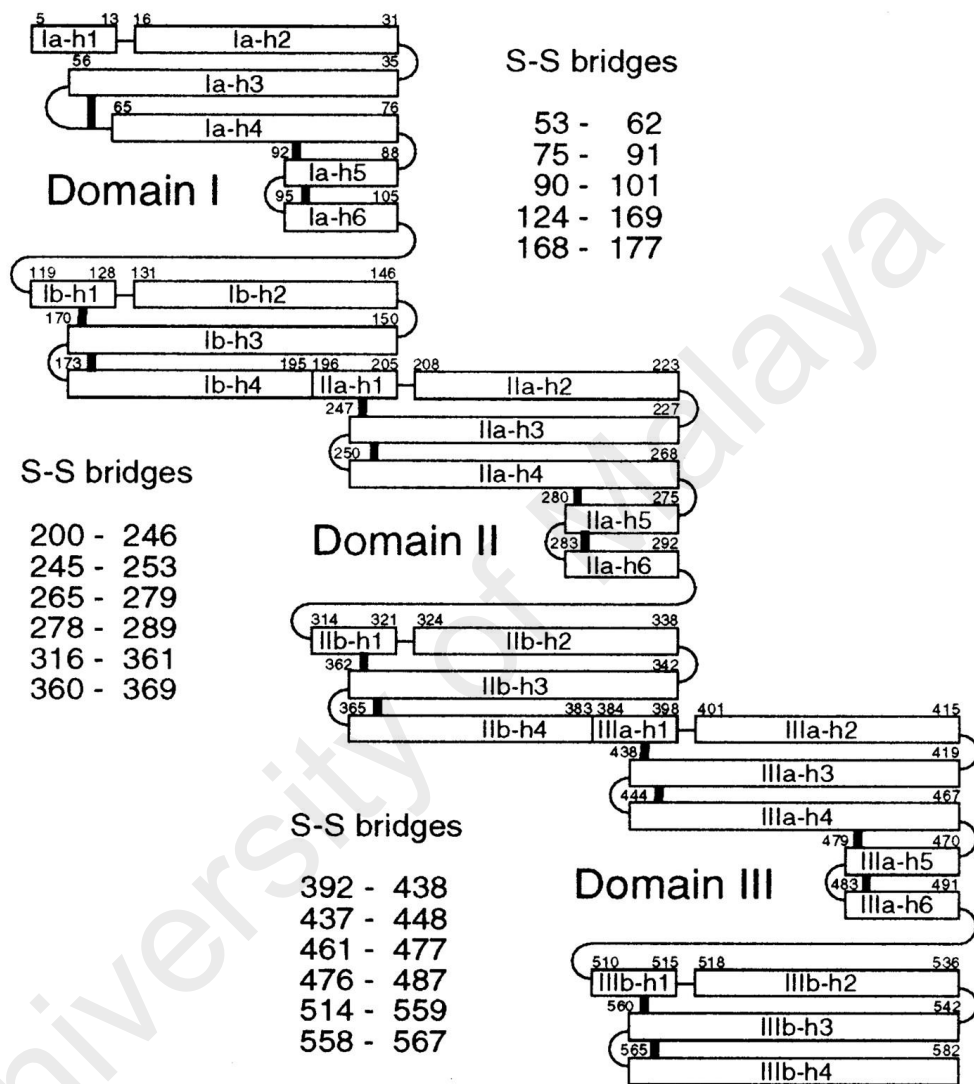


**Figure 1.6.** Helices and disulfide bridges of HSA. Helices are represented by rectangles, and loops and turns by thin lines. Disulfide bridges are drawn with thick lines. (Taken from Sugio et al., 1999).

I and III. Deep hydrophobic pockets with positively charged residues at the entrances are located at similar positions in subdomains IIA (site I) and IIIA (site II), while no such pocket is present in subdomain IA (Peters, 1996).

### **1.3.3. Genetics, synthesis and distribution of HSA**

Human serum albumin is coded by a single gene, which is expressed in a co-dominant manner with both alleles being transcribed and translated (Peters, 1996). Figure 1.7 shows the overall structure of the human albumin gene, as determined by Minghetti et al. (1986). The human albumin gene spans 16,961 nucleotides from the Cap site to the first poly(A) addition site and is split into 15 exons by 14 intervening sequences. The gene is located on the long arm of chromosome 4, near the centromere at position q11–22 (Harper & Dugaiczky, 1983). It lies 14.5 kb upstream of the gene for  $\alpha$ -fetoprotein and adjacent to the gene for vitamin D-binding protein (Cooke et al., 1986; Minghetti et al., 1986; Urano et al., 1984). The 15 exons are designated by the letters ‘ZABCDEFGHIJKLMN’ and are symmetrically placed within the three domains of HSA. The leader exon, Z, contains the 5'-untranslated portion of the albumin mRNA, including the initiation and capping sites. It encodes for the 18-residue signal peptide and the 6-residue propeptide (Peters, 1996). Domains I, II and III of HSA are encoded by quartets of exons, namely, A–D, E–H and I–L, respectively. The C-terminal end and the termination codon are encoded by exon M, whereas exon N codes for the polyadenylation site. The TATA box resides in the 5' region at position –32, downstream from the CAT box, which is located at position –88. A second TATA box is found at position –793, but a CAT box does not appear to accompany this upstream sequence (Minghetti et al., 1986).

The albumin mRNA contains ~2080 base pairs, with 39 base pairs preceding the initiation codon and 210 base pairs following the termination codon, which include a 24 base pairs long poly(A) segment (Peters, 1996). The first translated sequence is the 18-residue signal peptide which directs the growing polypeptide chain through the membrane

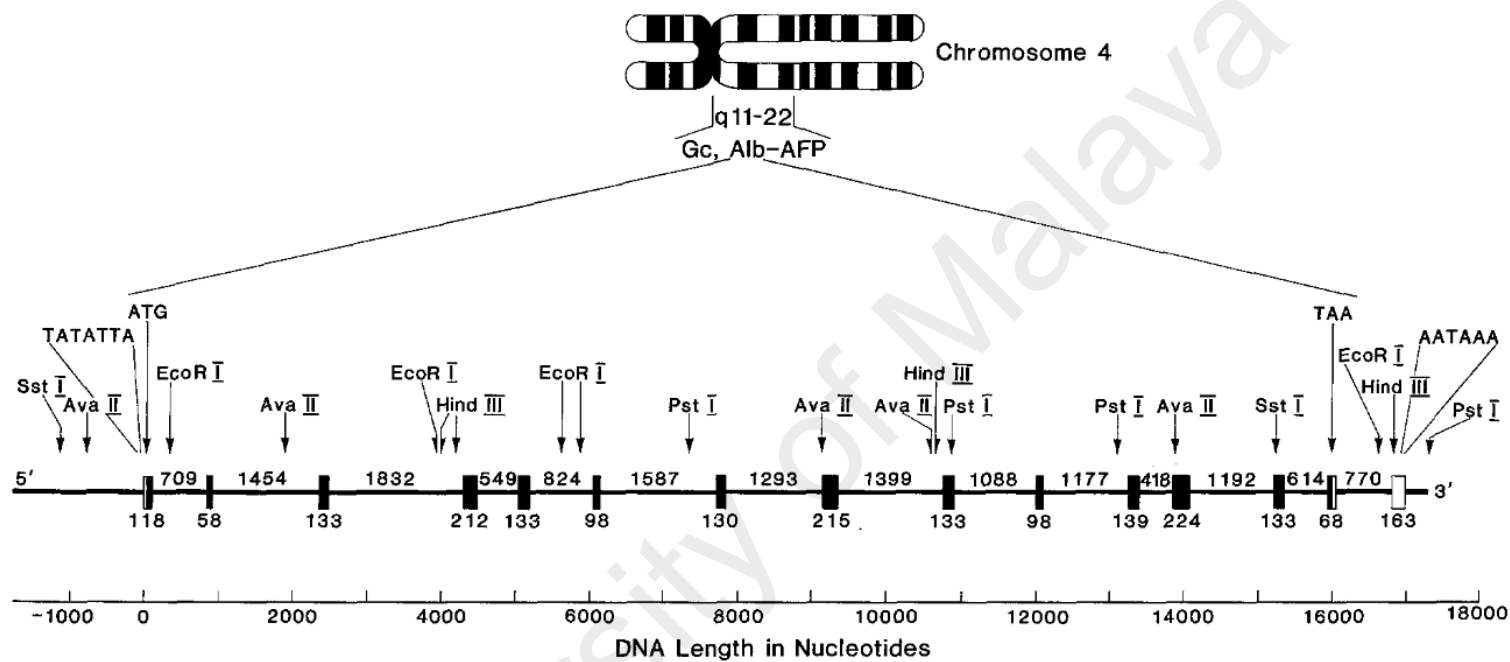


**Figure 1.7.** Map of the HSA gene. Exons are shown as boxes, while the introns are shown as thick lines. Solid boxes indicate the translated portion of the exons. The numbers represent their length in nucleotides. The gene begins at the Cap site of exon 1 and ends at the first polyadenylation site of exon 15. Major restriction endonuclease sites are listed above the map. (Taken from Minghetti et al., 1986).

of the endoplasmic reticulum (ER). It is cleaved off even before the translation process is completed. Formation of the disulfide bridges and protein folding occur immediately following the emergence of the polypeptide into the lumen of ER (Peters & Davidson, 1982). At this stage, the proalbumin contains a hexapeptide with the sequence Arg-Gly-Val-Phe-Arg-Arg attached to its N-terminal end (Russell & Geller, 1975). This leader peptide guides the protein from the ER to the Golgi apparatus for proteolytic processing and secretion. This peptide is also cleaved before the mature albumin is released from the cell in its biologically active form (Peters & Davidson, 1982). HSA is produced in the liver at a rate of ~13.9 g per day (Peters, 1996). It has an approximate half-life of 19 days (Waldmann, 1977), with about 4–5% of its population replaced daily by hepatic synthesis (Olufemi et al., 1990).

Human serum albumin is the most abundant protein in the blood plasma, with a concentration of ~40 mg mL<sup>-1</sup>. Interestingly, this only accounts for 40% of the total albumin content in the body, as the remaining albumin is distributed in extracellular locations such as skin, gut, muscle, cerebrospinal and pleural fluids as well as secretions including sweat, tears and milk. On the other hand, its intracellular concentration is very low (Evans, 2002; Peters, 1996). Upon secretion from hepatocytes, albumin enters the circulation and translocates to the extracellular space through the pores of sinusoidal or fenestrated endothelium in certain organs, such as liver, pancreas, small intestine and bone marrow (Merlot et al., 2014).

#### **1.3.4. Functions of HSA**

The concentration of albumin in the serum has long been recognized as an indicator of the state of general health and nutrition of an individual (Williams, 1992). Many important physiological functions have been ascribed to HSA. Due to its high concentration in the plasma, HSA is responsible for 80% of the colloidal osmotic pressure of blood (Lundsgaard-Hansen, 1986). In turn, its synthesis is closely regulated by the

blood osmotic pressure (Brown & Shockley, 1982). Additionally, HSA also plays a major role in maintaining blood pH (Figge et al., 1991). It has also been shown to possess several enzymatic or enzyme-like activities. For instance, it is involved in the conversion of PGE<sub>2</sub> to prostaglandin A<sub>2</sub>, and the latter to prostaglandin B<sub>2</sub> (Dieter et al., 1990). It has also been found to display esterase activity with a variety of substrates (Dubois-Presle et al., 1995; Salvi et al., 1997).

The most important function of HSA is the transport of a great variety of small molecules, particularly those with low aqueous solubility, through the circulatory system. These ligands include fatty acids, amino acids, steroid compounds such as bile acids, cholesterol, steroid hormones, etc., prostaglandins and many commonly prescribed drugs and their metabolites. It is also involved in transporting ions such as copper, zinc, calcium, iron and chloride in the circulation (Peters, 1996). HSA has also been identified as an important depot of NO, a key signaling molecule (Stamler et al., 1992). Furthermore, it also acts as a toxic waste carrier by binding to bilirubin, the product of heme catabolism, to deliver it to the liver for hepatic excretion (Knudsen et al., 1986). Interestingly, HSA is also believed to act as an anti-oxidant on account of its ability to protect bound substances such as fatty acids and lipoproteins from peroxidative damage. This is also reflected by binding to free copper, which limits its redox activity and thus, the production of free radicals. HSA also serves as a source of thiols that are avid reactive oxygen and nitrogen species scavengers (Evans, 2002; Peters, 1996).

### **1.3.5. Ligand binding sites of HSA**

Human serum albumin interacts reversibly with a broad spectrum of ligands. Generally, a vast number of drugs bind to one or very few high-affinity sites with an association constant, falling in the range,  $10^4$ – $10^6$  M<sup>-1</sup> (Table 1.4). Fluorescent probe displacement studies by Sudlow and coworkers (1975, 1976) first showed the presence of two specific drug binding sites, namely, site I (called the warfarin binding site) and site

**Table 1.4.** Binding of drugs to sites I and II of HSA.

Ligand	$K_a$ ( $M^{-1}$ )	Reference
<i>Site I</i>		
Acenocoumarol	$2.2 \times 10^5$	Yamasaki et al., 1996
Azapropazone	$2.8 \times 10^5$	Kragh-Hansen, 1988
Benzylthiouracil	$4.1 \times 10^4$	Zatón et al., 1988
Canrenoate	$2.0 \times 10^5$	Takamura et al., 1997
Carbenicillin	$2.4 \times 10^3$	Itoh et al., 1996
Chlorpropamide	$3.3 \times 10^5$	Kragh-Hansen, 1988
Furosemide	$1.9 \times 10^5$	Takamura et al., 1996
Indomethacin	$1.4 \times 10^6$	Montero et al., 1986
Iodipamide	$9.9 \times 10^6$	Yamasaki et al., 1996
Iophenoxic acid	$7.7 \times 10^7$	Mudge et al., 1978
Oxyphenbutazone	$3.5 \times 10^5$	Matsushita et al., 1998
Phenylbutazone	$1.5 \times 10^6$	Yamasaki et al., 1996
Piretanide	$9.5 \times 10^4$	Takamura et al., 1996
Quercetin	$2.7 \times 10^5$	Boulton et al., 1998
Salicylic acid	$1.9 \times 10^5$	Kragh-Hansen, 1988
Sulbenicillin	$5.2 \times 10^3$	Tsuda et al., 2001
Sulfadimethoxine	$9.0 \times 10^4$	Otagiri et al., 1989a
Sulfathiazole	$2.5 \times 10^4$	Kragh-Hansen, 1988
Tenoxicam	$3.7 \times 10^5$	Bree et al., 1993
Thymoquinone	$2.4 \times 10^4$	Lupidi et al., 2010
Tolbutamide	$4.0 \times 10^4$	Vallner, 1977
Valproic acid	$2.8 \times 10^5$	Takamura et al., 1998
Warfarin	$3.4 \times 10^5$	Yamasaki et al., 1996

**Table 1.4.** continued

Ligand	$K_a$ ( $M^{-1}$ )	Reference
<i>Site II</i>		
Benoxaprofen	$7.5 \times 10^6$	Albengres et al., 1982
Carprofen	$1.1 \times 10^6$	Rahman et al., 1993a
Chlofibric acid	$7.6 \times 10^5$	Meisner & Neet, 1978
Chlorothiazide	$5.5 \times 10^4$	Fenerty & Lindup, 1991
Costunolide	$9.7 \times 10^3$	Gao et al., 2011
Diazepam	$3.8 \times 10^5$	Kragh-Hansen, 1991
Diclofenac	$3.3 \times 10^6$	Yamasaki et al., 2000
Diflunisal	$5.0 \times 10^5$	Honore & Brodersen, 1984
Ethacrynic acid	$1.7 \times 10^6$	Bertucci et al., 1998
Etodolac	$2.0 \times 10^5$	Mignot et al., 1996
Fenoprofen	$3.4 \times 10^5$	Wang et al., 1998
Flurbiprofen	$1.0 \times 10^5$	Guo et al., 2011
Ibuprofen	$2.7 \times 10^6$	Kragh-Hansen, 1981
Iopanoic acid	$6.7 \times 10^6$	Mudge et al., 1978
Ketoprofen	$2.5 \times 10^6$	Rahman et al., 1993b
Naproxen	$3.7 \times 10^6$	Bischer et al., 1995
Oxazepam	$3.5 \times 10^5$	Boudinot et al., 1985
Pirprofen	$3.9 \times 10^5$	Otagiri et al., 1989b
Pranoprofen	$1.2 \times 10^6$	Nomura et al., 1992
Propofol	$1.5 \times 10^4$	Liu et al., 2004
Sulindac	$7.6 \times 10^6$	Russeva et al., 1994
Suprofen	$7.2 \times 10^4$	Maruyama et al., 1993
Thiamylal	$8.7 \times 10^4$	Sueyasu et al., 2000

II (the benzodiazepine binding site) on HSA. Using protein fragments derived from peptic and tryptic digestions, Bos et al. (1988a, 1988b) suggested the location of sites I and II in domains II and III, respectively. Crystallographic studies assigned the locations of sites I and II in subdomains IIA and IIIA, respectively (Carter & Ho, 1994; Curry et al., 1998; Sugio et al., 1999). Although Sudlow's classification of ligand binding sites of HSA remains useful, it cannot however, account for high affinity binding of many drugs. A number of locations in other HSA subdomains have since been identified as alternative drug binding sites, as defined by crystallographic studies (Figure 1.8). Details of the main and additional ligand binding sites are given in the following subsections.

#### *1.3.5.1. Site I*

Several investigations have been directed toward characterizing the environment of site I. Fehske and his group reported that site I contains a warfarin–azapropazone binding area, which consists of two overlapping binding sites for these drugs (Fehske et al, 1982). They also identified the presence of the sole Trp residue of HSA (Trp-214) in the non-overlapping region of the warfarin site. Results from other studies also indicated the existence of two independent binding regions within site I (Kragh Hansen, 1985, 1988). Site I appears to be more complex by the proposal of Yamasaki et al. (1996), who suggested the presence of three binding regions, i.e., subsites Ia, Ib and Ic within this site, characterized as warfarin, azapropazone and butamben binding loci, respectively.

Ligands possessing high affinity toward site I (Table 1.4) are generally grouped as dicarboxylic acids or bulky heterocyclic molecules with a negative charge localized in the middle of the molecule (Kragh Hansen et al., 2002; Otagiri, 2005). Due to the diversity of ligands and the ability to harbor more than one ligand simultaneously, site I is believed to be a large and flexible binding region (Kragh Hansen, 1988). Crystallographic studies on site I drug–HSA complexes revealed site I to be larger than site II and involvement of different parts of the subdomain IIA binding pocket, including the part adjacent to the

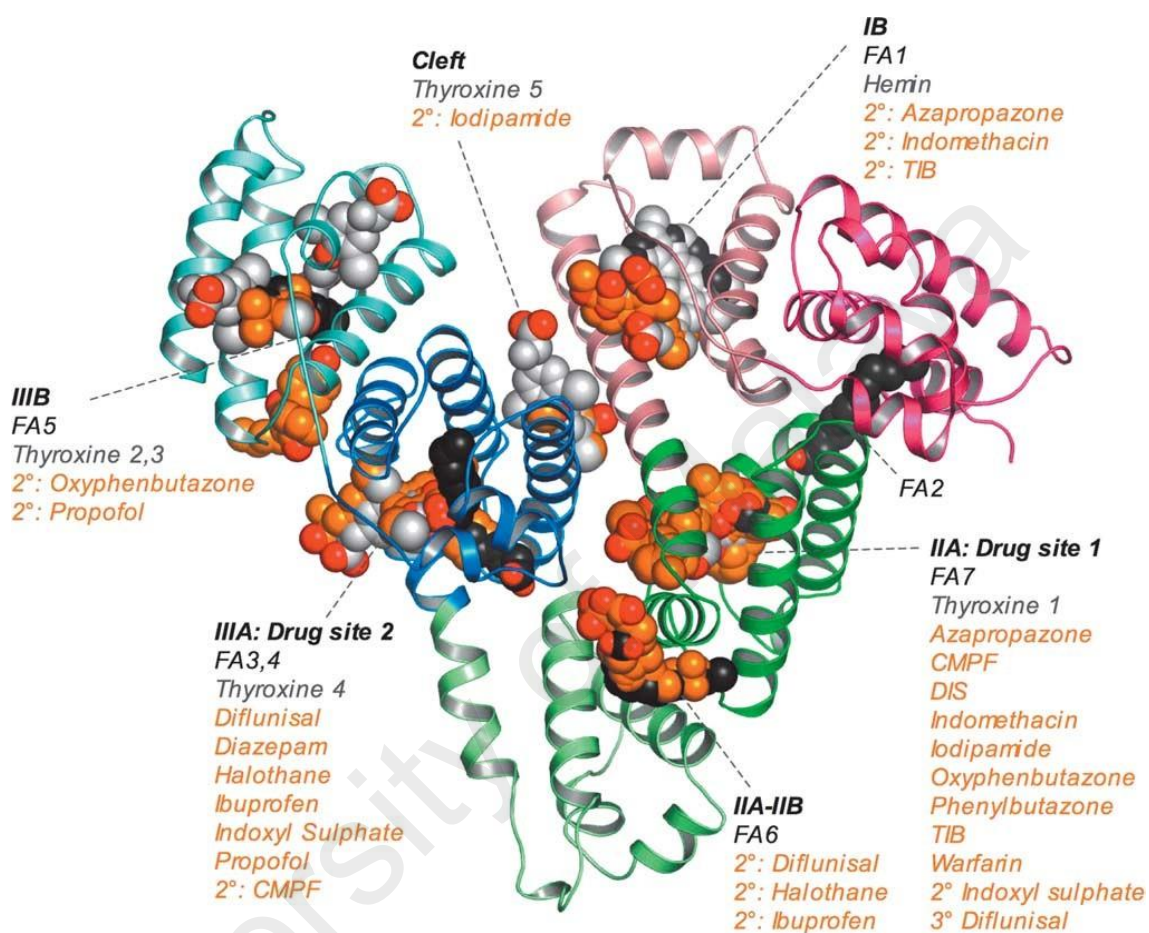


**Figure 1.8.** Ligand binding sites of HSA. Individual subdomains are colored differently and ligands are depicted as space-filling models. Oxygen atoms are colored red. All other atoms in fatty acids, other endogenous ligands (hemin and thyroxine) and drugs are colored black, grey and orange, respectively. (Taken from Ghuman et al., 2005).

interface with subdomain IB, in the complex formation with different drugs (Ghuman et al., 2005; Zhu et al., 2008). Site I is comprised of two nonpolar clusters with a pair of centrally-located polar features, formed by Tyr-150, His-242 and Arg-257 at the bottom of the pocket and by Lys-195, Lys-199, Arg-218 and Arg-222 at the entrance of the pocket. It has been suggested that flat aromatic compounds are able to fit snugly between the side-chains of Leu-238 and Ala-291 in the center of the cleft (Curry, 2011; Ghuman et al., 2005).

#### *1.3.5.2. Site II*

Site II is mainly an apolar cavity with a single dominant polar patch centered around Tyr-411 and Arg-410 near the pocket entrance (Curry, 2009). This arrangement of polar and apolar features seems to be consistent with the typical structures of site II drugs, which are aromatic carboxylic acids with a negatively charged group at one end of the molecule away from a hydrophobic center (Kragh Hansen et al., 2002; Yamasaki, 2013). Site II was proposed to be smaller and narrower compared to site I, as large molecules rarely bind to this locus (Kragh Hansen et al., 2002). Furthermore, site II is not comprised of overlapping subsites as seen in site I. It also appears to be less flexible, because ligand binding is often strongly affected by stereoselectivity. For instance, L-Trp binds to site II with ~100 times higher affinity than the D-isomer (Kragh Hansen et al., 2002). Furthermore, substitution of site II ligands with a relatively small group can strongly influence their binding (Curry, 2011). For example, fluorination of diazepam completely inhibits its binding to site II, which is the preferred binding site of diazepam (Chuang & Otagiri, 2011). Similarly, substitution of a methyl group for the  $\alpha$ -hydrogen in L-Trp also results in impediment in its binding (Peters, 1996). Although this site can bind to a variety of ligands, it appears to be more restricted than site I. However, crystallographic data suggest that site II also exhibits some degree of binding flexibility (Curry, 2009; Ryan et al., 2011). This is evident from the binding of diazepam with its relatively large and

branched structure, which induces large rotations in the side-chains of Leu-387 and Leu-453 to accommodate the phenyl moiety of the drug in this site (Yamasaki et al., 2013).

#### *1.3.5.3. Additional binding sites*

Despite the high affinity binding of many drugs to sites I and II, not all drugs bind to these sites on the HSA molecule. Even Sudlow and his group suggested that probenecid, amitriptyline and debrisoquine interact strongly with HSA, but do not bind significantly to either of the two sites (Sudlow et al., 1976). Crystallographic analysis revealed that propofol binds to site II as well as another location in subdomain IIIB (Bhattacharya et al., 2000). On the other hand, fusidic acid binds specifically to subdomain IB, the same region where the primary binding site for hemin is located (Zunzain et al., 2008). Subdomain IB was also identified as a primary binding site for lidocaine (Hein et al., 2010) and as a secondary binding site for site I drugs such as iophenoxic acid (Ryan et al., 2011), warfarin (Petitpas et al., 2001), triiodobenzoic acid (Curry et al., 1998), azapropazone and indomethacin (Yamasaki et al., 2013). A secondary binding site for ibuprofen and diflunisal was found at the interface between subdomains IIA and IIB, while that for oxyphenbutazone is located in subdomain IIIB (Ghuman et al., 2005). Interestingly, Cys-34 residue in subdomain IA, which is located in a crevice on the surface of the protein also appears to play a role in the binding of a few drugs to HSA. Due to its free sulfhydryl group, Cys-34 has been reported to participate in covalent interactions with several drugs and their metabolites including penicillamine (Keire et al., 1993), captopril (Narazaki et al., 1997), acetaminophen (Damsten et al., 2007), ethacrynic acid (Bertucci et al., 1998), cisplatin (Ivanov et al., 1998) and bucillamine derivatives (Narazaki et al., 1996).

### ***1.3.6. Clinical implications of ligand binding to HSA***

Due to the limited number of sites available for high-affinity ligand binding and the flexibility of the HSA molecule, drug binding to HSA can be affected by the binding of other drugs or endogenous compounds (Yamasaki et al., 2013). In addition to competitive binding for the same site, drugs and other ligands, which bind to a different site on HSA may also influence the binding of another drug by inducing conformational changes in the protein. Information about such influences is important since alterations in protein binding may affect the volume of distribution, clearance and elimination of a drug, which modulate its therapeutic effect (Kragh Hansen et al., 2002). When evaluating the effect of protein binding on drug therapy, it is also important to take into account not only potential drug-drug interactions but also the fact that drug metabolites may also bind to albumin with high affinity.

Drug-drug interactions are usually regarded as adverse secondary effects to the health. Although most of these interactions can be anticipated and managed by appropriate dosage adjustment, some may prove as potentially life-threatening (Lin & Lu, 1997). For example, co-administration of terfenadine, an antihistamine drug and ketoconazole led to fatal ventricular arrhythmias in some patients (Monahan et al., 1990). On the other hand, drug-drug interactions may also be useful for therapeutic purposes in certain cases. For example, patients suffering from nephrotic syndrome usually show a weak response to diuretics such as furosemide due to albumin binding. However, co-administration of a displacer such as bucolome significantly increased the diuretic effect of furosemide (Takamura et al., 2005). Furthermore, it has recently been reported that pain relief in rheumatoid arthritis patients prescribed with diclofenac was increased by concomitant administration of nabumetone (Setoguchi et al., 2013). Both diclofenac and the active metabolite of nabumetone, 6-methoxy-2-naphthylacetic acid bind strongly to site II on

HSA. Competition for the same binding site led to an increase in the free concentration of diclofenac and hence, its improved pharmacological action (Setoguchi et al., 2013).

Drug binding to albumin can also be modulated by simultaneous binding of several endogenous compounds. For instance, caprylic acid binds with high affinity to site II and has been reported to reduce the binding of thiamylal (Sueyasu et al., 2000), diazepam (Kragh-Hansen, 1991), ibuprofen and flurbiprofen (Wanwimolruk et al., 1983) at this site. On the other hand, long-chain fatty acids exhibited the opposite effect on some site I ligands such as furosemide (Takamura et al., 1998), warfarin and bilirubin (Kragh-Hansen, 1981), which showed increased binding to HSA. Such effect on the improved binding of certain site I ligands can be explained by fatty acid-induced conformational changes in HSA, which rendered site I more suitable for ligand binding. However, an alternative mechanism to address this phenomenon has also been proposed based on X-ray crystallographic studies. In the absence of fatty acids, triiodobenzoic acid binds to HSA at site I, as well as at site II with lower affinity (Kragh Hansen et al., 2002). However, in the presence of myristic acid, it is displaced from site II but rebinds at a new, myristic acid-induced binding site in subdomain IB (Curry et al., 1998).

Similarly, drug binding to HSA may also have a significant impact on the disposition of endogenous ligands. For example, several drugs including valproic acid (Yu & Shen, 1999), ceftriaxone (Brodersen & Robertson, 1989), sulfisoxazole (Brodersen, 1974), phenylbutazone, tolbutamide and warfarin (Maruyama et al., 1984) have shown strong displacing effects on bilirubin binding to HSA. Therefore, it is necessary that drugs needed to treat one disorder should also be tested for their displacing action against physiological ligands (Kremers, 2002).

### ***Objectives of the study***

Despite extensive documentation of the biological significance of FB, PS and 6S, their interactions with HSA have yet to be described. In view of the pharmacological importance of such interactions, the work presented in this thesis was undertaken to meet the following objectives:

1. To investigate the fluorescence quenching mechanism of HSA induced by FB, PS and 6S.
2. To determine the binding affinity of FB, PS and 6S to HSA.
3. To dissect the thermodynamic parameters and the intermolecular forces involved in the binding of FB, PS and 6S to HSA.
4. To analyze the effects of FB, PS and 6S binding to HSA on the microenvironment around the protein's fluorophores.
5. To study the thermal stability of HSA upon complexation with FB, PS and 6S.
6. To characterize the binding sites of FB, PS and 6S on HSA.
7. To validate the binding sites of FB, PS and 6S on HSA using molecular docking methods.



*Chapter 2*

---

# MATERIALS AND METHODS

---



## 2. MATERIALS AND METHODS

### 2.1. Materials

#### 2.1.1. Protein and bioactive compounds

Human serum albumin (HSA), essentially fatty acid-free (Lot 068K7538V) was purchased from Sigma-Aldrich Co., USA and was used as such throughout this study. Bioactive compounds used in this study, i.e., flavokawain B (FB), pinostrobin (PS) and 6-shogaol (6S) were kindly provided as a gift by Professor Datin Sri Nurestri Abdul Malek of the Institute of Biological Sciences, Faculty of Science, University of Malaya.

#### 2.1.2. Reagents used in drug displacement studies

Warfarin (WFN) (Lot 104K1261), bilirubin (BR) (Lot 055K0919), phenylbutazone (PBZ) (Lot 124K1625) and ketoprofen (KTN) (Lot BCBG9546V) were procured from Sigma-Aldrich Co., USA. Diazepam (DZP) (Lot 107.1B0.2) was the product of Lipomed AG, Switzerland.

#### 2.1.3. Miscellaneous

Analytical grade samples of sodium dihydrogen phosphate, disodium hydrogen phosphate, sodium hydroxide (NaOH), ethylenediaminetetraacetic acid (EDTA), disodium salt and hydrochloric acid (HCl) were obtained from System, Malaysia. Tris(hydroxymethyl)aminomethane (Tris) base was the product of Amresco, USA. Standard buffers of pH 7.0 and 10.0 were purchased from Sigma-Aldrich Co., USA. Analytical grade absolute ethanol and methanol as well as membrane filters (0.22 and 0.45  $\mu\text{m}$  pore size) were supplied by Merck Millipore, Germany. All-glass distilled water or ultrapure (Type 1) water produced by Milli-Q water purification system (Merck Millipore, Germany) was used throughout this study.

## 2.2. Methods

### 2.2.1. pH measurements

pH measurements were made on a Delta 320 pH meter (Mettler-Toledo GmbH, Switzerland) using a HA405-K2/120 combination electrode. The pH meter was routinely calibrated at room temperature with standard buffers of pH 7.0 and pH 10.0 for pH measurements in the neutral and alkaline pH ranges, respectively. The least count of the pH meter was 0.01 pH unit.

### 2.2.2. Analytical procedures

#### 2.2.2.1. Preparation of protein solution

HSA stock solution was prepared by dissolving a fixed amount of the protein in a fixed volume of 10 mM Tris-HCl buffer, pH 7.4 or 10 mM sodium phosphate buffer, pH 7.4. The protein solution was filtered using syringe-driven Millipore filters (0.45  $\mu\text{m}$ ). The concentration of the stock protein solution was determined spectrophotometrically using a specific extinction coefficient,  $\epsilon_{1\text{ cm}}^{1\%}$  of 5.3 at 280 nm (Wallevik, 1973). The protein stock solution was stored at 4 °C and was used within 2 weeks.

#### 2.2.2.2. Preparation of ligand solutions

The stock solution of FB was prepared by dissolving a known amount of its crystals in 10 mL of 0.5 M NaOH, while those of PS and 6S were prepared in 10 mL of ethanol. Working solutions of these ligands were made by diluting a constant volume of the stock solution to the desired concentration with either 10 mM Tris-HCl buffer, pH 7.4 or 10 mM sodium phosphate buffer, pH 7.4.

The stock solution of WFN was made by dissolution of its crystals in 1 mL of methanol and diluting it to 50 mL with 10 mM Tris-HCl buffer, pH 7.4. Its concentration was determined spectrophotometrically using a molar extinction coefficient,  $\epsilon_{1\text{ cm}}^{1M}$  of 13,610 at 310 nm (Twine et al., 2003).

BR stock solution was prepared by dissolving its crystals in 1 mL of 0.5 M NaOH containing 1 mM EDTA and diluting it to 50 mL with 10 mM Tris-HCl buffer, pH 7.4 (Faizul et al., 2008). A molar extinction coefficient,  $\epsilon_{1\text{ cm}}^{1\text{ M}}$  of 47,500 at 440 nm (Jacobsen & Wennberg, 1974) was used to determine its concentration using the spectrophotometric method. The BR solution was prepared fresh under dim light and was used within 2 h. All procedures involving BR were performed under dim light to avoid its photodegradation.

Both stock and working solutions of various drugs viz. PBZ, KTN and DZP were prepared in the same way as described above for PS and 6S.

### **2.2.3. Spectral measurements**

#### *2.2.3.1. Absorption spectroscopy*

Absorbance measurements were made on a Shimadzu UV-2450 double beam spectrophotometer (Shimadzu Corp., Japan) using quartz cuvettes of 1 cm path length. Scattering corrections, if required were made by extrapolation of the absorbance values in the wavelength range, 360–340 nm to the desired wavelength.

#### *2.2.3.2. Fluorescence spectroscopy*

Fluorescence measurements were performed on a Jasco FP-6500 spectrofluorometer (Jasco International Co., Japan), equipped with a thermostatically-regulated cell holder, using a quartz cuvette of 1 cm path length. The excitation and emission band widths were set at 10 nm each, while the scan speed was maintained at 500 nm min<sup>-1</sup>. Fluorescence spectra of HSA in the absence and the presence of a ligand were obtained by exciting the protein samples at 280 or 295 nm and recording the emission spectra in the wavelength range, 300–390 nm.

Synchronous fluorescence spectra of the protein samples were obtained after scanning them in the wavelength range, 280–320 nm and 310–370 nm, while maintaining the

difference between excitation and emission wavelengths ( $\Delta\lambda$ ) as 15 and 60 nm, respectively.

Three-dimensional fluorescence spectra of HSA and ligand–HSA systems were recorded by monitoring the emission spectra in the wavelength range, 220–500 nm, upon excitation of the samples in the wavelength range, 220–350 nm with 5/10 nm increments.

The concentration of HSA used in all fluorescence experiments was 3  $\mu\text{M}$ . Fluorescence spectra of the appropriate blanks were also recorded in the same way in order to subtract the fluorescence contributions of the ligand and the buffer from the fluorescence spectra of the samples.

#### 2.2.3.3. *Circular dichroism spectroscopy*

Circular dichroism (CD) spectral measurements were performed on a Jasco J-815 spectropolarimeter (Jasco International Co., Japan), equipped with a Jasco PTC-423S/15 temperature controller under constant nitrogen flow after calibrating the instrument with (+)-10-camphorsulfonic acid. CD spectra were collected at a scan speed of 100 nm min<sup>-1</sup> and a response time of 1 s. Each spectrum represented the average of three scans. Far-UV CD spectra were recorded with a protein concentration of 3  $\mu\text{M}$  using a 1 mm path length cell while a protein concentration of 10  $\mu\text{M}$  with a 10 mm path length cell were used for near-UV CD spectral measurements.

#### 2.2.4. *Ligand–HSA interaction studies*

##### 2.2.4.1. *Fluorescence quenching titration*

Binding of FB, PS and 6S to HSA was studied using fluorescence quenching titration method. In these experiments, HSA concentration was fixed at 3  $\mu\text{M}$  while ligand concentrations were varied in the following way in a total volume of 3 mL:

0 – 22.5  $\mu\text{M}$ , with 1.5  $\mu\text{M}$  intervals (FB)

0 – 22.5  $\mu\text{M}$ , with 1.5  $\mu\text{M}$  intervals (PS)

0 – 30.0  $\mu\text{M}$ , with 3.0  $\mu\text{M}$  intervals (6S)

After an incubation time of 1 h at 25 °C, the fluorescence spectra of the samples were recorded in the same way as described above.

In order to study the effect of temperature on the ligand–HSA interaction, titration experiments were carried out at either three (15, 25 and 35 °C) or four (15, 25, 35 and 45 °C) different temperatures, by recording the fluorescence intensity after an equilibration time of 6 min at each temperature (Lupidi et al., 2010; Silva et al., 2004; Yue et al., 2008).

#### 2.2.4.2. Spectrofluorimetric analysis

##### I. Inner filter effect correction

In order to nullify the inner filter effect, the fluorescence intensity values of the samples were corrected for their absorption at excitation and emission wavelengths using the following relationship (Lakowicz, 2006):

$$F_{\text{COR}} = F_{\text{OBS}} \times 10^{(A_{\text{EX}}+A_{\text{EM}}/2)} \quad (1)$$

where  $F_{\text{COR}}$  and  $F_{\text{OBS}}$  are the corrected and the observed fluorescence intensity values, while  $A_{\text{EX}}$  and  $A_{\text{EM}}$  represent changes in the absorbance values due to the addition of ligand at the excitation and emission wavelengths, respectively.

##### II. Quenching and binding parameters

The quenching of HSA fluorescence in the presence of increasing ligand concentrations was analyzed using the Stern-Volmer equation (Lakowicz, 2006):

$$F_0/F = K_{\text{SV}}[Q] + 1 = k_q\tau_0[Q] + 1 \quad (2)$$

where  $F_0$  and  $F$  represent the fluorescence intensity values of the protein in the absence and the presence of the quencher, respectively;  $K_{\text{SV}}$  is the Stern-Volmer constant;  $[Q]$  is the quencher concentration;  $k_q$  is the bimolecular quenching constant and  $\tau_0$  is the

fluorophore lifetime of HSA in the absence of any quencher, which was taken as  $6.38 \times 10^{-9}$  s (Abou-Zied & Al-Shihi, 2008).

Values of the association constant,  $K_a$  for the FB–HSA system at different temperatures were obtained by treating the titration data according to the modified Stern-Volmer equation (Lakowicz, 2006):

$$F_0/(F_0 - F) = 1/K_a f_a [Q] + 1/f_a \quad (3)$$

where  $F_0$ ,  $F$  and  $[Q]$  have the same significance as described above, while  $f_a$  represents the fraction of the accessible fluorescence.

Alternatively, titration data obtained with PS–HSA and 6S–HSA systems were treated according to the following double logarithmic equation (Bi et al., 2004), as it does not take into account any assumption for the ligand concentration.

$$\log [(F_0 - F)/F] = n \log K_a - n \log [1/([L_T] - (F_0 - F) [P_T]/F_0)] \quad (4)$$

where  $[L_T]$  and  $[P_T]$  refer to the total concentration of the ligand and the protein, respectively, while  $n$  represents the Hill coefficient.

### III. Thermodynamic parameters

Binding data at different temperatures were used to analyze the thermodynamic parameters using the van't Hoff equation (Raffa, 2003):

$$\ln K_a = -\Delta H/RT + \Delta S/R \quad (5)$$

where  $T$  is the absolute temperature ( $273 + ^\circ\text{C}$ ) and  $R$  is the gas constant ( $8.3145 \text{ J mol}^{-1} \text{ K}^{-1}$ ). Values of the enthalpy change ( $\Delta H$ ) and the entropy change ( $\Delta S$ ) were obtained from the slope and intercept, respectively, of the van't Hoff plot between  $\ln K_a$  and  $1/T$ . Values of  $\Delta H$  and  $\Delta S$ , thus obtained using the above method were assumed to be constant at all the four temperatures studied (Chi et al., 2011). The value of the free energy change,

$\Delta G$  of the binding reaction was subsequently obtained by fitting the  $\Delta H$  and  $\Delta S$  values into the following equation:

$$\Delta G = \Delta H - T\Delta S \quad (6)$$

### 2.2.5. *Thermal stability studies*

Thermal stability profiles of HSA and ligand–HSA complexes were obtained from CD spectral measurements. CD values of 3  $\mu\text{M}$  HSA both in the absence and the presence of each ligand (FB, PS and 6S) were recorded at 222 nm in the temperature ranges, 25–100  $^{\circ}\text{C}$  and 25–80  $^{\circ}\text{C}$ . The ligand–HSA mixtures were pre-incubated for 1 h at 25  $^{\circ}\text{C}$  to achieve equilibrium. The samples were further allowed to equilibrate for 3–6 min at each temperature in the given temperature range before the CD values were recorded. For checking the reversibility, CD measurements were made under identical conditions upon reversal of the temperature range (100–25  $^{\circ}\text{C}$  and 80–25  $^{\circ}\text{C}$ ).

### 2.2.6. *Competitive drug displacement studies*

Characterization of the binding sites of FB, PS and 6S on HSA was performed using BR, WFN and PBZ as the marker ligands for Sudlow's site I, while DZP and KTN were selected as the site markers for Sudlow's site II (Kragh-Hansen et al., 2002). All experiments were carried out at 25  $^{\circ}\text{C}$ .

#### 2.2.6.1. *Flavokawain B–HSA system*

BR displacement studies were carried out by recording the CD spectra of BR–HSA (1:1) complex (10  $\mu\text{M}$  each) in the wavelength range of 300–500 nm, both in the absence and the presence of increasing FB concentrations (15–75  $\mu\text{M}$ , with 15  $\mu\text{M}$  intervals). BR–HSA solutions were first incubated for 15 min (sufficient for equilibrium attainment) in the dark prior to the addition of FB, followed by another 15 min of incubation before CD spectral measurements.

To study the displacement of WFN in the presence of FB, fluorescence spectra of WFN–HSA (1:1) complex (3  $\mu\text{M}$  each) were recorded in the wavelength range of 360–480 nm upon excitation at 335 nm both in the absence and the presence of increasing FB concentrations (3–24  $\mu\text{M}$ , with 3  $\mu\text{M}$  intervals) under experimental conditions similar to those described in Section 2.2.3.2. WFN–HSA mixtures were preincubated for 1 h prior to the addition of FB. This was followed by another 1 h of equilibration before the spectra were recorded.

Site-specific experiments using DZP were performed by titrating 3  $\mu\text{M}$  HSA and FB–HSA mixture (3:1) with increasing concentrations of DZP (0.6–6.0  $\mu\text{M}$ , with 0.6  $\mu\text{M}$  intervals). The fluorescence spectra of HSA solutions were recorded between 300–380 nm upon excitation at 280 nm after 1 h of equilibration. The FB–HSA mixture was pre-incubated for 1 h before the titration was performed.

#### 2.2.6.2. *Pinostrobin–HSA system*

Displacement of BR by PS was studied by monitoring the effect of the addition of PS at increasing concentrations (10–80  $\mu\text{M}$ , with 10  $\mu\text{M}$  intervals) on the visible CD spectra of BR–HSA (1:1) complex (10  $\mu\text{M}$  each) in the wavelength range of 300–510 nm.

The displacing effect of PS on the binding of WFN to HSA was investigated by recording the fluorescence spectra of WFN–HSA (1:1) complex (3  $\mu\text{M}$  each) in the wavelength range of 360–480 nm upon exciting the complex at 335 nm, both in the absence and the presence of increasing PS concentrations (3–24  $\mu\text{M}$ , with 3  $\mu\text{M}$  intervals).

For competitive binding experiments involving DZP, CD spectra of DZP–HSA complex (20  $\mu\text{M}$  DZP + 10  $\mu\text{M}$  HSA) were recorded in the wavelength range of 250–350 nm both in the absence and the presence of increasing PS concentrations (10–80  $\mu\text{M}$ , with 10  $\mu\text{M}$  intervals).

The influence of PS on KTN–HSA complex (20  $\mu\text{M}$  KTN + 10  $\mu\text{M}$  HSA) was probed by recording the CD spectra of the complex in the wavelength range of 300–400 nm both

in the absence and the presence of increasing PS concentrations (10–80  $\mu\text{M}$ , with 10  $\mu\text{M}$  intervals).

Site marker–HSA mixtures were preincubated for 1 h before the addition of PS, followed by another 1 h of incubation with PS prior to spectral measurements. For experiments involving BR, both incubation times were set to 15 min.

#### 2.2.6.3. 6-Shogaol–HSA system

Titration of HSA was performed in the absence and the presence of drug/6S using fluorescence spectroscopy upon excitation at 295 nm. Fluorescence intensity values of HSA (3  $\mu\text{M}$ ) as well as 6S–HSA complex (5:1 molar ratio) were monitored at 338 nm with the addition of increasing drug concentrations (PBZ, 0–60  $\mu\text{M}$ ; KTN, 0–24  $\mu\text{M}$ ). The mixture of 6S and HSA was incubated for 1 h prior to the addition of the marker ligands. A further incubation of 1 h was allowed before fluorescence measurements.

The displacement experiments were also performed in the reverse order by titrating HSA (3  $\mu\text{M}$ ) and drug–HSA complexes (5:1 molar ratio) with increasing concentrations of 6S (0–30  $\mu\text{M}$ , with 3  $\mu\text{M}$  intervals).

#### 2.2.7. *Molecular docking studies*

ACD/ChemSketch 12 (Advanced Chemistry Development Inc., Toronto, Canada) was used to draw and optimize the structures of FB, PS and 6S. The geometry optimization of these compounds was refined with the help of Vega ZZ 2.08 (Pedretti et al., 2002) batch processing MOPAC script (mopac.r; keywords: MMOK, PRECISE, GEO-OK) using the AM1 semiempirical theory (Dewar et al., 1985). Three HSA crystal structures [PDB IDs: 1BM0, 2.5 Å resolution (Sugio et al., 1999); 2BXD, 3.05 Å and 2BXF, 2.95 Å (Ghuman et al., 2005)] were downloaded from the Protein Data Bank (Berman et al., 2000) for the docking analysis. AutoDock 4.2 (Goodsell et al., 1999) and AutoDockTools 1.5.4 (Sanner, 1999) were employed to perform molecular docking, visualization and rendering simulations at the Academic Grid Malaysia Infrastructure.

In the docking study, non-polar hydrogens of FB, PS and 6S were merged and their rotatable bonds were defined. On the other hand, all water and ligand molecules were removed before the atomic coordinates of the HSA crystal structures were used as input for AutoDockTools. After addition of polar hydrogens to the protein structures, the Kollman united atom partial charges and solvation parameters were assigned. The HSA structures were fixed at the initial input in a rigid conformation, while the torsional bonds of the ligands were allowed to orientate freely. The grid box in each simulation was defined by a  $70 \times 70 \times 70$  grid dimension of  $0.375 \text{ \AA}$  grid space and centered so that it enclosed the entire binding site and accommodated the free movement of the ligands. For Sudlow's site I, the grid boxes were centered at x, y and z coordinates of (35.26, 32.41, 36.46), (5.10, -13.35, 7.44) and (1.33, -10.09, 8.19) for 1BM0, 2BXD and 2BXF, respectively. On the other hand, the grid boxes were centered at (14.42, 23.55, 23.21), (15.23, 4.38, -7.69) and (5.28, 4.64, -10.08) for 1BM0, 2BXD and 2BXF, respectively, for docking at Sudlow's site II.

A total of 100 docking runs were performed for each binding site using Lamarckian genetic algorithm to evaluate the ligand binding energy. In each run, a population of 150 individuals with 27 000 generations and 250 000 energy evaluations were employed, with the operator weights for crossover, mutation and elitism set to 0.8, 0.02 and 1.0, respectively. A root-mean-square-deviation tolerance of  $2.0 \text{ \AA}$  was used for cluster analysis of the docking results.

#### **2.2.8. Statistical analysis**

All experiments were conducted independently at least three times and the data are presented as the mean  $\pm$  standard deviation. The statistical differences were analyzed using one way analysis of variance (ANOVA) and a value of  $p < 0.05$  was considered statistically significant.

Curve fitting and processing of statistical data were performed using OriginPro 9 (OriginLab Corp., Northampton, MA, USA).

University of Malaya



*Chapter 3*

---

# RESULTS AND DISCUSSION

---



### 3. RESULTS AND DISCUSSION

#### 3.1. Flavokawain B–human serum albumin interaction

Fluorescence spectroscopy has long been utilized in the characterization of ligand–protein interactions due to its high sensitivity toward conformational and microenvironmental changes in proteins. Investigations into binding of a ligand to a protein often involve quenching of the protein fluorescence as a result of its interaction with a particular ligand. Therefore, fluorescence spectroscopy was employed to study the interaction of a bioactive flavonoid (chalcone) from *Alpinia mutica*, flavokawain B (FB) with HSA.

##### 3.1.1. Quenching of HSA fluorescence and binding characteristics

Fluorescence quenching or a decrease in the fluorescence intensity of a system can be explained by a variety of molecular interactions such as excited-state reactions, molecular rearrangement, energy transfer, ground-state complex formation and collisional quenching (Lakowicz, 2006). As seen from Figure 3.1, HSA exhibited an emission spectrum in the wavelength range, 300–380 nm with an emission maximum at 337 nm upon excitation at 280 nm. This was in accordance with earlier reports (Kalanur et al., 2010; Kumar et al., 2004; Samari et al., 2012) and can be ascribed to the presence of a single Trp residue in the protein. Addition of FB led to a concentration-dependent quenching of the intrinsic fluorescence of HSA along with a blue shift of 6 nm in its emission maximum. The decrease in the fluorescence intensity of HSA upon addition of FB was more pronounced at lower FB/HSA molar ratios and sloped off at higher molar ratios (inset of Figure 3.1). About 72% quenching was observed at a FB/HSA molar ratio of 7.5. Increased hydrophobicity around the fluorophores can account for the blue shift in the emission maximum, whereas movement of the charged groups as well as hydrophobic changes in the microenvironment around fluorophores are responsible for the decrease in

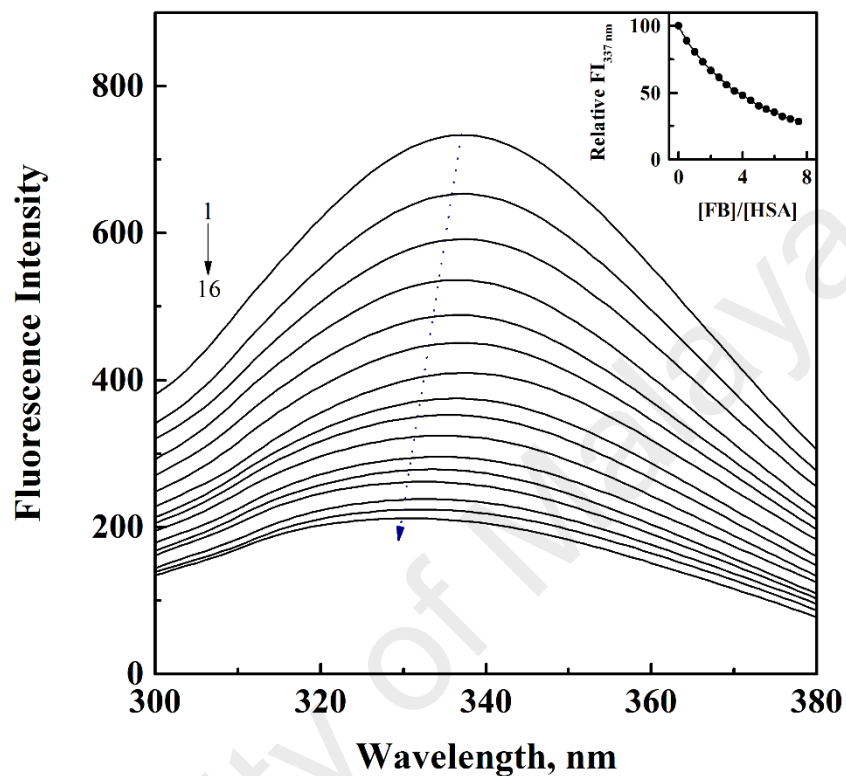


**Figure 3.1.** Fluorescence spectra of HSA in the absence and the presence of increasing FB concentrations, obtained in 10 mM Tris-HCl buffer, pH 7.4 at 25 °C upon excitation at 280 nm. The concentration of HSA was fixed at 3  $\mu\text{M}$ , while FB concentration was varied (from top to bottom, 1 $\rightarrow$ 16) in the range, 0–22.5  $\mu\text{M}$  at regular increments of 1.5  $\mu\text{M}$ . The arrow depicts the blue shift in the emission maximum of HSA with increasing FB concentrations. Inset shows the decrease in the relative fluorescence intensity at 337 nm ( $\text{FI}_{337 \text{ nm}}$ ) with increasing FB/HSA molar ratios.

the fluorescence intensity (Khanna et al., 1986). Hence, shift in the emission maximum is a better index to evaluate any alteration in the hydrophobicity in the vicinity of the fluorophores. Such changes in the fluorescence properties of HSA reflected microenvironmental alterations around the protein fluorophores upon FB addition and therefore, suggested the interaction of FB with HSA.

Quenching of the protein fluorescence can be classified as either a collisional or a static process. Both quenching mechanisms require molecular contacts between the fluorophores and the quenchers. Collisional quenching, a type of dynamic quenching process, results from random encounters between the excited fluorophore and the quencher. In other words, the quencher must diffuse to the fluorophore during the lifetime of its excited state. Upon contact, the fluorophore returns to the ground state, without emission of a photon. In general, quenching occurs without any permanent change in the molecule. On the other hand, in static quenching, a nonfluorescent ground state complex is formed between the fluorophore and the quencher. These two mechanisms can be distinguished on the basis of their dependence on temperature, as higher temperatures lead to more frequent collisions (higher extent of collisional quenching) and dissociation of the ground state complexes (smaller extent of static quenching) (Lakowicz, 2006).

In order to characterize the mechanism of the fluorescence quenching involved in the FB–HSA system, quenching experiments were performed at three different temperatures, i.e., 15, 25 and 35 °C. Figure 3.2 shows the Stern-Volmer plots for the FB–HSA system obtained at these temperatures. It should be noted that the plots showed an upward deviation at higher FB concentrations. This was not unusual, as many reports have shown upward deviation in the Stern-Volmer plots (Silva et al., 2004; Varlan & Hillebrand, 2010; Zhang et al., 2011). Therefore, results at lower ligand concentrations, showing linearity were selected for regression analysis. Values of the Stern-Volmer constant,  $K_{SV}$  were obtained from the slope of these plots and are listed in Table 3.1. As can be seen

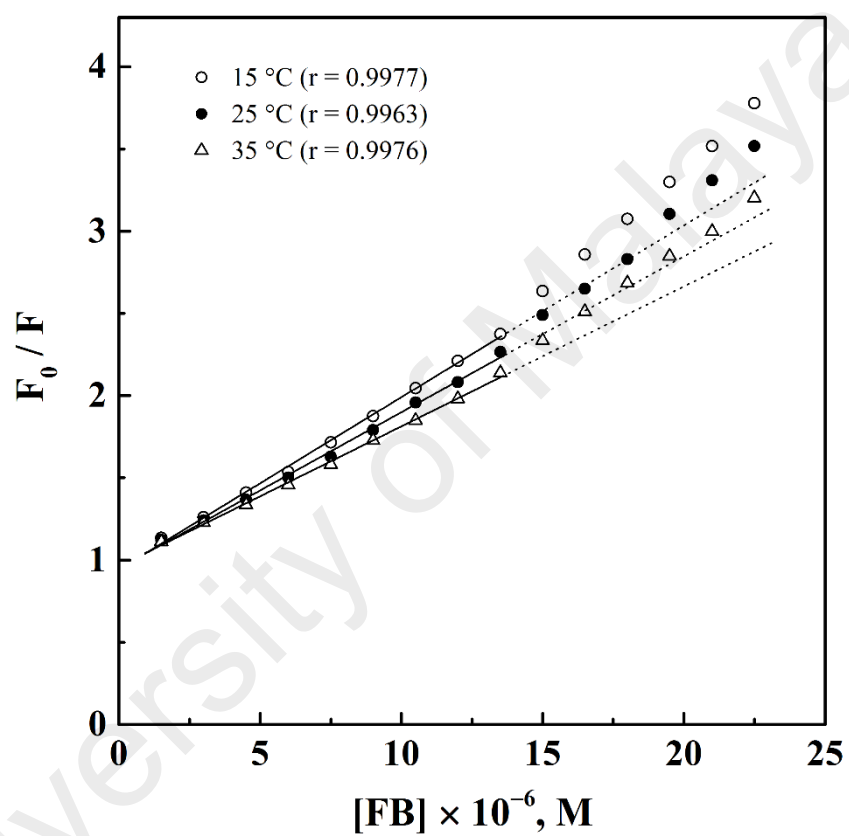


**Figure 3.2.** Stern-Volmer plots for the fluorescence quenching data of the FB-HSA system at three different temperatures, i.e., 15 °C, 25 °C and 35 °C.

**Table 3.1.** Quenching and binding parameters for the interaction of FB with HSA obtained from fluorescence quenching titration experiments at different temperatures, pH 7.4.

$T$ ( $^{\circ}\text{C}$ / $\text{K}$ )	$K_{\text{SV}}$ ( $\text{M}^{-1}$ )	$k_{\text{q}}$ ( $\text{M}^{-1} \text{s}^{-1}$ )	$K_{\text{a}}$ ( $\text{M}^{-1}$ )
15 / 288	$(1.05 \pm 0.02) \times 10^5$	$(1.65 \pm 0.04) \times 10^{13}$	$(7.52 \pm 0.14) \times 10^4$
25 / 298	$(9.52 \pm 0.34) \times 10^4$	$(1.49 \pm 0.06) \times 10^{13}$	$(6.88 \pm 0.25) \times 10^4$
35 / 308	$(8.51 \pm 0.26) \times 10^4$	$(1.33 \pm 0.04) \times 10^{13}$	$(6.24 \pm 0.19) \times 10^4$

from the table, an inverse correlation between  $K_{SV}$  and temperature was noticed. Because static quenching is characterized by the decrease in the quenching constant ( $K_{SV}$ ) with the increase in the temperature (Lakowicz, 2006), our results suggested that the quenching of HSA fluorescence by FB was due to the formation of FB–HSA complex. Furthermore, larger values of the bimolecular quenching constant,  $k_q$ , obtained for the FB–HSA system (Table 3.1) compared to the highest value reported for a diffusion-controlled process ( $\sim 10^{10} \text{ M}^{-1} \text{ s}^{-1}$ ) also opposed the involvement of collisional quenching in FB–HSA interaction (Lakowicz, 2006). Thus, overall quenching of HSA fluorescence by FB can be best described by the static quenching mechanism.

In view of the involvement of static quenching in the FB–HSA system, the fluorescence quenching titration data were also analyzed following the modified Stern-Volmer equation and the obtained plots at the three different temperatures are shown in Figure 3.3. It is important to note that all points in the modified Stern-Volmer plots had fallen on the straight line, when compared to the Stern-Volmer plots (Figure 3.2). Values of the association constant,  $K_a$ , obtained by dividing the y-intercept with the slope for each plot, are listed in Table 3.1. The  $K_a$  value was found to lie between  $6.24 \pm 0.19 \times 10^4$  and  $7.52 \pm 0.14 \times 10^4 \text{ M}^{-1}$  within the selected temperature range, which was typical for a moderate affinity binding system (Dufour & Dangles, 2005). Moderate affinity of a compound toward a protein helps in the diffusion of the compound from the circulatory system to reach its target site. Such a value of  $K_a$ , obtained for FB binding to HSA fulfills this criterion for its transport in the blood circulation and diffusion at the target site. Furthermore, the binding affinity of FB to HSA was found comparable to those generally observed for many drug–HSA complexes (Table 1.4). Interestingly, the trend of decreasing  $K_a$  value with increasing temperature was similar to that observed with the  $K_{SV}$  values. This can be explained on the basis of destabilization of the FB–HSA complex at

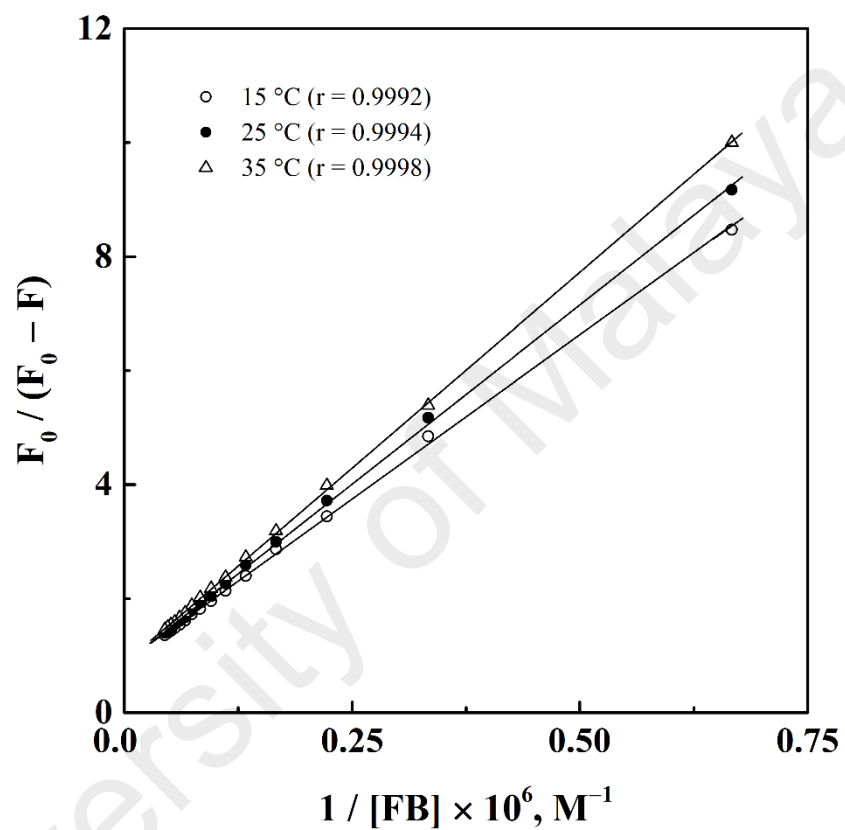


**Figure 3.3.** Modified Stern-Volmer plots for the fluorescence quenching data of the FB–HSA system at three different temperatures, i.e., 15 °C, 25 °C and 35 °C.

higher temperatures and further supported the static quenching mechanism for the FB–HSA system.

### 3.1.2. *Thermodynamic parameters and binding forces*

Quantitative evaluation of the energetics of ligand–protein interaction is crucial as it provides valuable information regarding binding forces (Sandhya et al., 2013). The interaction between a ligand and a biomacromolecule is facilitated by several intermolecular forces such as hydrogen bonds, electrostatic interactions, hydrophobic and van der Waals forces (Olsson et al., 2008; Qin et al., 2012; Trombley et al., 2011). To characterize the forces involved in the FB–HSA interaction, thermodynamic parameters ( $\Delta S$  and  $\Delta H$ ) for the binding reaction were determined from the van't Hoff plot (Figure 3.4) using  $K_a$  values obtained at different temperatures. Values of  $\Delta S$  and  $\Delta H$  as well that of  $\Delta G$ , obtained at three different temperatures using Eq. 6 are listed in Table 3.2.

The positive  $\Delta S$  ( $69.50 \text{ J mol}^{-1} \text{ K}^{-1}$ ) and negative  $\Delta H$  ( $-6.87 \text{ kJ mol}^{-1}$ ) values contributed favorably toward thermodynamic feasibility of the binding reaction with a negative sign of  $\Delta G$  values, obtained at different temperatures (Table 3.2). The favorable entropic contribution, as reflected from the positive  $\Delta S$  value, obtained for the FB–HSA interaction can be attributed to several phenomena including hydrophobic interactions and desolvation of the binding site, both of which involve the destruction of the ordered solvent layers surrounding the ligand and the protein binding site and removal of the solvent molecules from the binding pocket (Olsson et al., 2008; Ross & Subramanian, 1981; Ross & Rekharsky, 1996). Involvement of hydrophobic forces in the FB–HSA interaction seems understandable, as FB possesses benzenoid character as well as several nonpolar groups, which can interact with the protein's hydrophobic residues. Absence of any ionizable group in the FB structure coupled with a significant  $\Delta H$  value, obtained for the FB–HSA interaction excluded the involvement of electrostatic interactions in the complex formation, which are normally characterized by a very small or insignificant  $\Delta H$

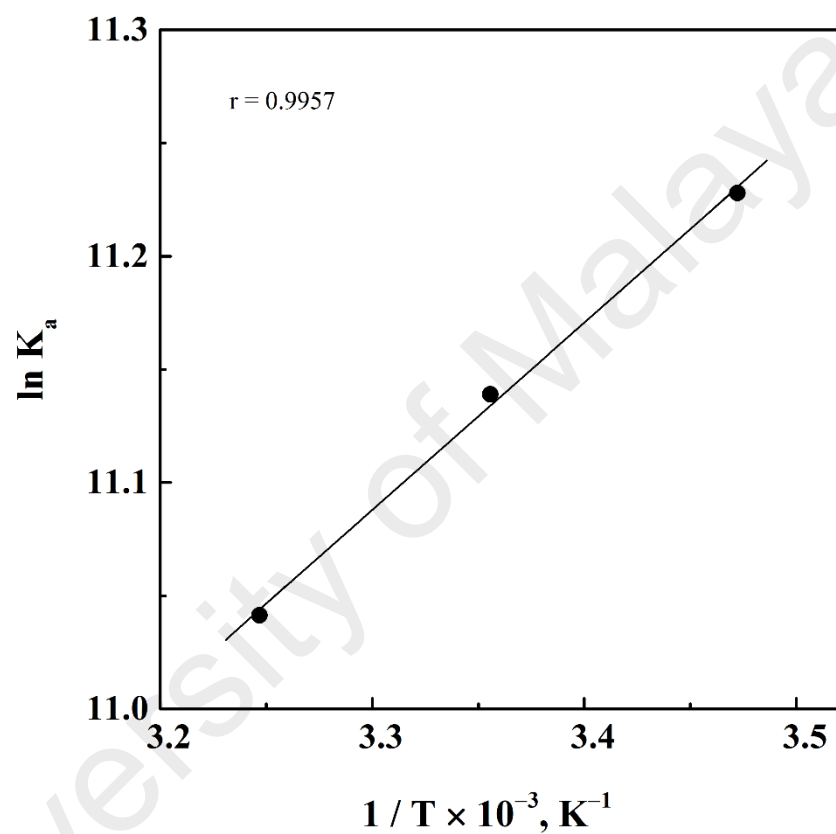


**Figure 3.4.** van't Hoff plot for the interaction between FB and HSA. Values of  $K_a$  were obtained from the modified Stern-Volmer plots shown in Figure 3.3.

**Table 3.2.** Thermodynamic parameters for the interaction of FB with HSA, obtained from fluorescence quenching titration experiments at different temperatures, pH 7.4.

$T$ (°C / K)	$\Delta S$ (J mol <sup>-1</sup> K <sup>-1</sup> )	$\Delta H$ (kJ mol <sup>-1</sup> )	$\Delta G$ (kJ mol <sup>-1</sup> )
15 / 288			-26.89
25 / 298	69.50	-6.87	-27.59
35 / 308			-28.28

value (Ross & Subramanian, 1981). Furthermore, a significantly higher  $pK_a$  value of the phenolic hydroxyl group in the FB molecule might have prevented its ionization at pH 7.4 to participate in electrostatic interactions. The negative  $\Delta H$  value on the other hand, may account for the participation of hydrogen bonding and/or van der Waals forces in the FB–HSA interaction (Ross & Subramanian, 1981). This was supported by the presence of functional groups in FB, capable of forming hydrogen bonds along with our molecular docking results, as discussed in the Section 3.1.6. Taking into consideration the possibility of several short-range interactions in the FB–HSA complexation, it would be inconceivable to assume the involvement of a single binding force in the interaction. Therefore, hydrophobic and van der Waals forces along with hydrogen bonds are believed to contribute collectively to the overall energetics of the FB–HSA interaction.

### **3.1.3. Microenvironmental alterations around HSA fluorophores**

FB-induced microenvironmental changes around protein fluorophores (Tyr and Trp) were investigated by synchronous and three-dimensional (3-D) fluorescence spectroscopy.

#### *3.1.3.1. Synchronous fluorescence spectra*

If the difference between excitation and emission wavelengths ( $\Delta\lambda$ ) is set to 15 or 60 nm, synchronous fluorescence spectra of the protein shows environmental perturbation around Tyr or Trp residues, respectively (Miller, 1979). Synchronous fluorescence spectra of HSA were recorded in the absence and the presence of increasing FB concentrations. Figures 3.5 and 3.6 show the effect of increasing concentrations of FB on the synchronous fluorescence spectra of HSA at the  $\Delta\lambda$  value of 15 and 60 nm, respectively. As can be seen from Figure 3.5, emission maximum of HSA (298 nm) remained unaltered in the presence of increasing FB concentrations, when  $\Delta\lambda$  was set at 15 nm. On the other hand, synchronous fluorescence spectra obtained with  $\Delta\lambda = 60$  nm (Figure 3.6) showed a blue shift in the emission maximum from 338 to 336 nm upon FB

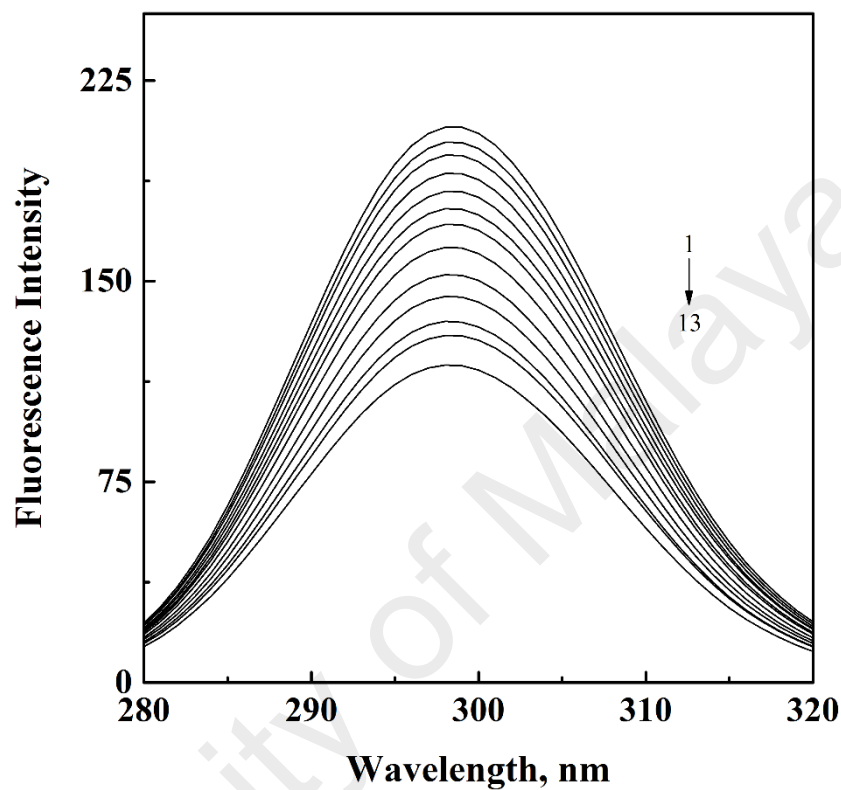


**Figure 3.5.** Synchronous fluorescence spectra of HSA in the absence and the presence of increasing FB concentrations at 25 °C, obtained in 10 mM Tris-HCl buffer, pH 7.4. The concentration of HSA was kept constant at 3  $\mu$ M, while FB concentration was varied (from top to bottom, 1 $\rightarrow$ 13) as 0, 0.6, 1.2, 1.8, 2.4, 3.0, 4.2, 5.4, 6.6, 7.8, 9.0, 10.5 and 12.0  $\mu$ M, respectively. The difference between excitation and emission wavelengths ( $\Delta\lambda$ ) was fixed at 15 nm.

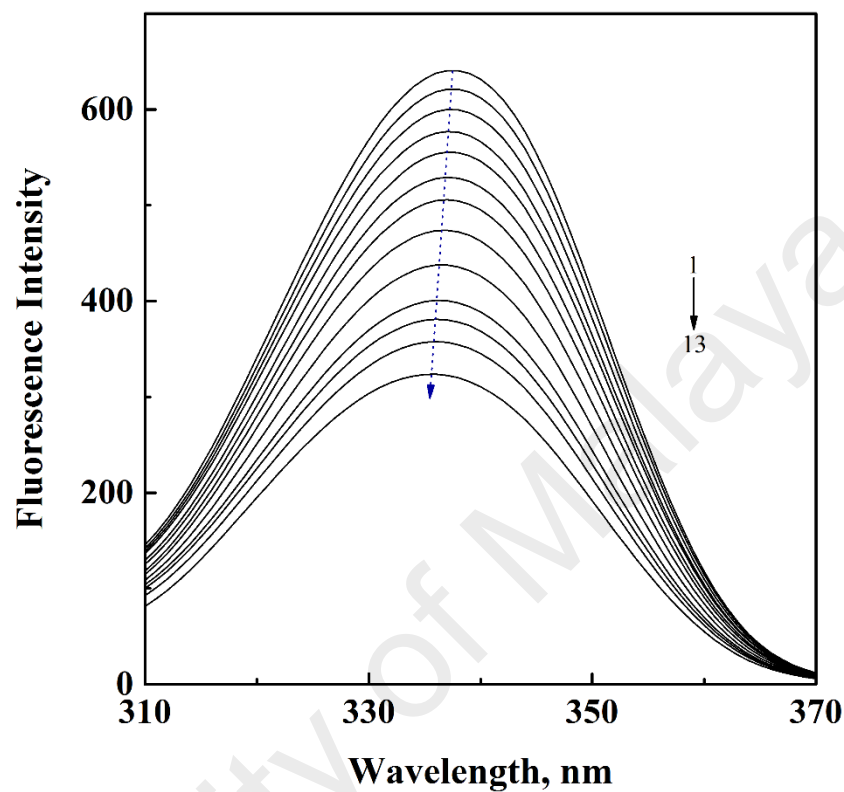


**Figure 3.6.** Synchronous fluorescence spectra of HSA in the absence and the presence of increasing FB concentrations at 25 °C, obtained in 10 mM Tris-HCl buffer, pH 7.4. The concentration of HSA was kept constant at 3  $\mu\text{M}$ , while FB concentration was varied (from top to bottom, 1 $\rightarrow$ 13) as 0, 0.6, 1.2, 1.8, 2.4, 3.0, 4.2, 5.4, 6.6, 7.8, 9.0, 10.5 and 12.0  $\mu\text{M}$ , respectively. The difference between excitation and emission wavelengths ( $\Delta\lambda$ ) was fixed at 60 nm. The arrow depicts the blue shift in the emission maximum of HSA with increasing FB concentrations.

addition. These results suggested that the binding of FB to HSA had little effect on the microenvironment around Tyr residues, but was sufficient to perturb the environment in the vicinity of the lone Trp residue (Trp-214), located in the subdomain IIA, in making it slightly more nonpolar. It is worth noting that while the blue shift shown in Figure 3.6 was in agreement with the intrinsic fluorescence results described above (Figure 3.1), difference in the extent of the shift in the emission maximum was noticed. Such variation in the magnitude of the shift in the emission maximum obtained from intrinsic and synchronous fluorescence measurements is not uncommon and has also been shown in several earlier reports (Khan et al., 2008; Paramaguru et al., 2010; Wang et al., 2008).

#### 3.1.3.2. Three-dimensional fluorescence spectra

Three-dimensional fluorescence spectroscopy was performed on HSA both in free form and in the presence of FB. Figures 3.7–3.9 show the 3-D fluorescence spectra and the corresponding contour maps of native HSA (Figure 3.7) and HSA in the presence of FB with FB/HSA molar ratios of 2:1 (Figure 3.8) and 4:1 (Figure 3.9). The 3-D fluorescence spectral characteristics in terms of peak position ( $\lambda_{\text{ex}}/\lambda_{\text{em}}$ ) and intensity are listed in Table 3.3.

Peaks labelled as ‘a’ and ‘b’ in Figure 3.7 referred to the Rayleigh and the second-order scattering peaks, respectively (Lakowicz, 2006), and were common in all spectra. It is important to note that both these scattering peaks were also present in the 3-D fluorescence spectra of the buffer (spectra not shown). The peaks designated as ‘1’ ( $\lambda_{\text{ex}} = 280 \text{ nm}$ ,  $\lambda_{\text{em}} = 337 \text{ nm}$ ) and ‘2’ ( $\lambda_{\text{ex}} = 230 \text{ nm}$ ,  $\lambda_{\text{em}} = 332 \text{ nm}$ ) represented protein fluorescence peaks due to the presence of Trp and Tyr residues and reflected the three-dimensional conformation of the protein. As evident from Figure 3.8, addition of FB to HSA in a 2:1 molar ratio produced a significant decrease in the fluorescence intensity along with a blue shift in the emission maximum, being 36%, 1 nm for peak ‘1’ and 33%, 6 nm for peak ‘2’ (Table 3.3). Increasing the molar ratio of FB/HSA to 4:1 further

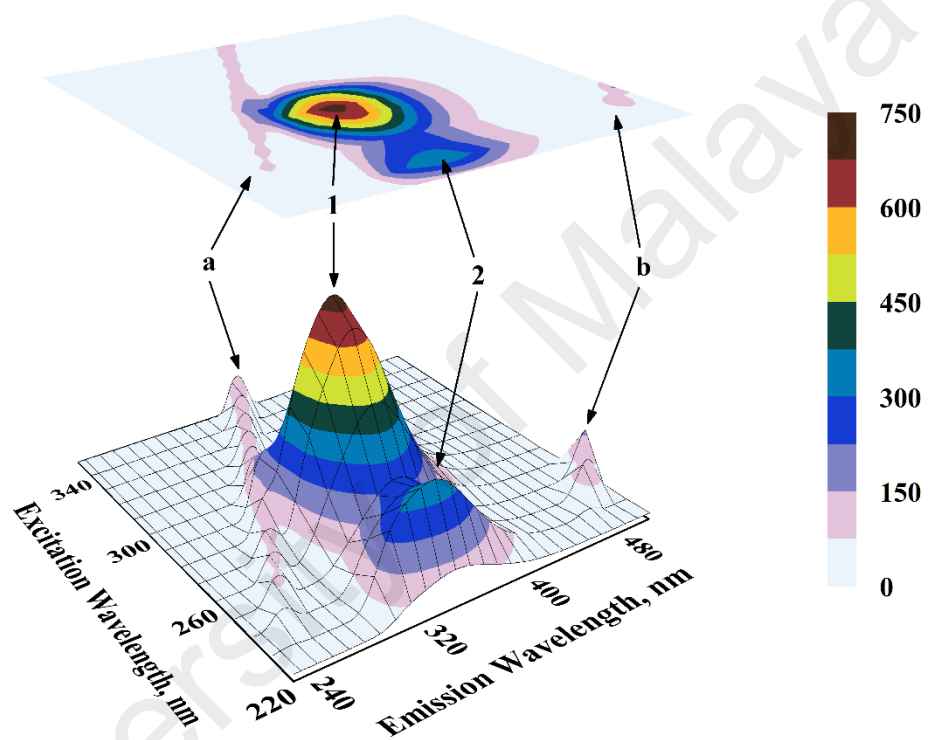


**Figure 3.7.** Three-dimensional fluorescence spectra and corresponding contour map of HSA (3  $\mu$ M), obtained in 10 mM Tris-HCl buffer, pH 7.4 at 25  $^{\circ}$ C.

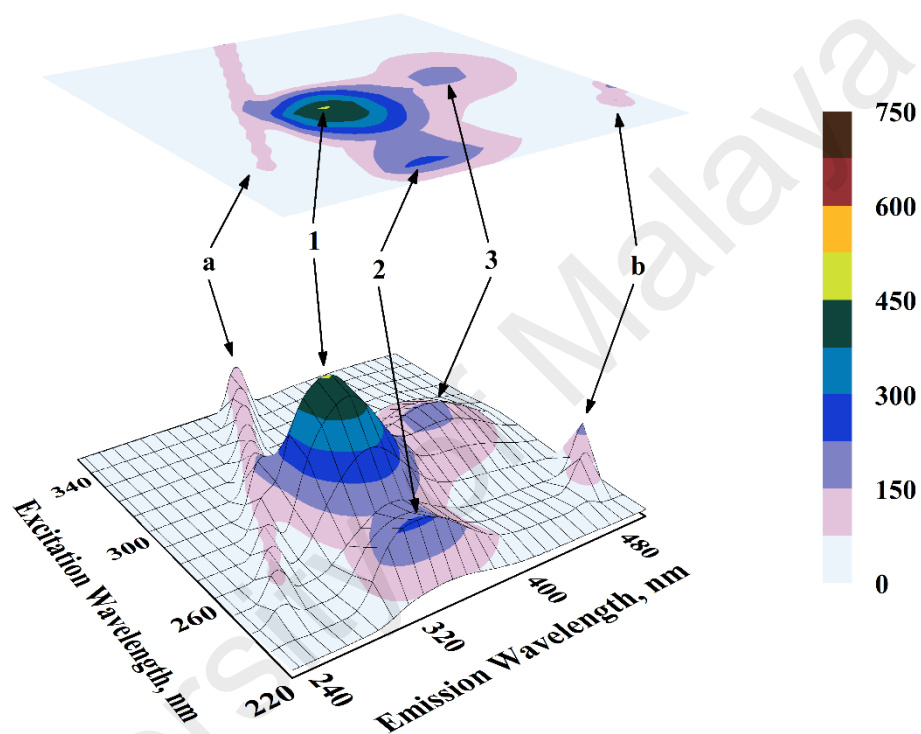


**Figure 3.8.** Three-dimensional fluorescence spectra and corresponding contour map of FB–HSA (2:1) complex, obtained in 10 mM Tris-HCl buffer, pH 7.4 at 25 °C, using HSA concentration of 3  $\mu$ M.

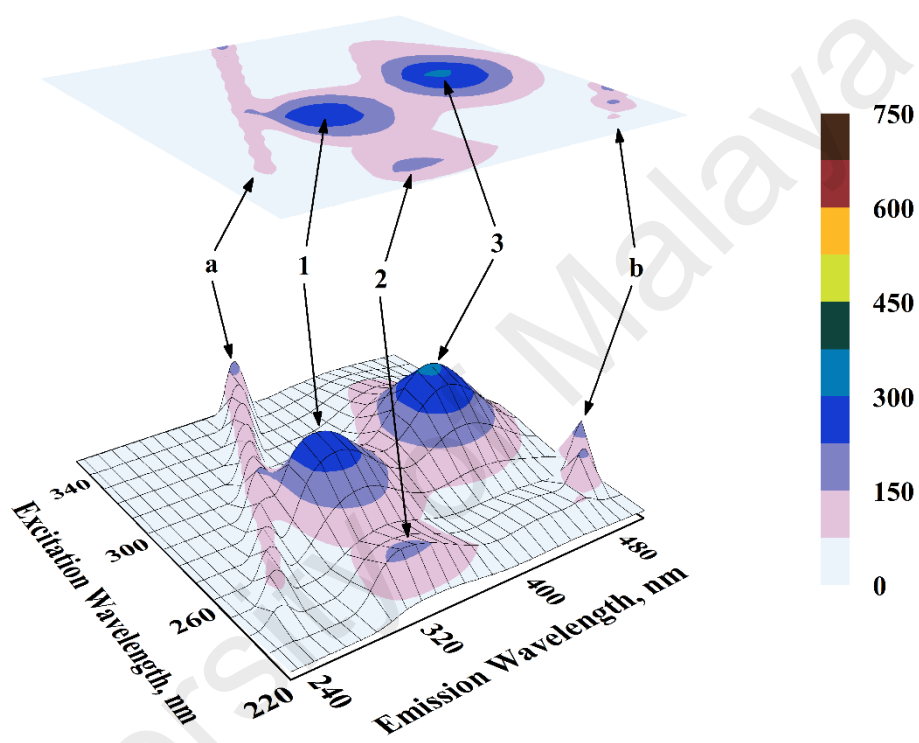


**Figure 3.9.** Three-dimensional fluorescence spectra and corresponding contour map of FB-HSA (4:1) complex, obtained in 10 mM Tris-HCl buffer, pH 7.4 at 25 °C, using HSA concentration of 3  $\mu$ M.

**Table 3.3.** Three-dimensional fluorescence spectral characteristics of HSA and FB–HSA complexes at pH 7.4, 25 °C.

System	Peak	Peak position [ $\lambda_{\text{ex}}/\lambda_{\text{em}}$ (nm/nm)]	Intensity
HSA	a	230/230 → 350/350	23.03 → 128.02
	b	250/500	165.38
	1	280/337	708.34
	2	230/332	359.12
[FB]:[HSA] = 2:1	a	230/230 → 350/350	24.06 → 153.48
	b	250/500	180.46
	1	280/336	453.91
	2	230/326	240.51
	3	290/428	169.92
[FB]:[HSA] = 4:1	a	230/230 → 350/350	24.79 → 181.44
	b	250/500	196.02
	1	280/335	280.52
	2	230/321	172.52
	3	290/432	315.32

aggravated these changes to 60%, 2 nm and 52%, 11 nm for peaks '1' and '2', respectively (Figure 3.9 and Table 3.3). The emergence of peak '3' ( $\lambda_{\text{ex}} = 290 \text{ nm}$ ,  $\lambda_{\text{em}} = 428/432 \text{ nm}$ ) in the 3-D fluorescence spectra of the FB–HSA systems represented the fluorescence characteristics due to FB. Similar changes in the 3-D fluorescence characteristics of HSA upon ligand binding have been reported earlier (Abdollahpour et al., 2011; Ding et al., 2010; Freitas et al., 2012; Li & Li, 2011, Shanmugaraj et al., 2014). Such changes in the fluorescence characteristics (fluorescence quenching and blue shift in the emission maximum) of HSA, observed in the presence of FB were suggestive of perturbation in the microenvironment around protein fluorophores, induced by FB binding.

#### **3.1.4. FB-induced thermal stabilization of HSA**

Any change in the thermal stability of a protein in the presence of a ligand points towards complexation between the ligand and the protein. In many instances, increased thermal stability of proteins has been observed in the presence of ligands (Celej et al., 2006; Gonzalez et al., 1999; Layton and Hellinga, 2010). This phenomenon results due to perturbation of the equilibrium between the native and the denatured protein species during thermal unfolding, which is coupled to the ligand binding equilibrium (Brandts & Lin, 1990; Shrake & Ross, 1990). Thus, ligand–protein interaction can also be verified by measuring thermal stability of a protein in the absence and the presence of its ligand.

The protein stability against heat denaturation in the absence and the presence of FB was examined using CD spectroscopy by recording the ellipticity value at 222 nm ( $\text{CD}_{222 \text{ nm}}$ ), a characteristic signal of the  $\alpha$ -helical structure in proteins (Kelly et al., 2005). Since HSA has a high (67%)  $\alpha$ -helical content (Peters, 1996), a decrease in the  $\text{CD}_{222 \text{ nm}}$  value upon heat treatment can be used to probe the thermal stability of the protein. Figure 3.10 shows thermal denaturation/renaturation profiles of HSA in the absence and the presence of FB (4:1 molar ratio) in the temperature range, 25–100 °C. The denaturation profile of free HSA suggested that the protein's  $\alpha$ -helical structure remained stable up to

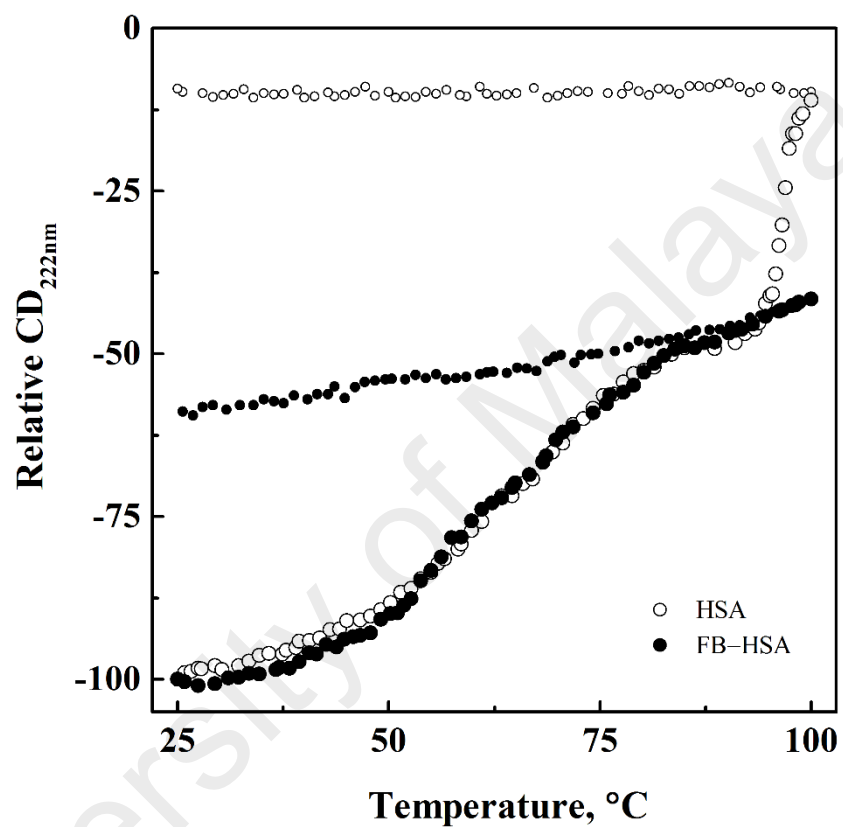


**Figure 3.10.** Thermal denaturation and renaturation curves of HSA (3  $\mu$ M) and FB-HSA (4:1) complex, as studied by  $CD_{222\text{ nm}}$  measurements in the temperature range, 25–100 °C in 10 mM Tris-HCl buffer, pH 7.4. Renaturation curves are shown with smaller symbols.

40 °C and showed significant disruption within the temperature range, 45–85 °C, indicating protein denaturation. The sharp decrease in the  $CD_{222\text{ nm}}$  value beyond 94 °C can be attributed to the irreversible unfolding of HSA leading to aggregation, which was in accordance with earlier reports (Heller, 2013; Mitra et al., 2007; Pico, 1997). This was reflected from the renaturation experiment, which showed no change in the  $CD_{222\text{ nm}}$  value, but the appearance of visible precipitates in the cuvette. The aggregation of unfolded protein at higher temperature can be ascribed to intermolecular hydrophobic interactions involving exposed hydrophobic patches in the unfolded protein molecules (Chi et al., 2003; Vermeer & Norde, 2000). Presence of FB in the incubation mixture significantly affected the thermal stability of HSA within the temperature range studied. This was evident from the gradual decrease in  $CD_{222\text{ nm}}$  at temperatures  $> 94\text{ °C}$  against the sharp decrease observed in its absence, as well as from the renaturation results, where a significant recovery (33%) in the  $CD_{222\text{ nm}}$  value was observed. Furthermore, no sign of precipitation was observed in the renaturation experiments in the presence of FB. Therefore, it is clear that the interaction between FB and HSA stabilized the protein structure against thermal denaturation by reducing the loss in the helicity and offering protection against protein aggregation.

The thermal denaturation/renaturation of HSA in the absence and the presence of FB were also studied within the temperature range, 25–80 °C and the results are shown in Figure 3.11. Although thermal denaturation curves of HSA and the FB–HSA complex showed a similar pattern, a significant difference was observed in the reversibility experiments. Whereas both solutions remained clear upon cooling, the FB–HSA complex exhibited a higher extent of recovery in terms of  $CD_{222\text{ nm}}$  value (51%) compared to HSA alone (40%). These results further suggested the stabilizing effect of bound FB on HSA against heat treatment. This was in accordance with previous reports suggesting higher

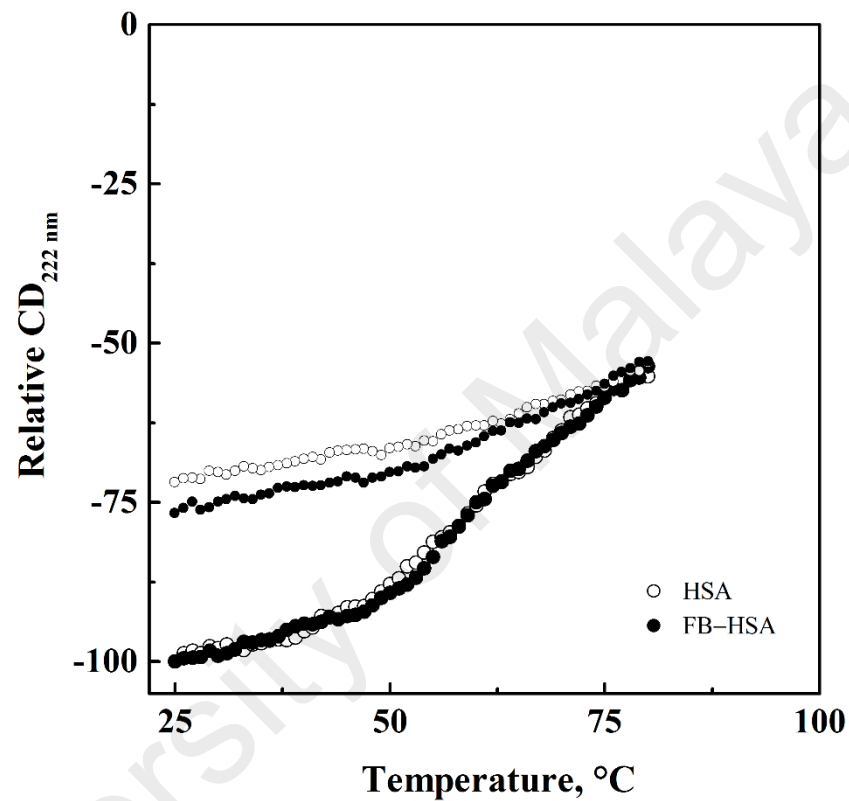


**Figure 3.11.** Thermal denaturation and renaturation curves of HSA (3  $\mu\text{M}$ ) and FB-HSA (4:1) complex, as studied by  $\text{CD}_{222 \text{ nm}}$  measurements in the temperature range, 25–80 °C in 10 mM Tris-HCl buffer, pH 7.4. Renaturation curves are shown with smaller symbols.

thermal stability of HSA upon ligand binding (Anraku et al., 2004; Lohner et al., 1994; Lupidi et al., 2010).

### **3.1.5. Binding site specificity of FB on HSA**

Several physiological ligands as well as a large number of drugs are known to bind to HSA with high affinity at one of two distinct binding sites namely, Sudlow's site I, located in subdomain IIA and Sudlow's site II, present in subdomain IIIA (Kragh-Hansen et al., 2002; Peters, 1996; Sudlow et al., 1975, 1976). Due to their higher affinities, a few drugs/ligands are often used as marker ligands for these sites. In view of this, displacement experiments were carried out using reporter ligands, bilirubin (BR) and warfarin (WFN) for site I and diazepam (DZP) for site II of HSA to establish the binding site of FB on HSA (Kragh-Hansen et al., 2002).

Figure 3.12 shows the displacing action of FB on the BR–HSA (1:1) complex as studied by CD spectroscopy. BR upon binding to HSA acquired chirality and resulted in a Cotton effect, marked by a bisignate CD spectra in the wavelength range, 350–500 nm, with a negative peak at lower wavelength (407 nm) and a positive peak at higher wavelength (458 nm) (Trynda-Lemiesz, 2004). It is important to note that free BR, HSA or FB solutions did not produce any CD spectral signal within this range, as represented by the spectra marked as 'a', 'b' and 'c', respectively in the Figure 3.12. Addition of increasing concentrations (15–75  $\mu\text{M}$ ) of FB to BR–HSA complex led to a significant reduction in the CD spectral characteristics, suggesting displacement of BR from its binding site on HSA. The CD spectral signal at 458 nm, obtained with the BR–HSA complex decreased continuously with increasing FB concentrations, showing 40% reduction at an FB/HSA molar ratio of 7.5:1 (Figure 3.14A). Thus, the binding site of FB on HSA seemed to be located in the close vicinity of the BR binding site, i.e., Sudlow's site I.

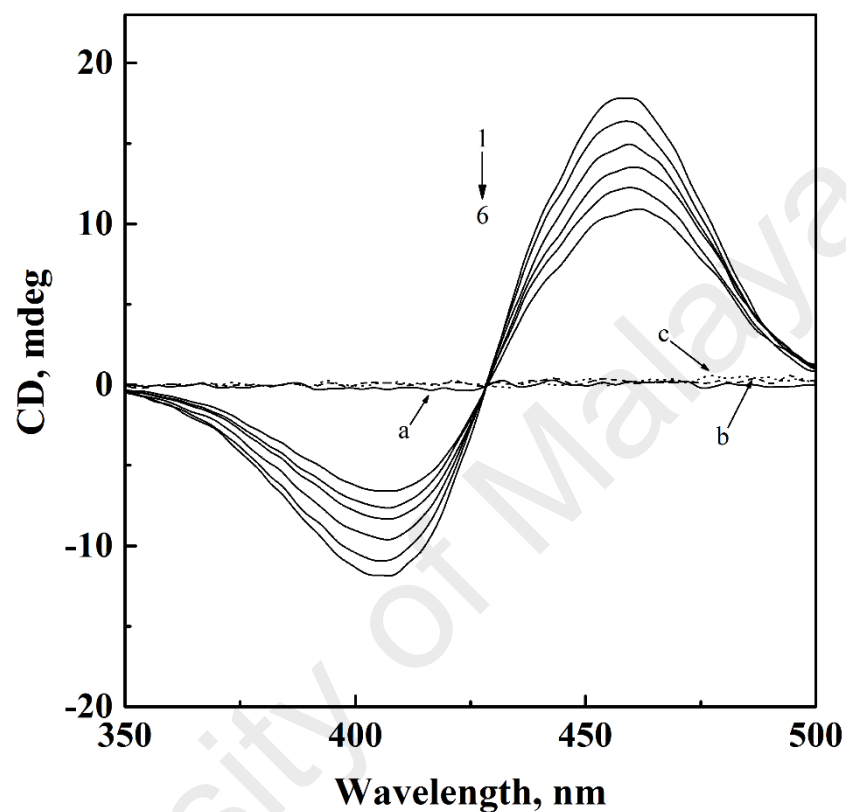


**Figure 3.12.** Displacing effect of FB on the visible CD spectrum of BR-HSA (1:1) complex at 25 °C. The concentrations of BR and HSA were 10  $\mu\text{M}$  each while the concentration of FB was varied (from top to bottom, 1 $\rightarrow$ 6) in the range, 0–75  $\mu\text{M}$  at regular increments of 15  $\mu\text{M}$ . CD spectra marked as ‘a’, ‘b’ and ‘c’ refer to 10  $\mu\text{M}$  BR, 10  $\mu\text{M}$  HSA and 75  $\mu\text{M}$  FB, respectively.

To strengthen the above finding, displacement experiments were also performed with the WFN–HSA complex using fluorescence spectroscopy. The WFN–HSA (1:1) complex produced a fluorescence spectrum in the wavelength range, 360–480 nm with an emission maximum at 383 nm, when excited at 335 nm (Figure 3.13) (Trynda-Lemiesz, 2004). Addition of increasing FB concentrations (3–24  $\mu\text{M}$ ) to the WFN–HSA complex produced a progressive decrease in the fluorescence intensity, which was indicative of WFN displacement by FB. About 35% decrease in the fluorescence intensity was observed at an FB/HSA molar ratio of 8:1 (Figure 3.14B). FB, a fluorescent compound, also produced a fluorescence spectrum in the same wavelength range, when excited at 335 nm. However, the emission maximum was found to appear at 433 nm, far from the 383 nm signal (emission maximum) of the WFN–HSA complex. Furthermore, free WFN and HSA produced weak or significant signals in the wavelength range studied. Taken together, displacement of BR as well as WFN in the presence of FB suggested the binding of FB to Sudlow's site I of HSA.

In order to assess the involvement of site II in the interaction between FB and HSA, competitive displacement experiments were also performed using DZP as the marker ligand. Figure 3.15 shows the effect of increasing DZP concentrations (0.6–6.0  $\mu\text{M}$ ) on the fluorescence spectra of HSA (A) and FB–HSA (3:1) complex (B). Titration of HSA alone as well as its complex with FB (FB–HSA) with DZP produced a similar decrease in the fluorescence intensity at 337 nm in both samples, reaching to ~20% quenching at 6  $\mu\text{M}$  DZP (Figure 3.16). These observations suggested that the presence of FB in the incubation mixture did not alter the quenching of HSA induced by DZP, hence alluding to the noninvolvement of Sudlow's site II in FB–HSA interaction.

### **3.1.6. Molecular docking**

A molecular docking study was conducted to predict the binding site of FB in HSA and to confirm the results of the displacement experiments described above. The ligand

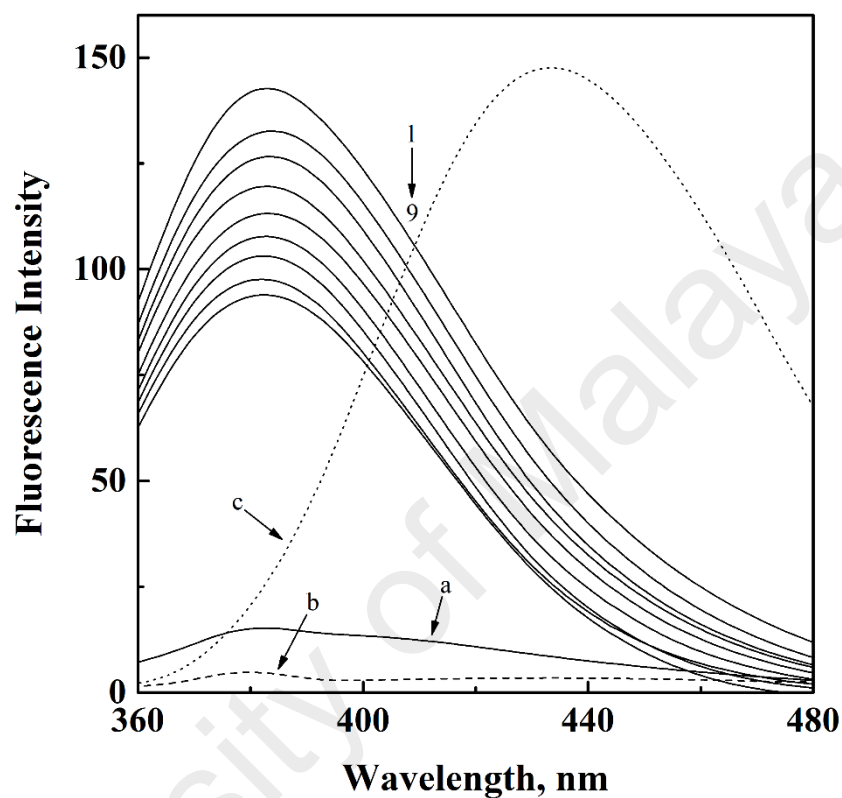


**Figure 3.13.** Displacing effect of FB on the fluorescence spectrum of WFN–HSA (1:1) complex at 25 °C. The concentrations of WFN and HSA were 3  $\mu\text{M}$  each while the concentration of FB was varied (from top to bottom, 1 $\rightarrow$ 9) in the range, 0–24  $\mu\text{M}$  at regular increments of 3  $\mu\text{M}$ . Emission spectra marked as ‘a’, ‘b’ and ‘c’ refer to 3  $\mu\text{M}$  WFN, 3  $\mu\text{M}$  HSA and 24  $\mu\text{M}$  FB, respectively. The excitation wavelength was 335 nm.

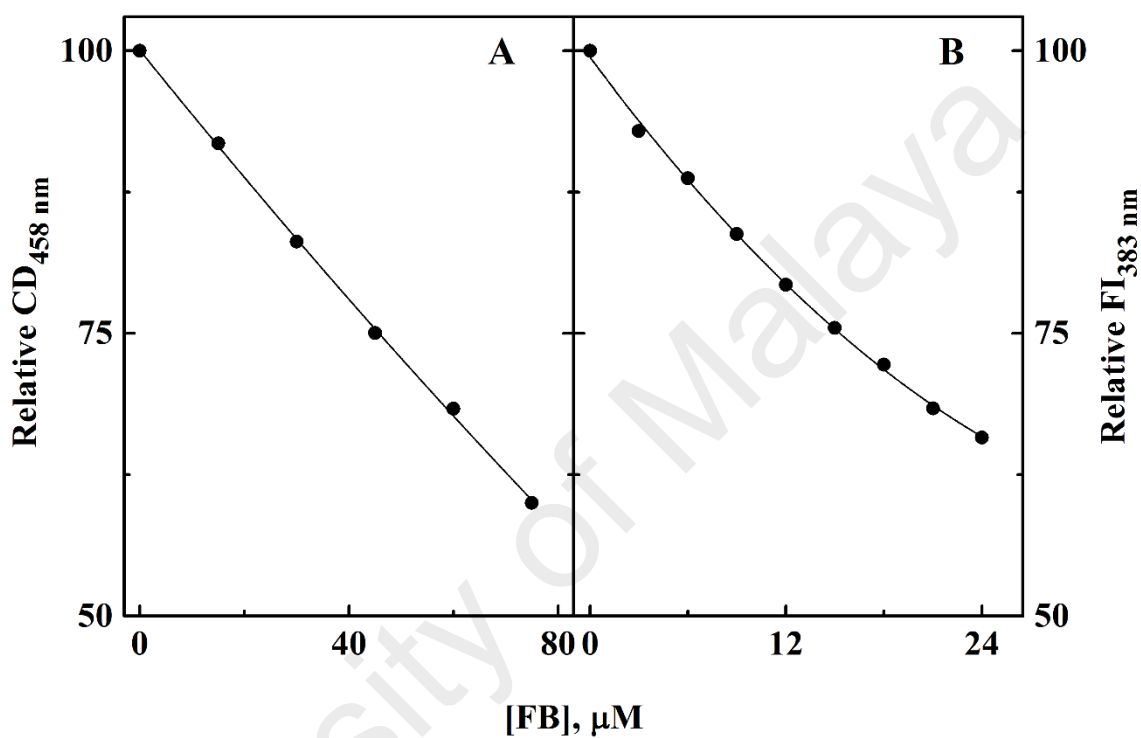


**Figure 3.14.** Plots showing the decrease in the relative CD value at 458 nm ( $CD_{458\text{ nm}}$ ) of BR-HSA complex (A) and the relative fluorescence intensity at 383 nm ( $FI_{383\text{ nm}}$ ) of WFN-HSA complex (B) with increasing FB concentrations. Values of the relative  $CD_{458\text{ nm}}$  and the relative  $FI_{383\text{ nm}}$  were obtained from the spectra shown in Figures 3.12 and 3.13, respectively.

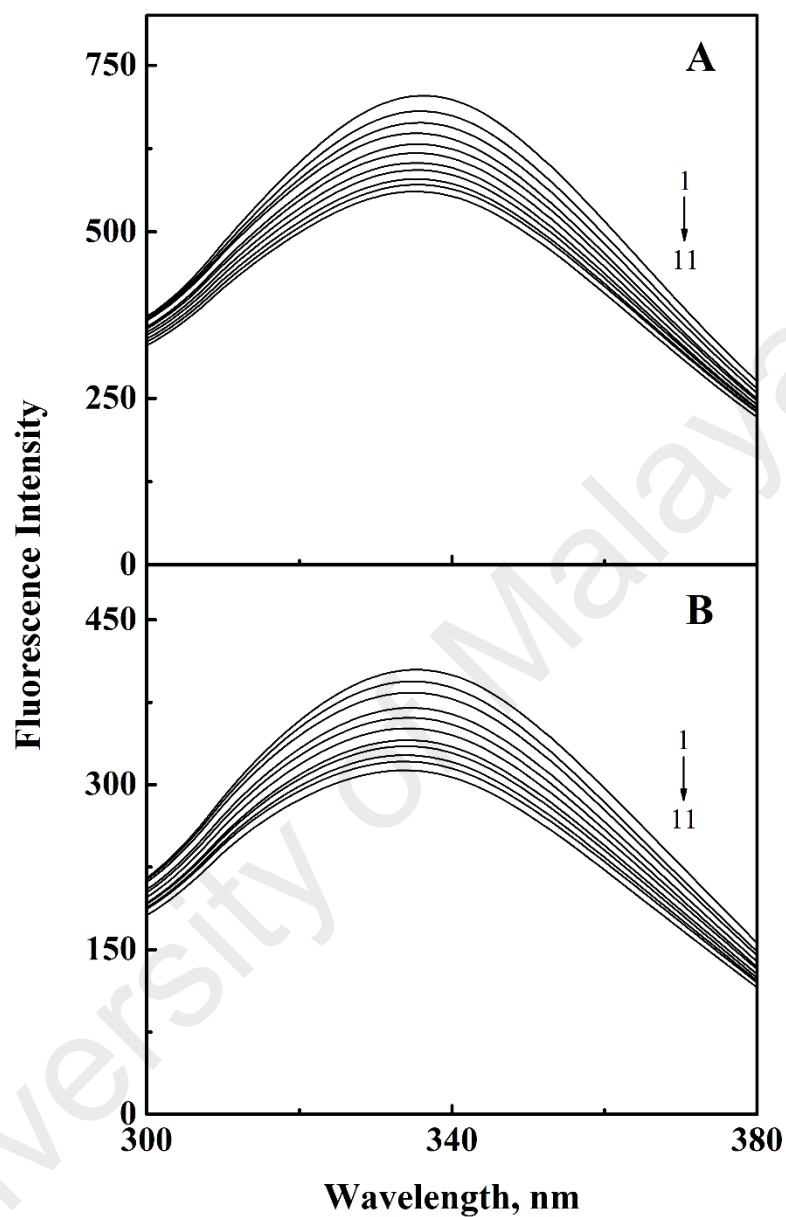


**Figure 3.15.** Fluorescence spectra of (A) HSA (3  $\mu$ M) and (B) FB-HSA (3:1) complex in the absence and the presence of increasing DZP concentrations, obtained in 10 mM Tris-HCl buffer, pH 7.4 at 25  $^{\circ}$ C upon excitation at 280 nm. The DZP concentration was varied (from top to bottom, 1 $\rightarrow$ 11) in the range, 0–6  $\mu$ M at regular increments of 0.6  $\mu$ M.

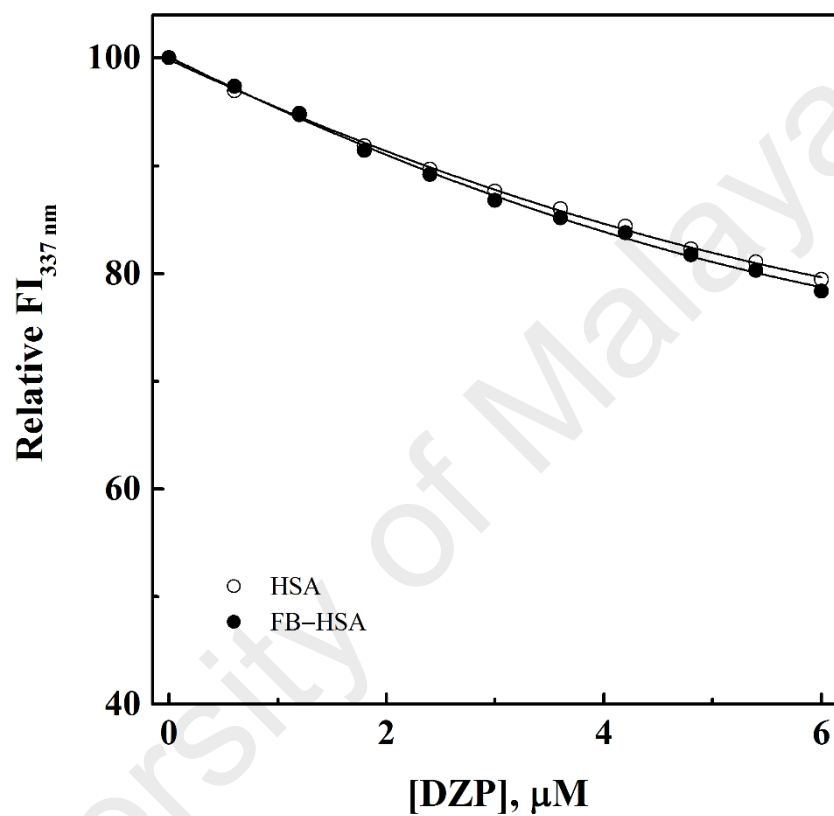


**Figure 3.16.** Plots showing the decrease in the relative fluorescence intensity at 337 nm ( $\text{FI}_{337 \text{ nm}}$ ) of HSA ( $3 \mu\text{M}$ ) and FB-HSA complex (3:1) with increasing DZP concentrations. Values of the relative  $\text{FI}_{337 \text{ nm}}$  were obtained from the spectra shown in Figure 3.15.

was constructed, geometrically optimized and docked to a high resolution X-ray crystal structure of HSA (PDB code: 1BM0). The binding mode of FB was predicted for the two main drug binding sites, Sudlow's sites I and II.

A total of 9 multimember conformational clusters were obtained from 100 docking runs for site I. The highest populated cluster contained more than half of the analyzed conformations (53 out of 100 conformations) and was found to be the lowest on the energy scale. Hence, it was the most energetically favorable cluster, possessing an estimated docking energy of about  $-31.8 \text{ kJ mol}^{-1}$  (Figure 3.17A). Whereas for the binding site II, using the same approach, about 26 distinct conformational clusters were obtained. However, the most populated cluster (14 out of 100 conformations) was not the most energetically favorable ( $-17.6 \text{ kJ mol}^{-1}$ ) cluster (Figure 3.17B). Accordingly, FB showed a binding preference for the drug binding site I (subdomain IIA) of HSA. The results of these docking studies were in good agreement with the displacement experiments discussed above.

The predicted binding model with the lowest docking energy ( $-31.8 \text{ kJ mol}^{-1}$ ) was then used for binding orientation analysis (Figure 3.18). The binding site (defined as amino acid residues within a  $5 \text{ \AA}$  distance to FB) was found to be deep inside the protein structure and was mostly located in a hydrophobic cleft lined by the following amino acid residues: Tyr-150, Glu-153, Ser-192, Lys-195, Gln-196, Lys-199, Leu-219, Leu-238, Arg-222, Val-241, His-242, Arg-257, Leu-260, Ala-261, Ile-264, Ser-287, His-288, Ile-290, Ala-291 and Glu-292. The interaction between FB and HSA cannot be presumed to be exclusively hydrophobic in nature, as there were several ionic as well as polar residues in the proximity of the bound ligand. Five hydrogen bonds were predicted from the conformation. These hydrogen bonds between the amino acid residues of HSA to the oxygen atom of the hydroxyl, carbonyl and methoxy group of FB are summarized in Table 3.4. The benzene rings of the ligand seemed to be buried inside the hydrophobic

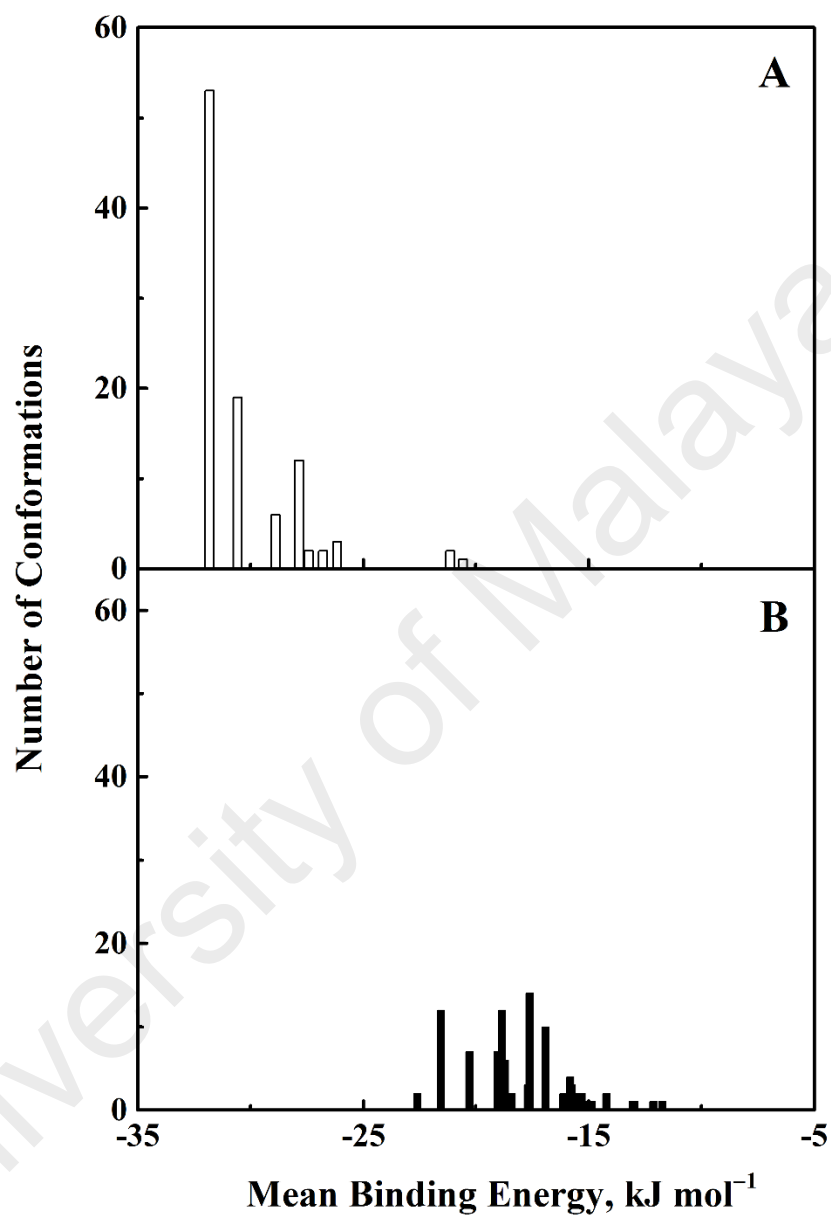


**Figure 3.17.** Cluster analysis of the docking of FB to Sudlow's sites I (A) and II (B) of HSA crystal structure (1BM0). A total of 100 runs were performed for each binding site.

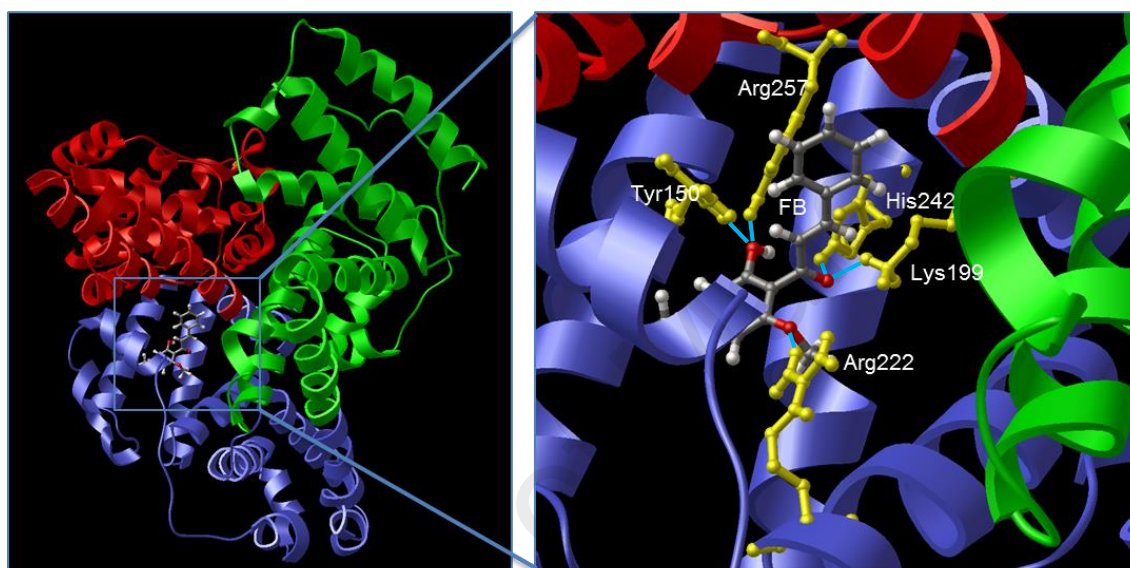


**Figure 3.18.** Binding orientation of the lowest docking energy conformation of FB (ball and stick rendered) in Sudlow's site I (subdomain IIA) of HSA (1BM0). Domains I, II and III of HSA are represented in red, blue and green, respectively. The zoomed-in view of the binding site shows the hydrogen bonds (turquoise lines) formed between FB and amino acid side chains of HSA (yellow).

**Table 3.4.** Distance of the predicted hydrogen bonds formed between interacting atoms of the amino acid residues of HSA (site I) and FB.

HSA atom	FB atom	Distance (Å)
Tyr-150: HH	O (hydroxyl)	1.76
Lys-199: HZ3	O (carbonyl)	1.93
Arg-222: HH11	O (methoxy)	2.24
His-242: HE2	O (carbonyl)	2.10
Arg-257: HE	O (hydroxyl)	1.82

cleft and stabilized the docking conformation through hydrophobic interactions with other hydrophobic residues of the protein clustered within the binding site.

In conclusion, the interaction of FB with HSA was found to be comparable to many other flavonoids in terms of binding affinity, when investigated by fluorescence spectroscopy. The binding reaction mainly involved hydrophobic and van der Waals interactions as well as hydrogen bonding, as revealed by thermodynamic parameters and docking results. Binding of FB to HSA also led to microenvironmental changes around protein fluorophores, as analyzed by intrinsic, synchronous and 3-D fluorescence. Sudlow's site I of HSA, located in domain IIA, was assigned to be the most probable binding site for FB on HSA, as suggested by competitive ligand displacement experiments as well as molecular docking studies.

University of Malaya

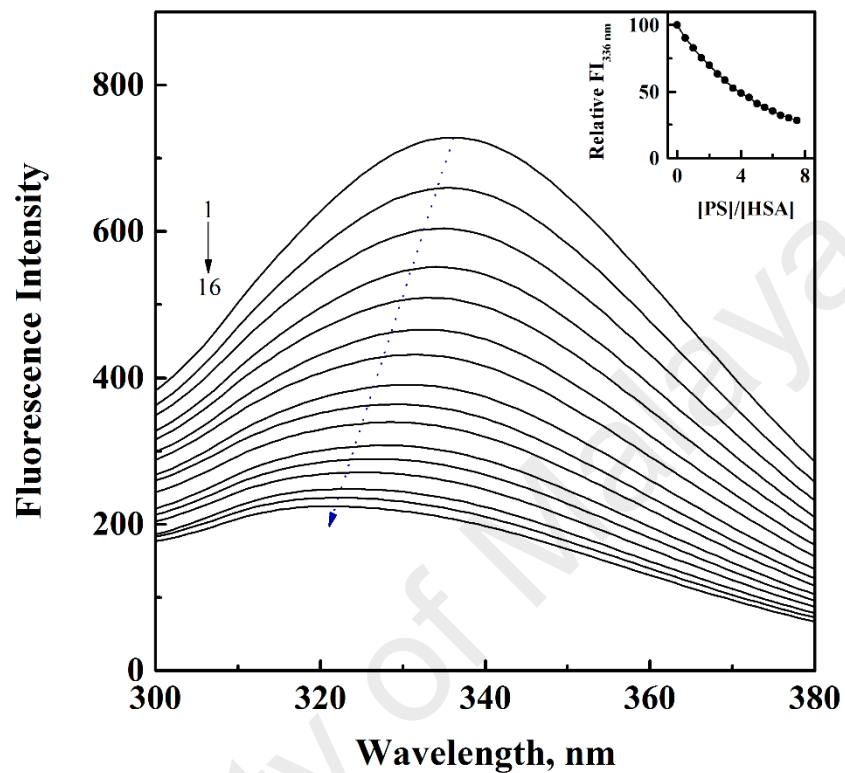
### 3.2. Pinostrobin–human serum albumin interaction

Similar to FB–HSA binding studies described in the Section 3.1, the interaction of another bioactive flavonoid (flavanone) from *Boesenbergia rotunda*, pinostrobin (PS) with HSA was also studied using fluorescence spectroscopy.

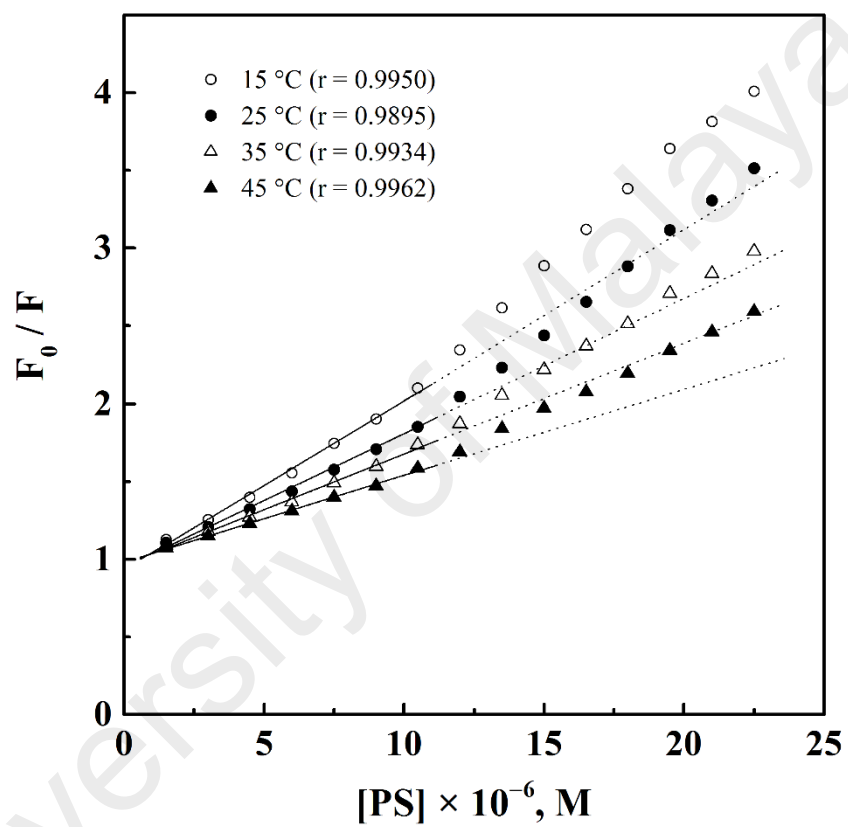
#### 3.2.1. Quenching of HSA fluorescence and binding characteristics

Figure 3.19 shows the intrinsic fluorescence spectra of HSA in the wavelength range, 300–380 nm upon excitation at 280 nm, obtained in the absence and the presence of PS at 25 °C. Addition of increasing PS concentrations (0–22.5 µM) to HSA solution produced a progressive decrease in the fluorescence intensity and a significant blue shift in the emission maximum. About 72% decrease in the fluorescence intensity at the emission maximum, 336 nm (inset of Figure 3.19) and 14 nm blue shift were observed at the highest PS concentration (22.5 µM) used in this study. Apart from the difference in the magnitude of the blue shift in the emission maximum, quenching of HSA fluorescence was found similar to that observed with FB (Figure 3.1). The fluorescence characteristics exhibited by HSA upon addition of PS were highly suggestive of the conformational change in the protein, representing transfer of the fluorophores to a more hydrophobic environment, thus indicating the interaction of PS to HSA.

In order to validate the mode of quenching, titration experiments of HSA with PS were performed at four different temperatures, i.e., 15, 25, 35 and 45 °C and the data were analyzed according to Eq. 2. The Stern-Volmer plots (Figure 3.20), obtained at these temperatures showed linearity in the initial PS concentration zone and produced an upward curvature at higher PS concentrations. Therefore, only the linear zones of the Stern-Volmer plots were selected for regression analysis in order to determine the values of the Stern-Volmer constant,  $K_{SV}$ , which are listed in Table 3.5. A progressive decrease in the  $K_{SV}$  value with increasing temperature clearly suggested that the static quenching mechanism, involving the formation of a non-covalent PS–HSA binary complex was



**Figure 3.19.** Fluorescence spectra of HSA in the absence and the presence of increasing PS concentrations, obtained in 10 mM Tris-HCl buffer, pH 7.4 at 25 °C upon excitation at 280 nm. The concentration of HSA was fixed at 3  $\mu\text{M}$ , while PS concentration was varied (from top to bottom, 1 $\rightarrow$ 16) in the range, 0–22.5  $\mu\text{M}$  at regular increments of 1.5  $\mu\text{M}$ . The arrow depicts the blue shift in the emission maximum of HSA with increasing PS concentrations. Inset shows the decrease in the relative fluorescence intensity at 336 nm ( $\text{FI}_{336 \text{ nm}}$ ) with increasing PS/HSA molar ratios.



**Figure 3.20.** Stern-Volmer plots for the fluorescence quenching data of the PS-HSA system at four different temperatures, i.e., 15 °C, 25 °C, 35 °C and 45 °C.

**Table 3.5.** Quenching and binding parameters for the interaction of PS with HSA obtained from fluorescence quenching titration experiments at different temperatures, pH 7.4.

$T$ (°C / K)	$K_{sv}$ (M <sup>-1</sup> )	$k_q$ (M <sup>-1</sup> s <sup>-1</sup> )	$K_a$ (M <sup>-1</sup> )
15 / 288	$(1.09 \pm 0.03) \times 10^5$	$(1.71 \pm 0.05) \times 10^{13}$	$(1.28 \pm 0.04) \times 10^5$
25 / 298	$(8.60 \pm 0.27) \times 10^4$	$(1.35 \pm 0.04) \times 10^{13}$	$(1.03 \pm 0.03) \times 10^5$
35 / 308	$(7.15 \pm 0.32) \times 10^4$	$(1.12 \pm 0.05) \times 10^{13}$	$(8.57 \pm 0.38) \times 10^4$
45 / 318	$(5.60 \pm 0.22) \times 10^4$	$(8.78 \pm 0.35) \times 10^{12}$	$(6.92 \pm 0.27) \times 10^4$

followed. This was further supported by the values of the bimolecular quenching constant,  $k_q$  obtained from the  $K_{SV}$  values using Eq. 2, which were found to fall in the range of  $0.88\text{--}1.71 \times 10^{13} \text{ M}^{-1} \text{ s}^{-1}$  at all the temperatures studied (Table 3.5). Values of  $k_q$  higher than the diffusion-controlled limit ( $\sim 10^{10} \text{ M}^{-1} \text{ s}^{-1}$ ) indicated complex formation between PS and HSA (Lakowicz, 2006).

Values of the association constant,  $K_a$  for PS–HSA interaction at different temperatures were obtained from the double logarithmic plots, shown in Figure 3.21 and the values thus obtained, are listed in Table 3.5. As can be seen from the table,  $K_a$  values were relatively higher compared to those, obtained for FB–HSA interaction (Table 3.1). Nevertheless, these values were found in the range of  $1\text{--}15 \times 10^4 \text{ M}^{-1}$  and thus, pointed toward the intermediate affinity between PS and HSA (Dufour & Dangles, 2005). As anticipated,  $K_a$  values showed inverse correlation with temperature, since the forces involved in the complex formation would have been weakened with increasing temperature. Such intermediate value of the binding constant seems appropriate for the transport of PS in the blood circulation and its dissociation at the target site, as a large value of  $K_a$  would prevent the release of the ligand from the protein, thus hindering its action in the body (Peters, 1996).

### 3.2.2. *Thermodynamic parameters and binding forces*

In order to characterize the forces involved in the PS–HSA interaction, thermodynamic parameters for the binding reaction were determined from the van't Hoff plot (Figure 3.22) and the values of  $\Delta H$  and  $\Delta S$  are listed in Table 3.6. The negative  $\Delta H$  and positive  $\Delta S$  values contributed significantly toward making the  $\Delta G$  value more negative for the reaction and therefore, suggested the formation of a complex between PS and HSA as thermodynamically favorable. It is interesting to note that the signs of these parameters ( $+\Delta S$  and  $-\Delta H$ ) were identical to those found with the FB–HSA (Table 3.2), suggesting participation of the same intermolecular forces in the interactions of these ligands to HSA.

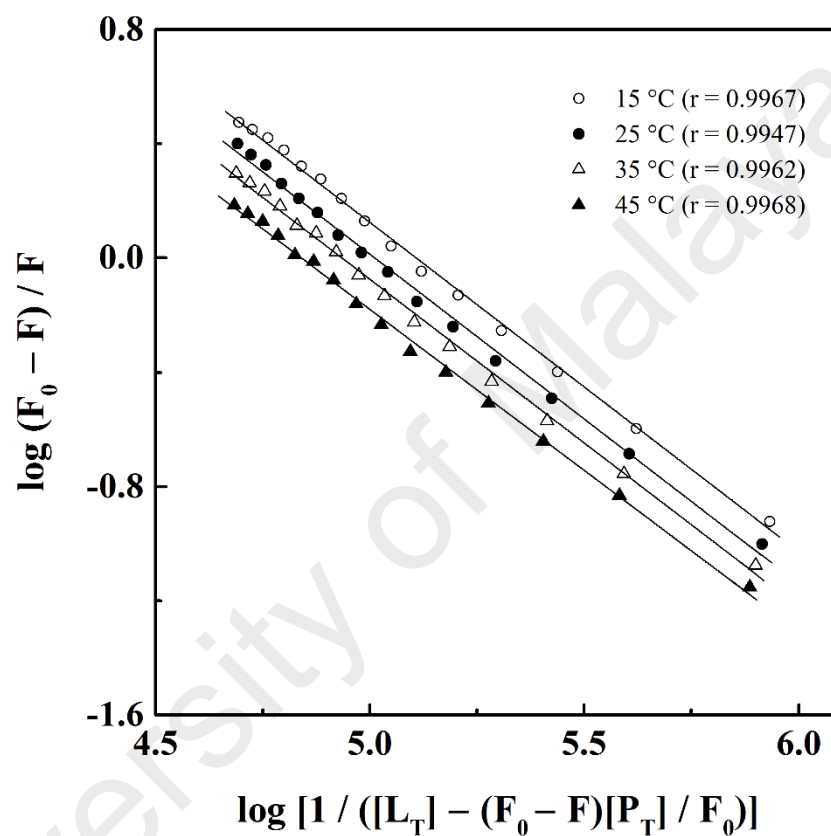


**Figure 3.21.** Double logarithmic plots of  $\log (F_0 - F) / F$  versus  $\log [1 / ([L_T] - (F_0 - F)[P_T] / F_0)]$  for the fluorescence quenching data of the PS-HSA system at four different temperatures, i.e., 15 °C, 25 °C, 35 °C and 45 °C.

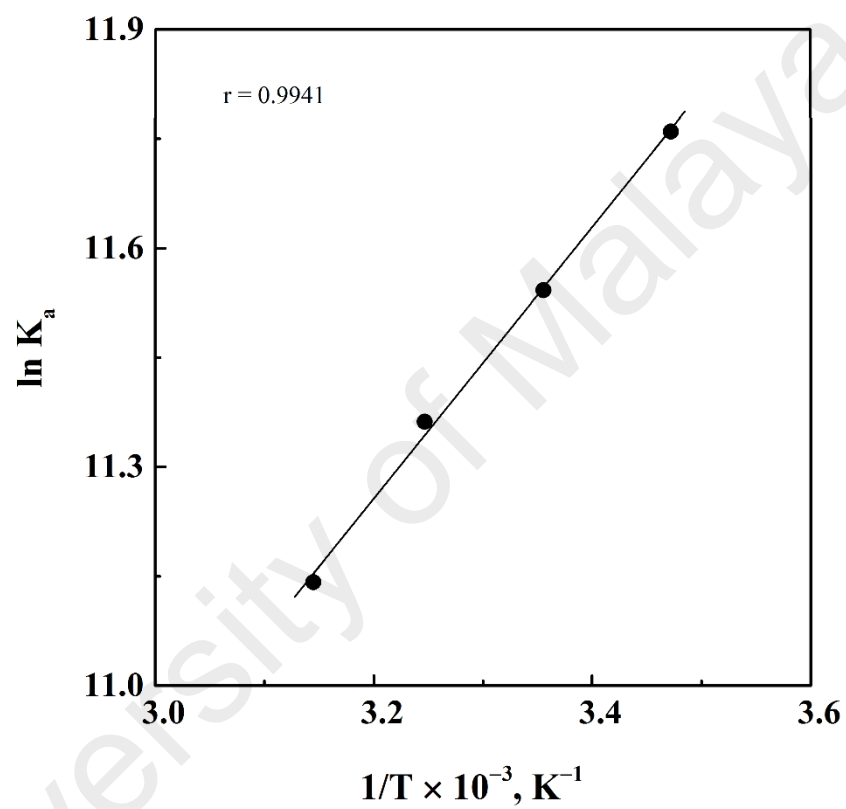


**Figure 3.22.** van't Hoff plot for the interaction between PS and HSA. Values of  $K_a$  were obtained from the double logarithmic plots shown in Figure 3.21.

**Table 3.6.** Thermodynamic parameters for the interaction of PS with HSA, obtained from fluorescence quenching titration experiments at different temperatures, pH 7.4.

$T$ ( $^{\circ}\text{C}$ / $\text{K}$ )	$\Delta S$ ( $\text{J mol}^{-1} \text{K}^{-1}$ )	$\Delta H$ ( $\text{kJ mol}^{-1}$ )	$\Delta G$ ( $\text{kJ mol}^{-1}$ )
15 / 288			-28.17
25 / 298	44.06	-15.48	-28.61
35 / 308			-29.05
45 / 318			-29.49

For a number of processes involving hydrophobic interactions, values of  $\Delta S$  were found to be positive, whereas  $\Delta H$  values were either close to zero or negative (Olsson et al., 2008; Ross & Rekharsky, 1996). The role of hydrophobic interactions in the PS–HSA complexation can be rationalized from the structural features of PS, which possesses two benzene rings connected by a tetrahydropyran ring system, giving it a non-polar character. The involvement of ionic forces in the binding reaction between PS and HSA is highly improbable due to a significantly higher value of  $\Delta H$  obtained for this reaction, as these forces are characterized by a  $\Delta H \approx 0$  (Ross & Subramanian, 1981). In addition, absence of any ionizable group in PS further rules out the participation of ionic forces in PS–HSA interaction. As mentioned earlier in the Section 3.1.2, a negative  $\Delta H$  value, obtained for PS–HSA system can account for the involvement of hydrogen bonding and/or van der Waals forces (Ross & Subramanian, 1981). This was further confirmed by docking experiments, which predicted the details of the hydrogen bonds likely to form between the functional groups of PS and the amino acid residues of the protein in the vicinity of the binding site, as discussed later in the Section 3.2.6. It would be an oversimplification to presume the involvement of a single force in the ligand–protein interaction. Taken together, evaluation of the energetics of PS–HSA interaction suggested the involvement of hydrophobic and van der Waals forces, together with hydrogen bonding in the complexation.

### **3.2.3. Microenvironmental alterations around HSA fluorophores**

Alteration in the microenvironment around the fluorophores (Tyr and Trp) in the three-dimensional structure of HSA upon PS binding was elucidated by synchronous and 3-D fluorescence spectroscopy.

#### **3.2.3.1. Synchronous fluorescence spectra**

Synchronous fluorescence spectra of HSA in the absence and the presence of increasing PS concentrations at 25 °C are shown in Figures 3.23 and 3.24, when  $\Delta\lambda$  was

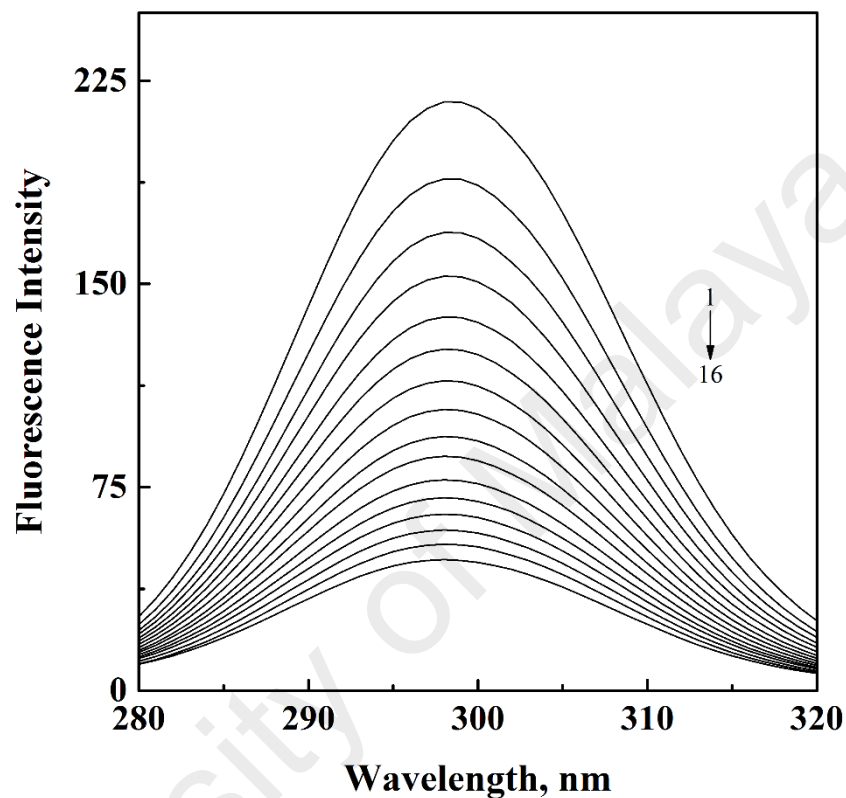


**Figure 3.23.** Synchronous fluorescence spectra of HSA in the absence and the presence of increasing PS concentrations at 25 °C, obtained in 10 mM Tris-HCl buffer, pH 7.4. The concentration of HSA was kept constant at 3  $\mu\text{M}$ , while PS concentration was varied (from top to bottom, 1 $\rightarrow$ 16) in the range, 0–22.5  $\mu\text{M}$  at regular increments of 1.5  $\mu\text{M}$ . The difference between excitation and emission wavelengths ( $\Delta\lambda$ ) was fixed at 15 nm.

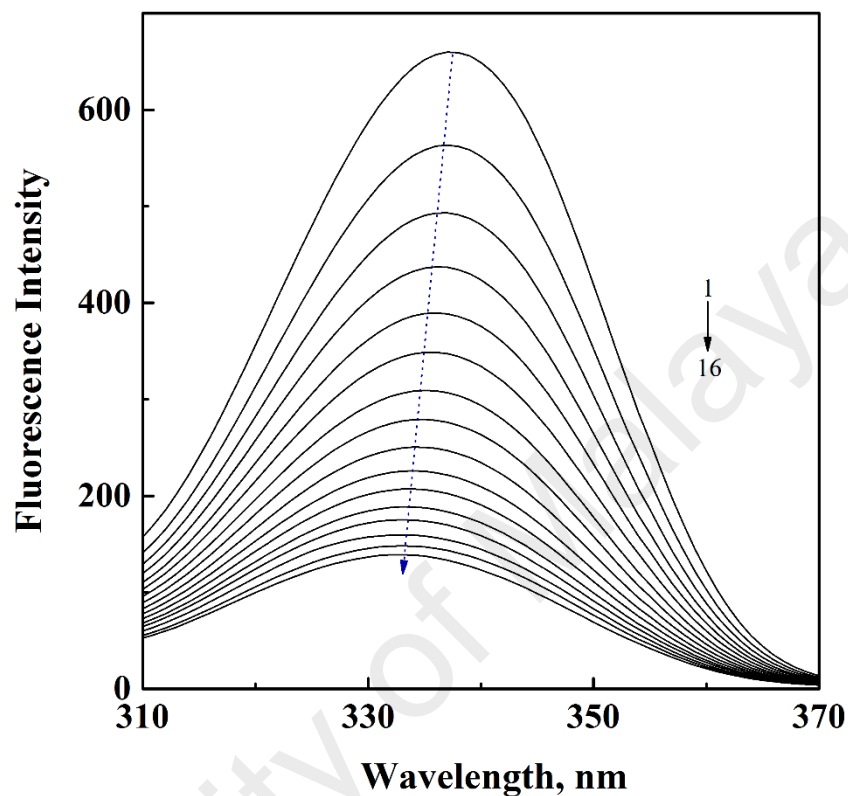


**Figure 3.24.** Synchronous fluorescence spectra of HSA in the absence and the presence of increasing PS concentrations at 25 °C, obtained in 10 mM Tris-HCl buffer, pH 7.4. The concentration of HSA was kept constant at 3  $\mu\text{M}$ , while PS concentration was varied (from top to bottom, 1 $\rightarrow$ 16) in the range, 0–22.5  $\mu\text{M}$  at regular increments of 1.5  $\mu\text{M}$ . The difference between excitation and emission wavelengths ( $\Delta\lambda$ ) was fixed at 60 nm. The arrow depicts the blue shift in the emission maximum of HSA with increasing PS concentrations.

kept at 15 and 60 nm, respectively. There was no change in the emission maximum of HSA (298 nm) upon addition of PS, when  $\Delta\lambda$  was 15 nm (Figure 3.23), suggesting that the microenvironment around Tyr residues was not significantly affected by the binding reaction. In contrast, a blue shift of 5 nm was observed, when  $\Delta\lambda$  was fixed at 60 nm (Figure 3.24), indicating perturbation in the microenvironment around Trp-214 towards a less polar milieu during PS–HSA complexation. These results were qualitatively similar to those obtained with the FB–HSA system (Figure 3.6).

Movement of the Trp residue to a more non-polar region as well as binding of a non-polar ligand to the binding pocket may account for the observed blue shift in the synchronous fluorescence spectra. Irrespective of the events that led to this phenomenon, it is possible to conclude from these results that the blue shift observed in the fluorescence spectrum of HSA upon PS binding (Figure 3.19) probably reflects the increased hydrophobicity in the microenvironment around the Trp residue.

### 3.2.3.2. Three-dimensional fluorescence spectra

Ligand-induced alteration in the fluorophores' microenvironment was also evident from the 3-D fluorescence spectra of HSA, obtained in the absence and the presence of different PS concentrations. The 3-D fluorescence spectra and the corresponding contour maps of native HSA and 1:1 PS–HSA complex are shown in Figure 3.25, while those of 2:1 and 3:1 PS–HSA complexes are presented in Figure 3.26. The spectral characteristics (peak position and peak intensity) of the 3-D fluorescence spectra are given in Table 3.7.

As can be seen from the Figures 3.25 and 3.26, both Rayleigh scattering and second order scattering peaks represented as peaks 'a' and 'b' were present in all 3-D fluorescence spectra. The protein fluorescence peaks, '1' ( $\lambda_{\text{ex}} = 280$  nm) and '2' ( $\lambda_{\text{ex}} = 235$  nm), characterizing the fluorescence spectral behavior of Trp and Try residues, were significantly affected in the presence of PS (Figures 3.25 and 3.26). A clear trend of decreasing fluorescence intensity, accompanied by the blue shift in both peaks '1' and '2'

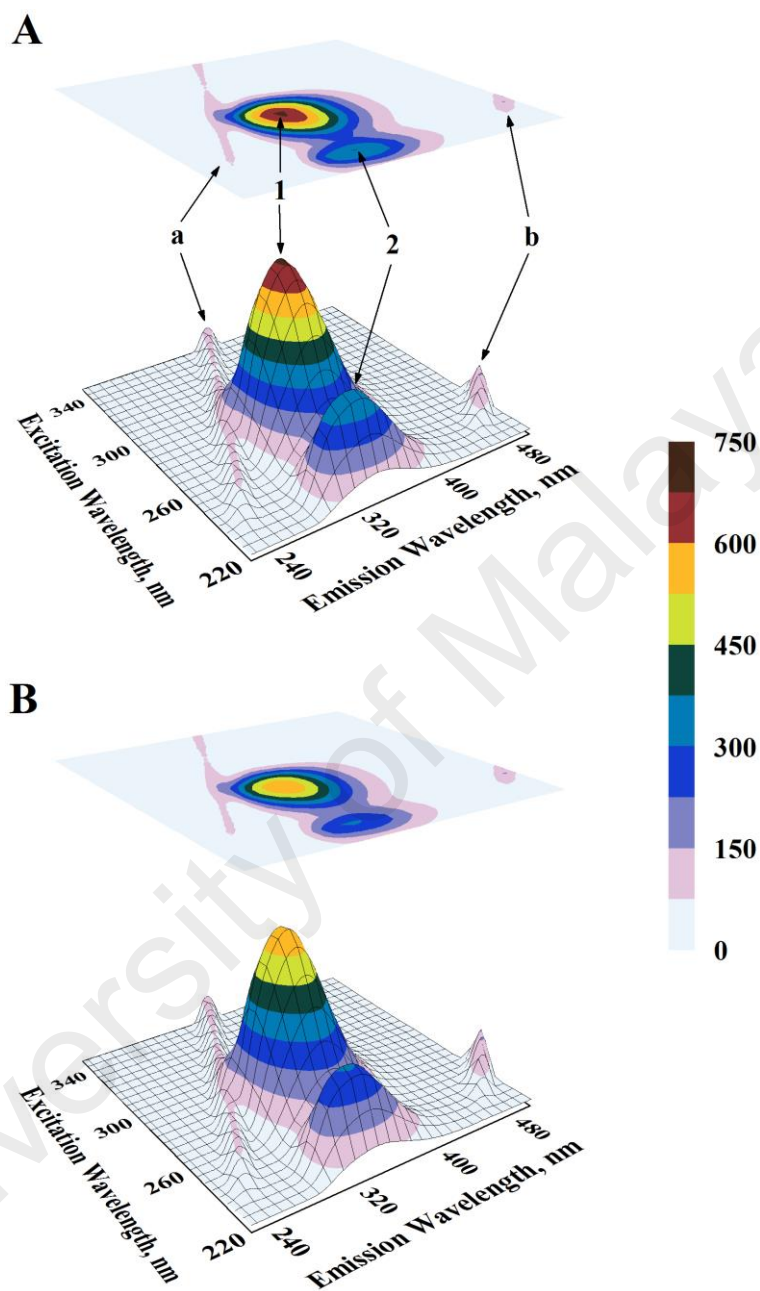


**Figure 3.25.** Three-dimensional fluorescence spectra and corresponding contour maps of (A) HSA (3  $\mu$ M) and (B) PS-HSA (1:1) complex, obtained in 10 mM Tris-HCl buffer, pH 7.4 at 25  $^{\circ}$ C.

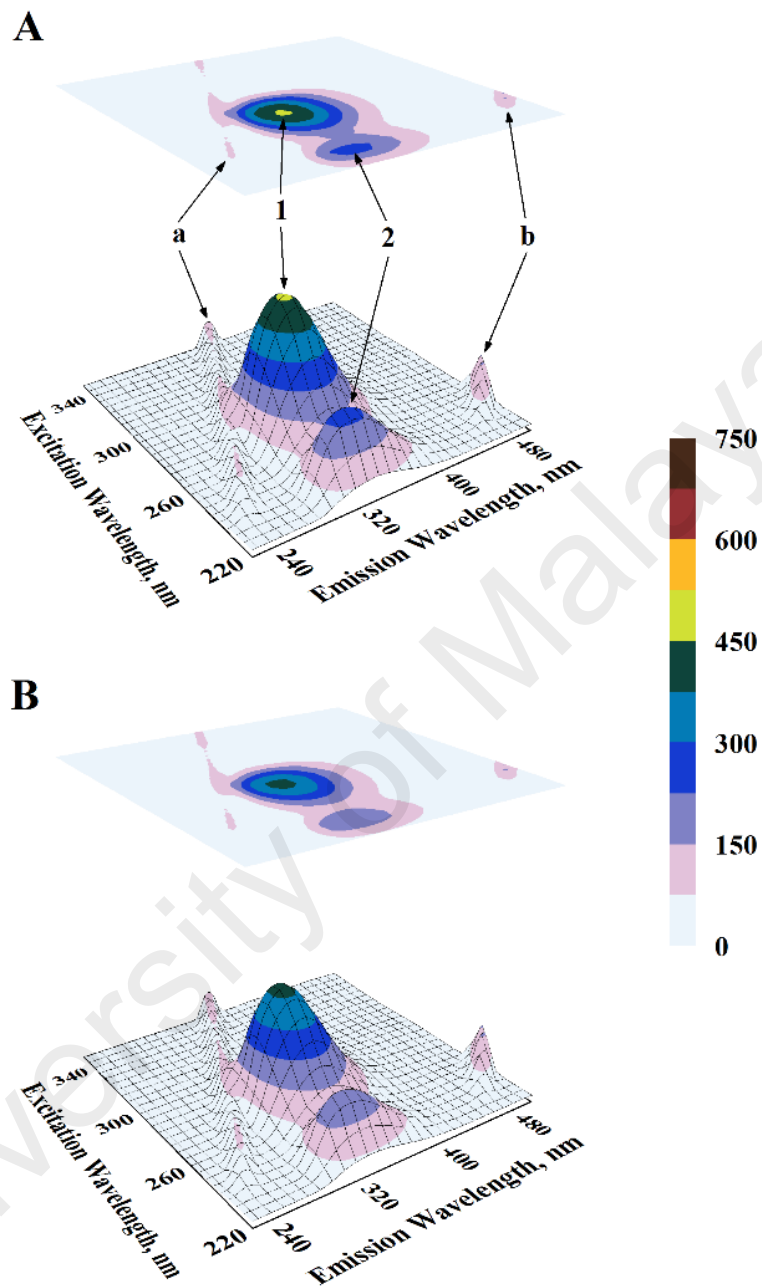


**Figure 3.26.** Three-dimensional fluorescence spectra and corresponding contour maps of (A) PS-HSA (2:1) complex and (B) PS-HSA (3:1) complex, obtained in 10 mM Tris-HCl buffer, pH 7.4 at 25 °C, using HSA concentration of 3  $\mu$ M.

**Table 3.7.** Three-dimensional fluorescence spectral characteristics of HSA and PS–HSA complexes at pH 7.4, 25 °C.

System	Peak	Peak position [ $\lambda_{ex}/\lambda_{em}$ (nm/nm)]	Intensity
HSA	a	230/230 → 350/350	23.39 → 96.41
	b	250/500	153.61
	1	280/335	683.13
	2	235/330	359.12
[PS]:[HSA] = 1:1	a	230/230 → 350/350	23.02 → 93.68
	b	250/500	155.66
	1	280/332	580.78
	2	235/326	307.91
[PS]:[HSA] = 2:1	a	230/230 → 350/350	22.53 → 91.79
	b	250/500	153.36
	1	280/330	448.23
	2	235/323	252.40
[PS]:[HSA] = 3:1	a	230/230 → 350/350	22.03 → 92.69
	b	250/500	157.06
	1	280/329	389.85
	2	235/320	219.38

of HSA was noticed with increasing PS/HSA molar ratios (Table 3.7). These results were suggestive of PS-induced alteration in the microenvironment around HSA fluorophores. In view of the binding of PS to Sudlow's site I of HSA, as reflected from our drug displacement and molecular docking results described in the Sections 3.2.5 and 3.2.6, respectively, it seems probable that such alteration in the microenvironment might have been confined to Trp-214, which is located in Sudlow's site I.

#### **3.2.4. PS-induced thermal stabilization of HSA**

CD spectroscopy was employed to study the effect of PS binding to HSA on its thermal stability by determining the loss in the  $CD_{222\text{ nm}}$  value of HSA with increasing temperature (25–100 °C) both in the absence and the presence of PS. Thermal denaturation curves of HSA and PS–HSA complex showed similar cooperative transition up to 94 °C, beyond which there was a steep loss in the  $CD_{222\text{ nm}}$  value of HSA against a gradual decrease, observed with the PS–HSA complex (Figure 3.27A). To validate these findings, cooling experiments were performed in the same way after equilibrating the samples for 6 min at each temperature in the reverse order. As can be seen from the Figure 3.27A, HSA alone did not show any recovery in the  $CD_{222\text{ nm}}$  value upon cooling, while a clear precipitate was noticed at 25 °C, suggesting irreversible protein unfolding and aggregation. On the contrary, a significant increase in the  $CD_{222\text{ nm}}$  signal from –49 at 100 °C to –67 at 25 °C and a clear state of the solution upon cooling to 25 °C, was observed with the PS–HSA complex. Both these results suggested relatively higher thermal stability of HSA in the presence of PS which not only prevented precipitation but also produced a significant reversal in the  $CD_{222\text{ nm}}$  value upon cooling.

Since exposure of the protein to higher temperatures was found to be the cause of irreversible protein denaturation and aggregation, the experiment was repeated within the temperature range, 25–80 °C (Figure 3.27B). Although no significant change in the denaturation profiles was seen, when compared to those shown in the Figure 3.27A,

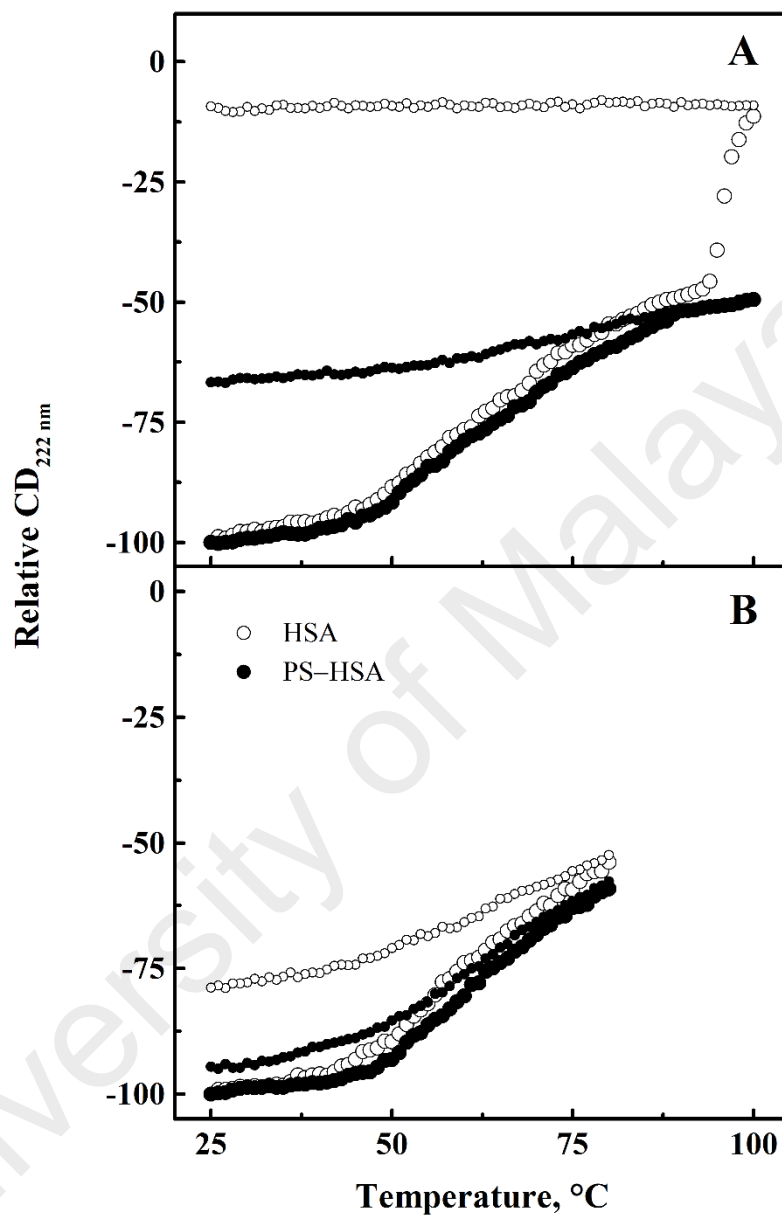


**Figure 3.27.** Thermal denaturation and renaturation curves of HSA (3  $\mu$ M) and PS-HSA (5:1) complex, as studied by CD<sub>222 nm</sub> measurements in the temperature range, 25–100 °C (A) and 25–80 °C (B) in 10 mM Tris-HCl buffer, pH 7.4. Renaturation curves are shown with smaller symbols.

remarkable alterations in the renaturation profiles of HSA were noticed. A significant recovery in the native structural characteristics was observed, showing 87% regain in the  $CD_{222\text{ nm}}$  value at 5:1 PS/HSA molar ratio, compared to only 55% recovery, obtained with HSA alone. Greater recovery in the  $CD_{222\text{ nm}}$  value (55%) observed with HSA compared to 40% shown in the Section 3.1.4 can be attributed to the shorter duration of equilibration (3 min) used in these experiments against 6 min employed in the previous study. Hence, these results unequivocally suggested thermal stabilization of HSA induced by PS binding.

### 3.2.5. *Binding site specificity of PS on HSA*

In order to investigate the binding preference of PS towards Sudlow's sites I and II, displacement experiments were performed using site marker ligands. The selected markers for site I were BR and WFN; whereas site II was probed using DZP and KTN as the reporter ligands (Kragh-Hansen et al., 2002).

Figure 3.28 shows the effect of increasing PS concentrations on the visible CD spectrum of BR–HSA (1:1) complex. As can be seen from the figure, BR–HSA complex exhibited a bisignate CD spectrum with a maximum at 458 nm and a minimum at 407 nm. In the absence of any chirality in the free BR molecule (spectrum 'a'), the above Cotton effect is believed to be the result of the dissymmetry produced in the BR structure upon binding to HSA (Trynda-Lemiesz, 2004). Free forms of PS (spectrum 'c') and HSA (spectrum 'b') as well as their complex (spectrum 'd') did not contribute any CD signal in the wavelength range studied; thus, any signal in this wavelength range can be attributed to the complexation between BR and HSA. Addition of increasing PS concentrations to BR–HSA complex led to a gradual decrease in the induced CD signal at 458 nm, producing around 80% loss at a PS/HSA molar ratio of 8:1 (Figure 3.30A). Such a decrease in the  $CD_{458\text{ nm}}$  signal clearly indicated the displacement of BR from its

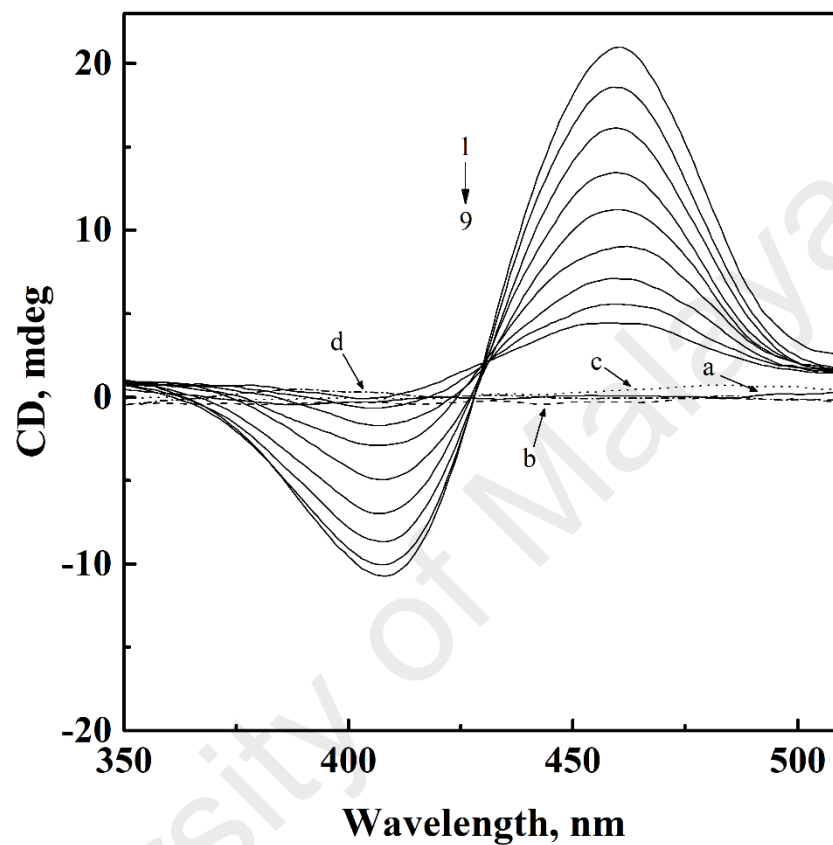


**Figure 3.28.** Displacing effect of PS on the visible CD spectrum of BR-HSA (1:1) complex at 25 °C. The concentrations of BR and HSA were 10 μM each while the concentration of PS was varied (from top to bottom, 1→9) in the range, 0–80 μM at regular increments of 10 μM. CD spectra marked as ‘a’, ‘b’, ‘c’ and ‘d’ refer to 10 μM BR, 10 μM HSA and 50 μM PS and PS-HSA (5:1) complex, respectively.

binding site on HSA in the presence of PS, which was suggestive of the site I of HSA as the preferred binding site for PS.

To substantiate the above finding, another site I marker ligand, WFN was used and the displacing action of PS on WFN–HSA complex was monitored by fluorescence spectroscopy (Figure 3.29). WFN in free form produced a weak fluorescence spectrum in the wavelength range, 360–480 nm, when excited at 335 nm (spectrum ‘a’). However, a pronounced emission spectrum with an emission maximum at 383 nm was observed upon its complexation with HSA (Trynda-Lemiesz, 2004). It is important to note that free PS (spectrum ‘c’) and HSA (spectrum ‘b’) as well as PS–HSA complex (spectrum ‘d’) did not produce any significant fluorescence spectra in this range. The intensity of the fluorescence spectra of WFN–HSA complex decreased with the addition of PS in a concentration-dependent manner, showing 75% reduction at a PS/HSA molar ratio of 8:1 (Figure 3.30B). Decrease in the fluorescence intensity of WFN–HSA complex in the presence of PS suggested the removal of WFN from site I of HSA by PS. These results corroborated the earlier finding, obtained with BR displacement experiments.

In order to investigate the possibility of PS binding to site II of HSA, CD spectra of DZP–HSA complex were recorded in the wavelength range, 250–350 nm both in the absence and the presence of increasing PS concentrations (Figure 3.31). Free DZP (spectrum ‘a’) and PS (spectrum ‘c’) did not show any significant CD spectra in this wavelength range. However, binding of DZP to HSA produced a CD spectrum, characterized by the presence of two maxima at 259 and 289 nm and a minimum at 319 nm (Watanabe et al., 2000). On the other hand, HSA (spectrum ‘b’) as well as its complex with PS (spectrum ‘d’) produced CD spectra, which showed negative CD values throughout the wavelength range studied. Addition of PS to DZP–HSA complex produced little effect on the complexation, as reflected from the small change (24%) in the relative CD signal at 259 nm at a PS/HSA molar ratio of 8:1 (Figure 3.33A). This

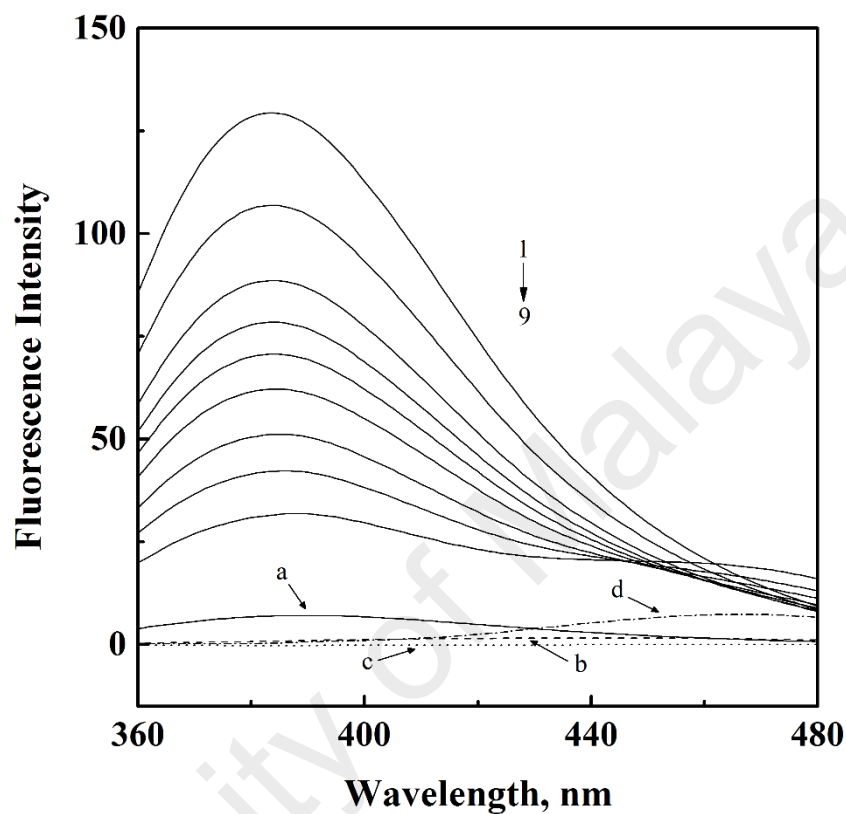


**Figure 3.29.** Displacing effect of PS on the fluorescence spectrum of WFN–HSA (1:1) complex at 25 °C. The concentrations of WFN and HSA were 3  $\mu$ M each while the concentration of PS was varied (from top to bottom, 1 $\rightarrow$ 9) in the range, 0–24  $\mu$ M at regular increments of 3  $\mu$ M. Emission spectra marked as ‘a’, ‘b’, ‘c’ and ‘d’ refer to 3  $\mu$ M WFN, 3  $\mu$ M HSA, 15  $\mu$ M PS and PS–HSA (5:1) complex, respectively. The excitation wavelength was 335 nm.

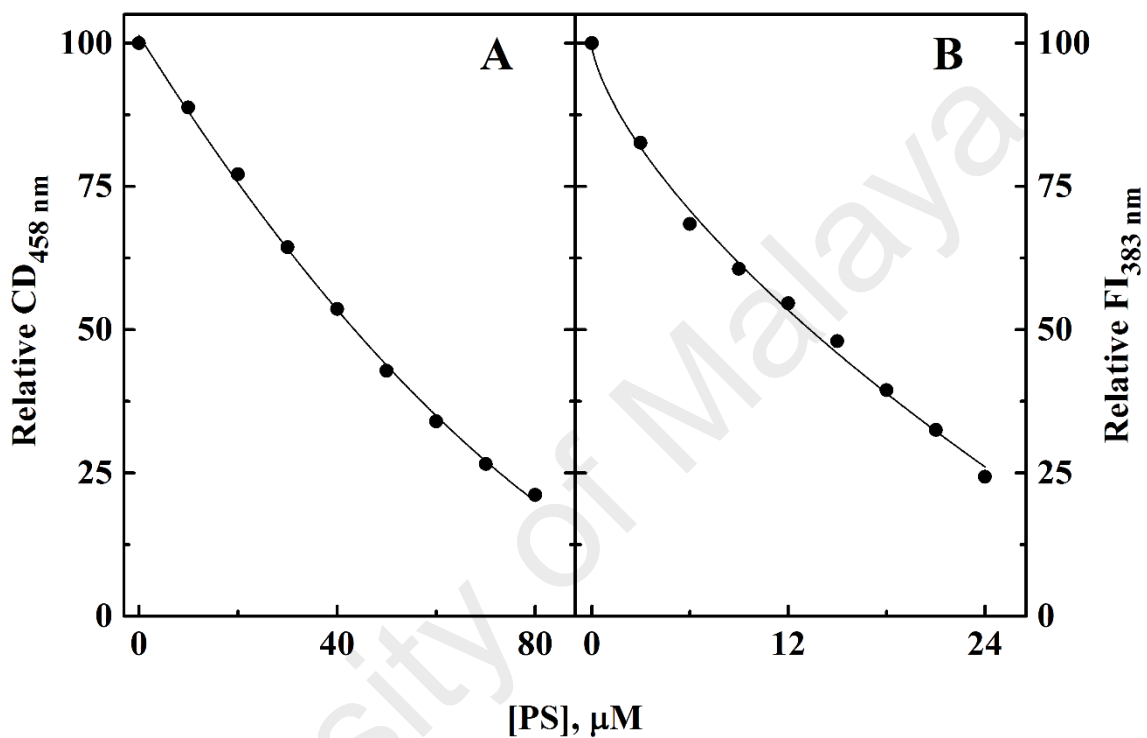


**Figure 3.30.** Plots showing the decrease in the relative CD value at 458 nm ( $CD_{458\text{ nm}}$ ) of BR-HSA complex (A) and the relative fluorescence intensity at 383 nm ( $FI_{383\text{ nm}}$ ) of WFN-HSA complex (B) with increasing PS concentrations. Values of the relative  $CD_{458\text{ nm}}$  and the relative  $FI_{383\text{ nm}}$  were obtained from the spectra shown in Figures 3.28 and 3.29, respectively.

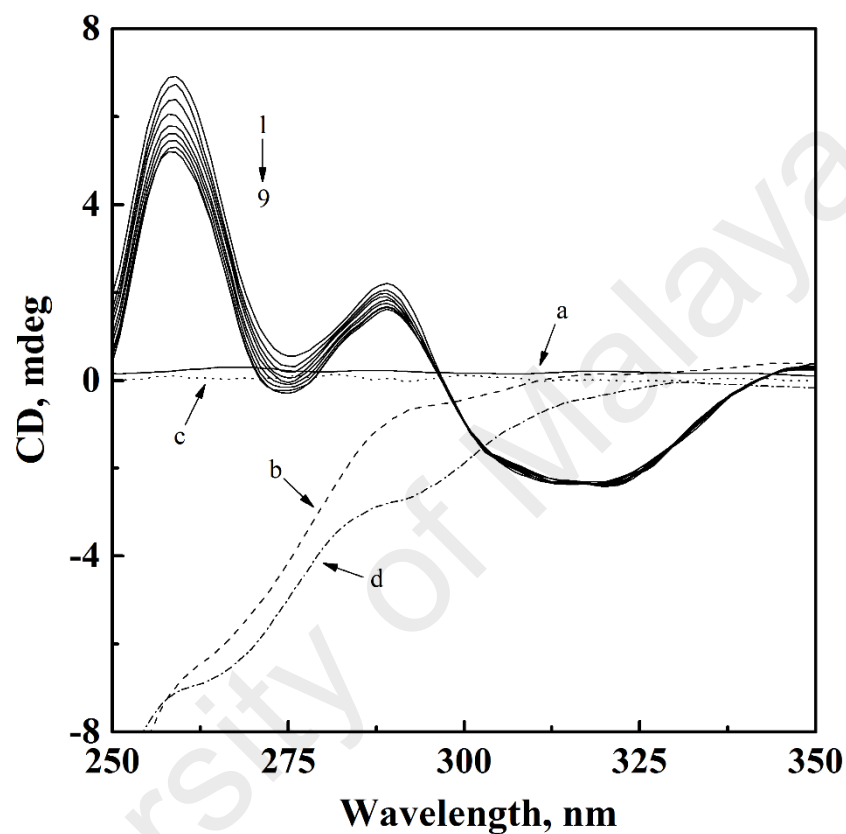


**Figure 3.31.** Displacing effect of PS on the CD spectrum of DZP–HSA (20  $\mu\text{M}$  DZP + 10  $\mu\text{M}$  HSA) complex at 25  $^{\circ}\text{C}$ . The concentration of PS was varied (from top to bottom, 1 $\rightarrow$ 9) in the range, 0–80  $\mu\text{M}$  at regular increments of 10  $\mu\text{M}$ . CD spectra marked as ‘a’, ‘b’, ‘c’ and ‘d’ refer to 20  $\mu\text{M}$  DZP, 10  $\mu\text{M}$  HSA, 50  $\mu\text{M}$  PS and PS–HSA (5:1) complex, respectively.

decrease in the CD signal was much smaller compared to the decrease observed with either BR–HSA or WFN–HSA complexes (Figure 3.30). In view of the negative CD signal at 259 nm shown by PS–HSA complex, one should expect a much larger decrease in the  $CD_{259\text{ nm}}$  value in the presence of PS, had there been displacement of DZP from its binding site on HSA by PS. Therefore, a small decrease in the relative  $CD_{259\text{ nm}}$  value, observed with DZP–HSA complex in the presence of PS cannot be taken to indicate DZP displacement by PS.

The displacement of KTN, another site II marker ligand, by PS was also studied using CD spectroscopy in the wavelength range, 300–400 nm. Figure 3.32 depicts the effect of the addition of increasing PS concentrations on the induced CD spectrum of KTN–HSA complex. As evident from the figure, a negative Cotton effect was induced with a minimum at around 340 nm upon binding of KTN to HSA (Watanabe et al., 2000). On the other hand, free KTN (spectrum ‘a’) and PS (spectrum ‘c’) exhibited negligible CD signals in the same wavelength range. However, HSA (spectrum ‘b’) as well as its conjugate with PS (spectrum ‘d’) displayed significant negative CD values in the wavelength range, 300–335 nm, beyond which CD signals became insignificant. The CD spectra of KTN–HSA complex showed slight variation in the presence of increasing PS concentrations. Only 10% decrease in the relative  $CD_{340\text{ nm}}$  signal was observed at a PS/HSA molar ratio of 8:1 (Figure 3.33B). These results suggested that KTN binding to HSA remained largely unaffected in the presence of increasing PS concentrations, thus reflecting differential preference of PS for the two binding sites on HSA. These results were in accordance with the outcome of the above displacement experiments in assigning site I as the preferred binding site of PS on HSA.

### **3.2.6. Molecular docking**

A docking simulation of the interaction between PS and HSA was conducted using the AutoDock software package to predict the binding mode of the ligand on the protein for

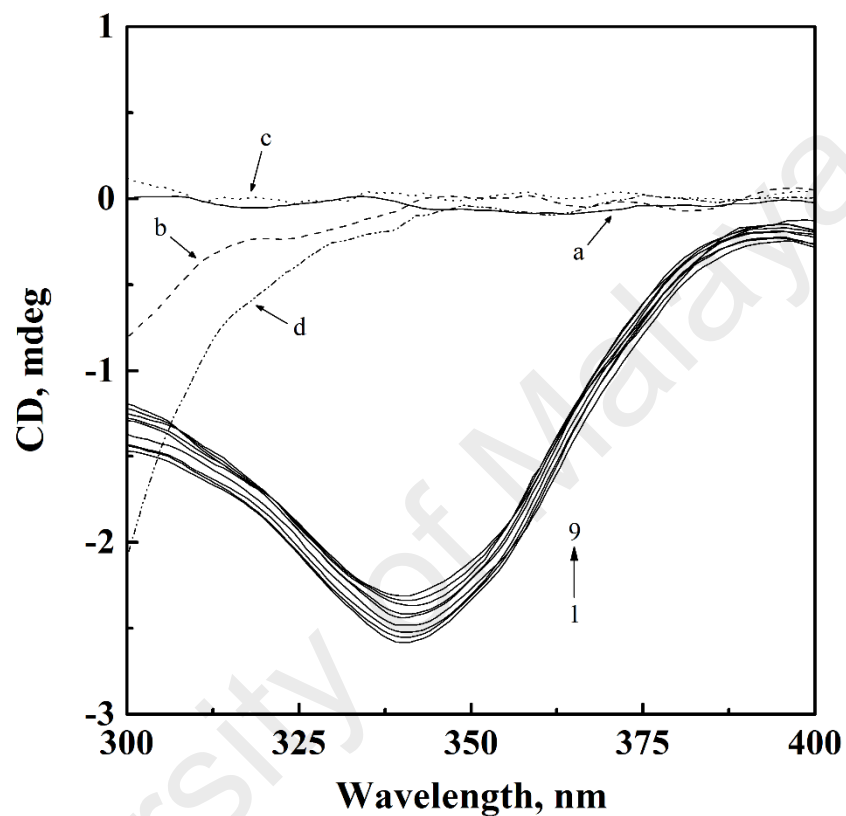


**Figure 3.32.** Displacing effect of PS on the CD spectrum of KTN-HSA (20  $\mu\text{M}$  KTN + 10  $\mu\text{M}$  HSA) complex at 25  $^{\circ}\text{C}$ . The concentration of PS was varied (from bottom to top, 1 $\rightarrow$ 9) in the range, 0–80  $\mu\text{M}$  at regular increments of 10  $\mu\text{M}$ . CD spectra marked as ‘a’, ‘b’, ‘c’ and ‘d’ refer to 20  $\mu\text{M}$  KTN, 10  $\mu\text{M}$  HSA, 50  $\mu\text{M}$  PS and PS-HSA (5:1) complex, respectively.

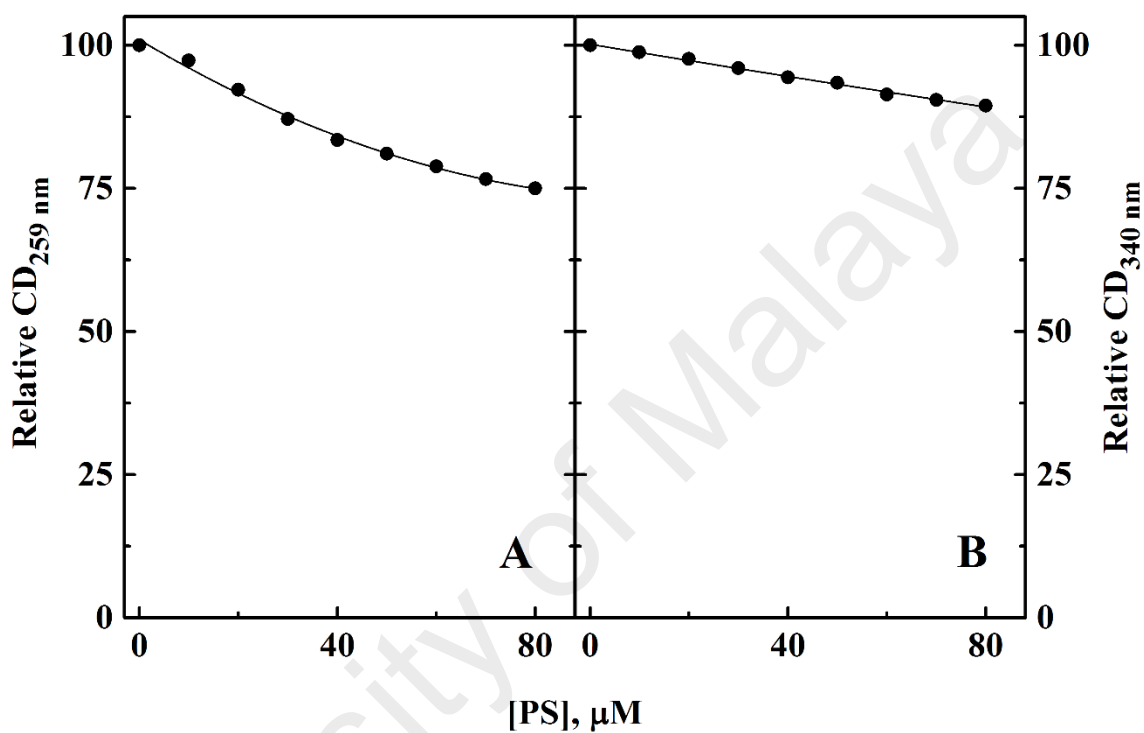


**Figure 3.33.** Plots showing the decrease in the relative CD value at 259 nm ( $CD_{259\text{ nm}}$ ) of DZP-HSA complex (A) and the relative CD value at 340 nm ( $CD_{340\text{ nm}}$ ) of KTN-HSA complex (B) with increasing PS concentrations. Values of the relative  $CD_{259\text{ nm}}$  and the relative  $CD_{340\text{ nm}}$  were obtained from the spectra shown in Figures 3.31 and 3.32, respectively.

the two main ligand binding sites, I and II; and to confirm the results of the ligand displacement experiments described above. Multiple crystal structures of HSA, i.e., 1BM0, 2BXD and 2BXF were analyzed to ensure the robustness of the simulation method. The additional crystal structures, 2BXD and 2BXF were chosen as they represented HSA complexes with WFN and DZP, respectively (Ghuman et al., 2005). Since HSA is known to bind to WFN at site I and DZP at site II (Kragh-Hansen et al., 2002; Peters, 1996), docking analysis using these structures could reveal the binding preference of PS to either site I or site II of HSA. The docking simulation of 1BM0–PS was analyzed due to the fact that 1BM0 is the highest resolution HSA crystal structure available (Sugio et al., 1999).

At site I of the 1BM0–PS complex, cluster analysis of 100 docking results revealed a total of 7 multimember conformational clusters, as shown in Figure 3.34A. The cluster with the lowest binding energy was also found to be the highest populated cluster, having more than 70% of the analyzed conformations (72 out of 100 conformations). Therefore, it was the most energetically favorable cluster, possessing a mean docking energy of about  $-31.10 \text{ kJ mol}^{-1}$ . Using the same approach for site II, 24 distinct conformational clusters were obtained. However, the most populated cluster (22 out of 100 conformations) was not the most energetically favorable cluster ( $-20.88 \text{ kJ mol}^{-1}$ ). Hence, PS showed a binding preference for binding site I of HSA and these docking results were in good agreement with the displacement results, discussed above. Clustering analysis of the 2BXD–PS and 2BXF–PS complexes (Figures 3.35 and 3.36) also showed similar results in terms of the lowest binding energy and highly populated clusters with site I, strengthening our conclusion about site I of HSA as the primary binding site of PS.

The predicted binding model with the lowest docking energy conformation, as obtained from the 1BM0–PS complex ( $-31.10 \text{ kJ mol}^{-1}$ ) was then used for binding orientation analysis (Figure 3.37). The binding site (defined as amino acid residues within

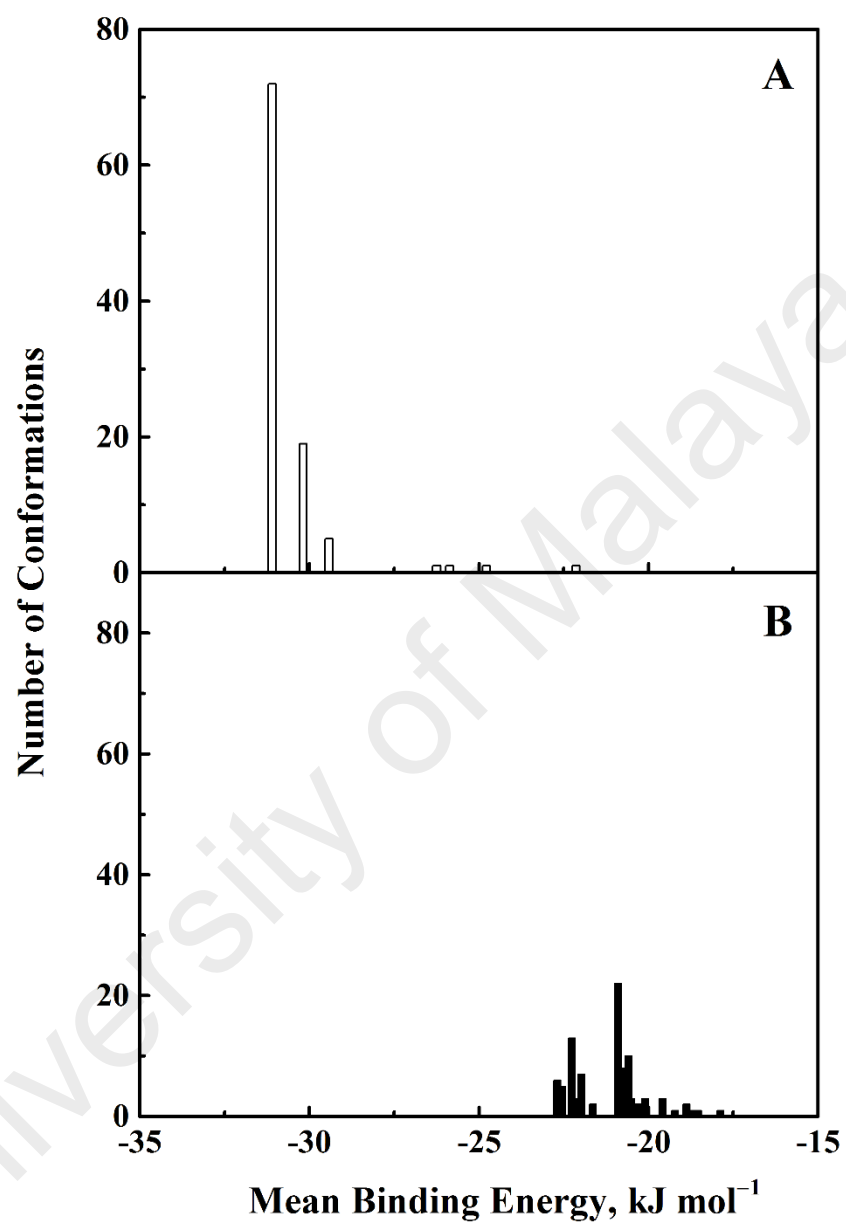


**Figure 3.34.** Cluster analysis of the docking of PS to Sudlow's sites I (A) and II (B) of HSA crystal structure (1BM0). A total of 100 runs were performed for each binding site.

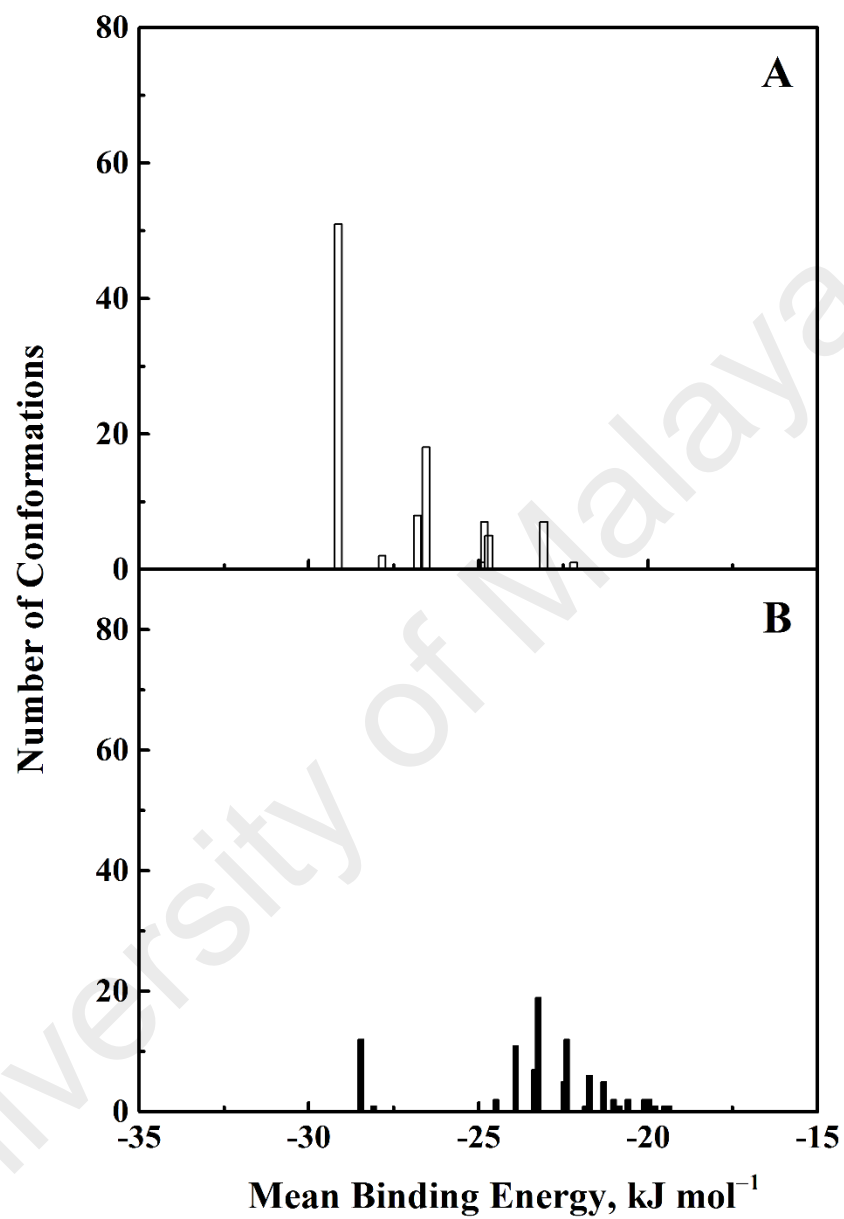


**Figure 3.35.** Cluster analysis of the docking of PS to Sudlow's sites I (A) and II (B) of HSA crystal structure (2BXD). A total of 100 runs were performed for each binding site.

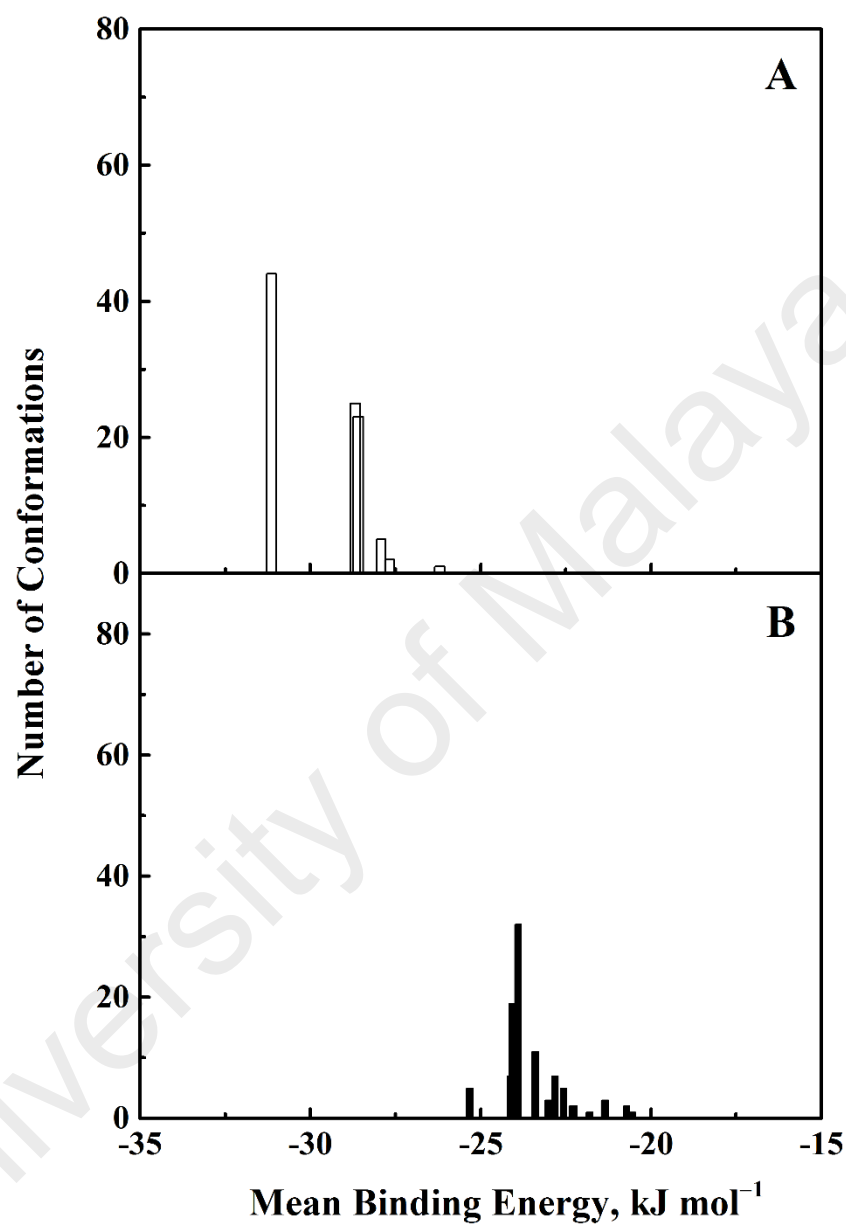


**Figure 3.36.** Cluster analysis of the docking of PS to Sudlow's sites I (A) and II (B) of HSA crystal structure (2BXF). A total of 100 runs were performed for each binding site.

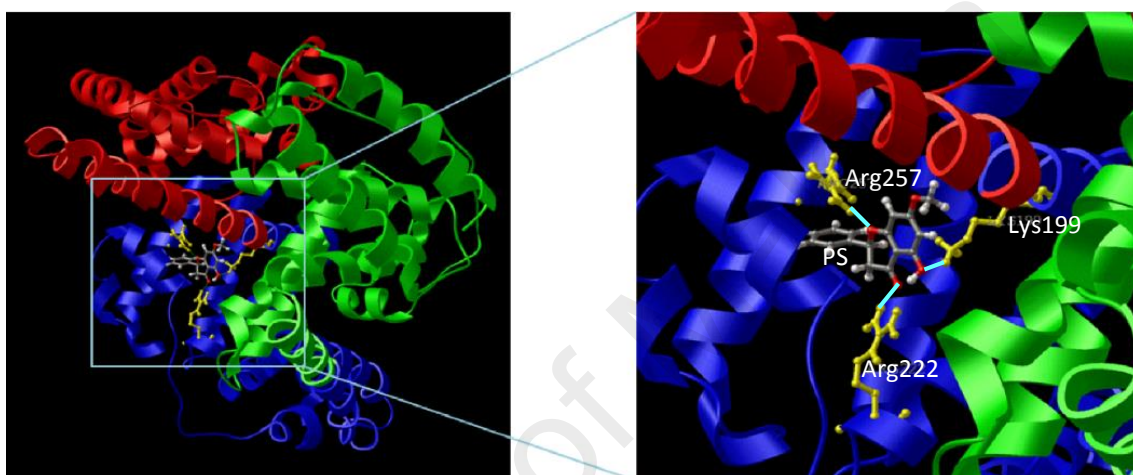


**Figure 3.37.** Binding orientation of the lowest docking energy conformation of PS (ball and stick rendered) in Sudlow's site I (subdomain IIA) of HSA (1BM0). Domains I, II and III of HSA are represented in red, blue and green, respectively. The zoomed-in view of the binding site shows the hydrogen bonds (turquoise lines) formed between PS and amino acid side chains of HSA (yellow).

5 Å distance with the ligand) was found to be located deep within the protein structure in a hydrophobic cleft, walled by the 18 amino acid residues: Glu-153, Ser-192, Lys-195, Gln-196, Lys-199, Trp-214, Arg-218, Leu-219, Arg-222, Leu-238, Val-241, His-242, Arg-257, Leu-260, Ala-261, Ser-287, Ile-290 and Ala-291. Hydrophobic interactions between hydrophobic residues of the cleft and the benzene rings of the ligand are believed to contribute towards the stability of the docking conformation of PS inside this binding pocket. However, the interaction between PS and HSA cannot be presumed to be exclusively hydrophobic in nature; as there were several polar residues in the proximity of the bound ligand that may participate in polar interactions with the hydrophilic groups of PS. Indeed, three hydrogen bonds were also predicted from the model involving hydrogen atoms of three different amino acid residues of HSA (Lys-199, Arg-222 and Arg-257) and the oxygen atoms of the hydroxyl, carbonyl and oxacyclohexane groups of PS (Table 3.8). Hence, it can be concluded that PS binds to a hydrophobic pocket located in subdomain IIA, involving both hydrophobic interactions and hydrogen bonding; in accordance with our thermodynamic data.

In summary, the above quantitative analysis of PS–HSA interaction describes a binding reaction that, in general, is analogous to that of the FB–HSA system. The thermodynamic and molecular modeling data suggested the involvement of van der Waals force, hydrophobic interaction and hydrogen bonding in the complexation between PS and HSA. Alterations in the microenvironment around protein fluorophores upon PS binding were evident from multiple spectroscopic results. Binding of PS to HSA increased the thermal stability of the protein and the binding site of PS on HSA was confirmed as site I, based on competitive ligand displacement results as well as docking analysis.

**Table 3.8.** Distance of the predicted hydrogen bonds formed between interacting atoms of the amino acid residues of HSA (site I) and PS.

HSA atom	PS atom	Distance (Å)
Lys-199: HZ1	O (hydroxyl)	2.18
Arg-222: HH11	O (carbonyl)	2.03
Arg-257: HH22	O (oxacyclohexane)	1.97

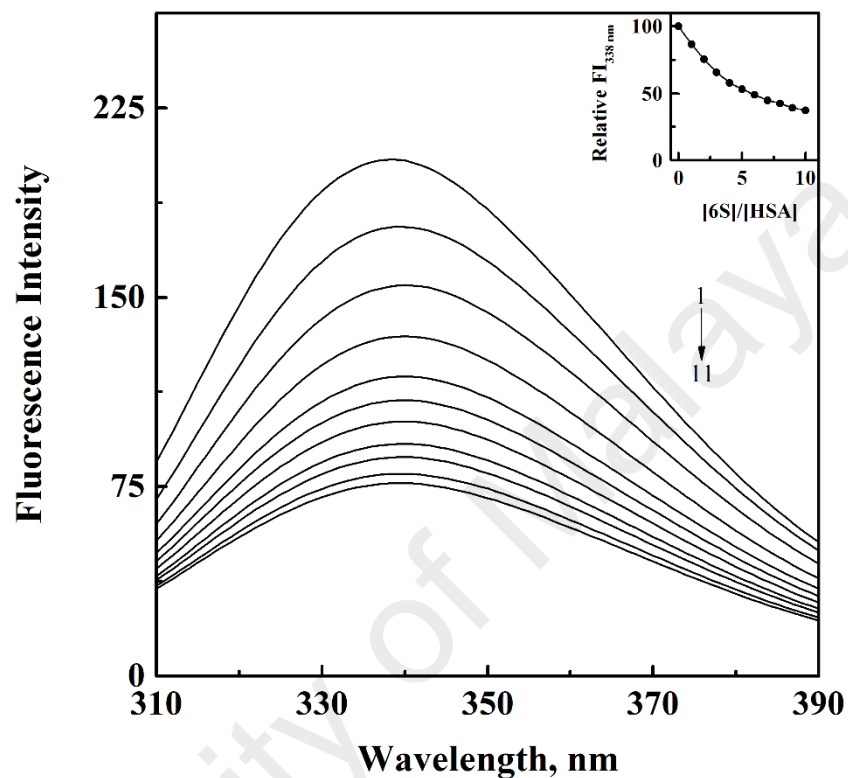
### 3.3. 6-Shogaol–human serum albumin interaction

The interaction of the main chemical constituent of the dried ginger (*Zingiber officinale*), 6-shogaol (6S) with HSA was also investigated using the fluorescence quenching titration method.

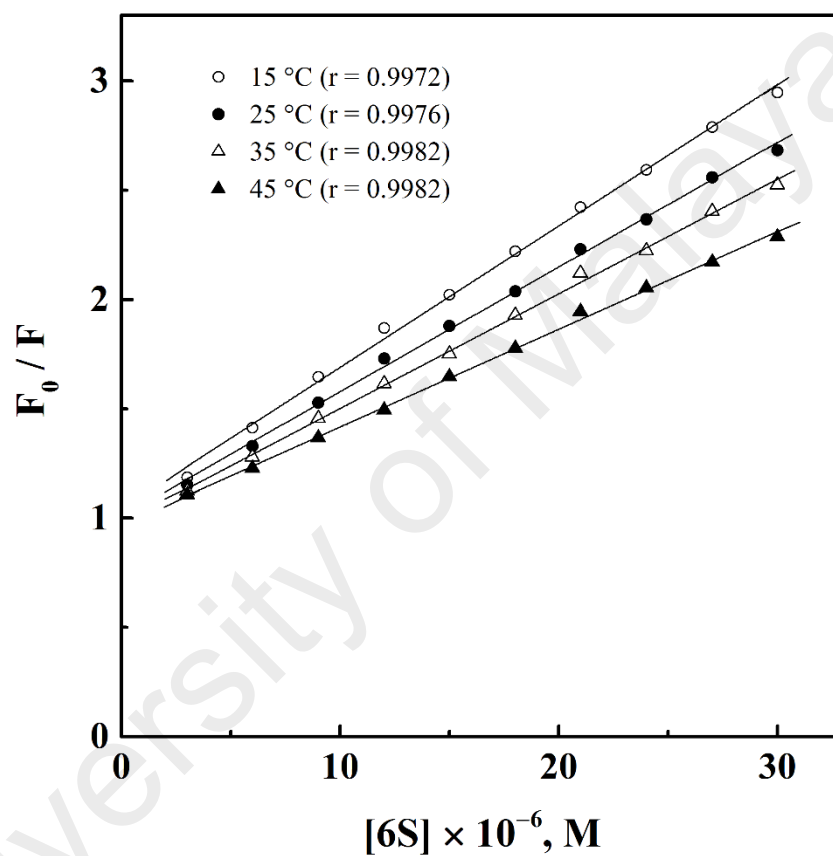
#### 3.3.1. Quenching of HSA fluorescence and binding characteristics

Figure 3.38 shows fluorescence spectra of HSA (3  $\mu\text{M}$ ) in the wavelength range, 310–390 nm, obtained in the absence and the presence of increasing 6S concentrations (0–30  $\mu\text{M}$ ) at 25 °C. The emission spectrum with a maximum at 338 nm was originated due to the presence of the solitary Trp residue (Trp-214) of HSA, which was selectively targeted upon excitation at 295 nm. Addition of 6S to HSA induced a concentration-dependent decrease in its fluorescence intensity, producing ~63% quenching at a 6S/HSA molar ratio of 10:1 (inset of Figure 3.38). While considerable quenching was observed in the presence of 6S, the emission maximum remained unchanged throughout the titration. Considering Trp as a relatively sensitive fluorophore, it appears that addition of 6S to HSA had little effect on the polarity of microenvironment in the vicinity of Trp-214 or its accessibility to the solvent (Ladokhin, 2000). The quenching of the tryptophanyl fluorescence as shown in Figure 3.38 thus, seems to arise due to collisional or static quenching phenomena (Lakowicz, 2006).

In view of the temperature dependence of collisional and static quenching mechanisms, fluorescence quenching titration experiments were performed at four different temperatures (15, 25, 35 and 45 °C) to predict the quenching mechanism involved in the 6S–HSA system. Treatment of the fluorescence data according to Eq. 2 produced Stern-Volmer plots (Figure 3.39), which were used to determine the  $K_{\text{SV}}$  values (Table 3.9). The inverse correlation between the  $K_{\text{SV}}$  values and the temperature suggested involvement of the static quenching mechanism in the 6S-induced quenching of HSA fluorescence. In addition, appreciably larger values ( $0.70\text{--}1.01 \times 10^{13} \text{ M}^{-1} \text{ s}^{-1}$ ) of



**Figure 3.38.** Fluorescence spectra of HSA in the absence and the presence of increasing 6S concentrations, obtained in 10 mM sodium phosphate buffer, pH 7.4 at 25 °C upon excitation at 295 nm. The concentration of HSA was fixed at 3  $\mu$ M, while 6S concentration was varied (from top to bottom, 1 $\rightarrow$ 11) in the range, 0–30  $\mu$ M at regular increments of 3  $\mu$ M. Inset shows the decrease in the relative fluorescence intensity at 338 nm ( $FI_{338 \text{ nm}}$ ) with increasing 6S/HSA molar ratios.



**Figure 3.39.** Stern-Volmer plots for the fluorescence quenching data of the 6S-HSA system at four different temperatures, i.e., 15 °C, 25 °C, 35 °C and 45 °C.

**Table 3.9.** Quenching and binding parameters for the interaction of 6S with HSA, obtained from fluorescence quenching titration experiments at different temperatures, pH 7.4.

$T$ ( $^{\circ}\text{C}$ / $\text{K}$ )	$K_{\text{SV}}$ ( $\text{M}^{-1}$ )	$k_{\text{q}}$ ( $\text{M}^{-1} \text{s}^{-1}$ )	$K_{\text{a}}$ ( $\text{M}^{-1}$ )
15 / 288	$(6.47 \pm 0.20) \times 10^4$	$(1.01 \pm 0.04) \times 10^{13}$	$(7.51 \pm 0.36) \times 10^4$
25 / 298	$(5.71 \pm 0.16) \times 10^4$	$(8.95 \pm 0.25) \times 10^{12}$	$(6.29 \pm 0.33) \times 10^4$
35 / 308	$(5.25 \pm 0.23) \times 10^4$	$(8.23 \pm 0.35) \times 10^{12}$	$(5.56 \pm 0.27) \times 10^4$
45 / 318	$(4.47 \pm 0.27) \times 10^4$	$(7.01 \pm 0.43) \times 10^{12}$	$(4.68 \pm 0.42) \times 10^4$

the bimolecular quenching constant,  $k_q$ , calculated for the 6S–HSA system (Table 3.9) in comparison to that obtained for a typical diffusion-controlled phenomenon ( $\sim 10^{10} \text{ M}^{-1} \text{ s}^{-1}$ ) further supported the complex formation between 6S and HSA (Lakowicz, 2006).

The fluorescence data were also analyzed according to the double logarithmic equation (Eq. 4) to determine the association constant,  $K_a$  of the binding reaction. Figure 3.40 shows linear plots between  $\log [(F_0 - F) / F]$  and  $\log [1 / ([L_T] - (F_0 - F)[P_T] / F_0)]$  for 6S–HSA system, obtained at different temperatures. The values of  $K_a$  were calculated from the y-axis intercept of these plots and are listed in Table 3.9. The magnitude of the  $K_a$  values ( $4.68\text{--}7.51 \times 10^4 \text{ M}^{-1}$ ), obtained at different temperatures clearly revealed a moderate binding affinity between 6S and HSA. Such value of  $K_a$  is favorable for efficient transportation of the ligand in circulation and its release at the target site (Dufour & Dangles, 2005). A comparison of the  $K_a$  values, obtained for the three phytochemicals (FB, PS and 6S) used in this study, revealed that the binding affinity between 6S and HSA closely matched to those obtained for the FB–HSA and PS–HSA systems (Tables 3.1 and 3.5). In view of this, it is reasonable to suggest that the pharmacokinetic properties of 6S such as the ratio of its free/bound concentrations, duration of the pharmacological efficacy and *in vivo* half-life would be more or less similar to FB, PS and other therapeutic compounds, possessing similar binding characteristics (Table 1.4).

### 3.3.2. *Thermodynamic parameters and binding forces*

In order to determine thermodynamic parameters associated with the binding reaction, van't Hoff plot (Figure 3.41) was used to obtain the values of  $\Delta S$  and  $\Delta H$ . These values were incorporated into Eq. 6 to calculate  $\Delta G$  at different temperatures as described in the Section 2.2.4.2. The values of thermodynamic parameters are listed in Table 3.10. The spontaneity of the binding reaction was evident from the negative values of  $\Delta G$ . The overall 6S–HSA association can be viewed as proceeding through hydrophobic interactions between the ligand and the protein, as indicated by the positive entropy

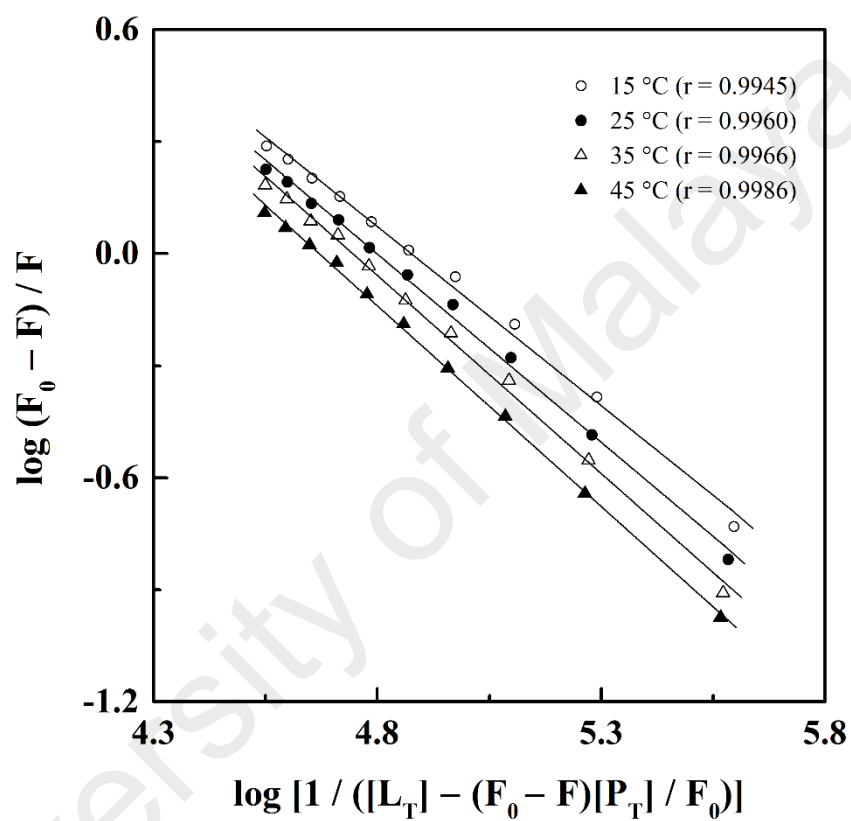


**Figure 3.40.** Double logarithmic plots of  $\log (F_0 - F) / F$  versus  $\log [1 / ([L_T] - (F_0 - F)[P_T] / F_0)]$  for the fluorescence quenching data of the 6S-HSA system at four different temperatures, i.e., 15 °C, 25 °C, 35 °C and 45 °C.

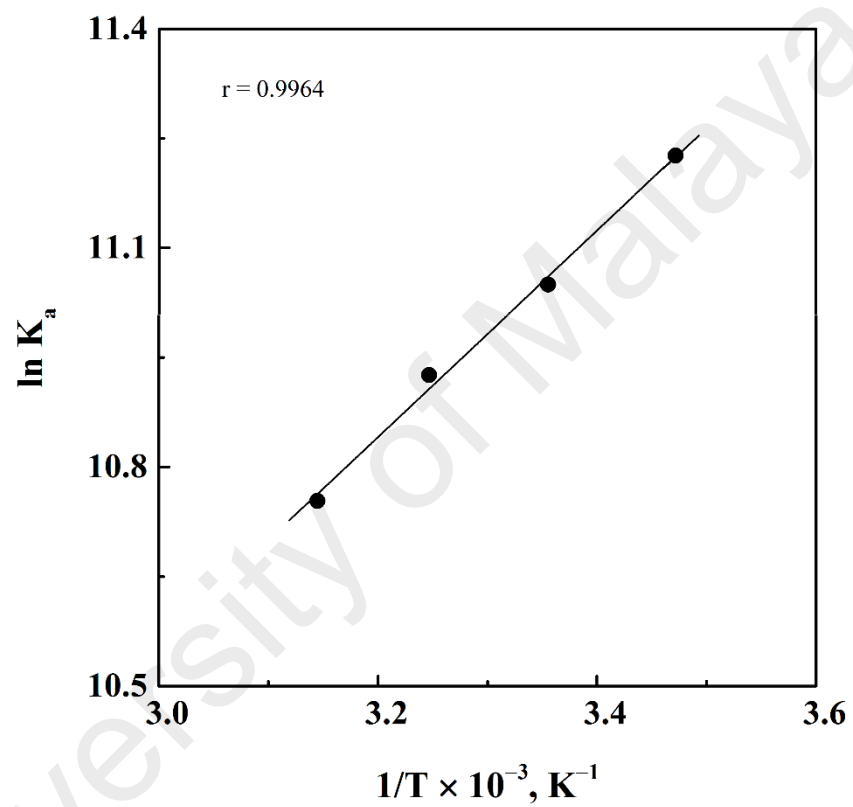


**Figure 3.41.** van't Hoff plot for the interaction between 6S and HSA. Values of  $K_a$  were obtained from the double logarithmic plots shown in Figure 3.40.

**Table 3.10.** Thermodynamic parameters for the interaction of 6S with HSA, obtained from fluorescence quenching titration experiments at different temperatures, pH 7.4.

$T$ ( $^{\circ}\text{C}$ / $\text{K}$ )	$\Delta S$ ( $\text{J mol}^{-1} \text{K}^{-1}$ )	$\Delta H$ ( $\text{kJ mol}^{-1}$ )	$\Delta G$ ( $\text{kJ mol}^{-1}$ )
15 / 288			-26.88
25 / 298	52.52	-11.76	-27.41
35 / 308			-27.93
45 / 318			-28.46

change ( $\Delta S = 52.52 \text{ J mol}^{-1} \text{ K}^{-1}$ ) (Ross & Subramanian, 1981). The partial disordering of the highly organized solvent structures around the ligand and the protein may account for the positive entropic contribution, observed in the binding reaction. This is supported by the apolar nature of 6S due to the presence of a 10-carbon long hydrocarbon chain and benzenoid structure. A variety of short range interactions seem to occur between the closely associated (hydrophobically) ligand and protein molecules. Formation of hydrogen bonds is always accompanied by the liberation of heat, resulting in a negative  $\Delta H$  value and it is highly likely to occur between 6S and HSA due to the presence of several polar groups in the ligand. This is further supported by our molecular docking results (Section 3.3.6), which predicted hydrogen bonding between the polar moieties of 6S and the amino acid residues of HSA. van der Waals forces also exhibit similar thermodynamic characteristics as shown by hydrogen bonds (Ross and Subramanian, 1981); thus, participation of van der Waals forces in the binding process cannot be excluded. While positive  $\Delta S$  value of the reaction points toward the involvement of electrostatic forces, this seems rather improbable in practice. Analysis of 6S structure using ALOGPS 2.1 software (Tetko et al., 2005) predicted a  $pK_a$  value of 9.8. Hence, at the experimental pH of 7.4, its only ionizable group ( $-\text{OH}$ ) remained in protonated form (neutral compound), which eliminates the role of electrostatic interactions in the 6S–HSA system.

### **3.3.3. *Microenvironmental alterations around HSA fluorophores***

In view of the absence of any shift in the emission maximum as shown in the titration results (Figure 3.38), synchronous fluorescence spectra of HSA in the presence of 6S were not measured. Since 3-D fluorescence spectra of a protein is the cumulative reflection of the change in the microenvironment around protein fluorophores, protein samples were subjected to 3-D fluorescence spectroscopy in the absence and the presence of 6S.

### 3.3.3.1. Three-dimensional fluorescence spectra

The 3-D fluorescence spectra and corresponding contour maps of free HSA (A) as well as 6S-bound HSA at a 6S/HSA molar ratio of 2:1 (B) and 4:1 (C) are shown in Figure 3.42. The fluorescence characteristics (peak position and intensity) of these spectra are given in Table 3.11. As described earlier in the Sections 3.1.3.2 and 3.2.3.2, the peaks marked as '1' and '2' represent protein fluorescence peaks due to Trp and Tyr residues. Addition of 6S to the protein in a 2:1 molar ratio produced significant reduction in the fluorescence intensity, as 22% and 25% quenching was observed for peaks '1' and '2', respectively. This was accompanied by a blue shift in the emission maximum of 2 and 3 nm for peaks '1' and '2', respectively. These changes became more pronounced at 4:1 6S/HSA molar ratio, where peak '1' showed 38% quenching and a blue shift of 3 nm in the emission maximum, compared to 40% quenching and 6 nm blue shift in the emission maximum, obtained for peak '2'. Such changes in the fluorescence characteristics, observed in the presence of 6S were suggestive of microenvironmental alteration around protein fluorophores induced by 6S binding. A comparative analysis of the 3-D fluorescence spectral results of HSA in the presence of FB (Table 3.3), PS (Table 3.7) and 6S (Table 3.11) showed relatively lesser microenvironmental perturbation around HSA fluorophores upon interaction with 6S. Absence of shift in the emission maximum in the titration results, shown in Figure 3.38 against the blue shift observed in the 3-D fluorescence spectra (Table 3.11) may be ascribed to different excitation wavelengths, used in these experiments.

### 3.3.4. 6S-induced thermal stabilization of HSA

In order to investigate the influence of 6S–HSA complexation on the thermal stability of HSA,  $CD_{222\text{ nm}}$  values of the protein were recorded in the absence and the presence of 6S in the temperature ranges, 25–100 °C and 25–80 °C. Renaturation experiments were also performed upon cooling the heated samples down to 25 °C to examine the

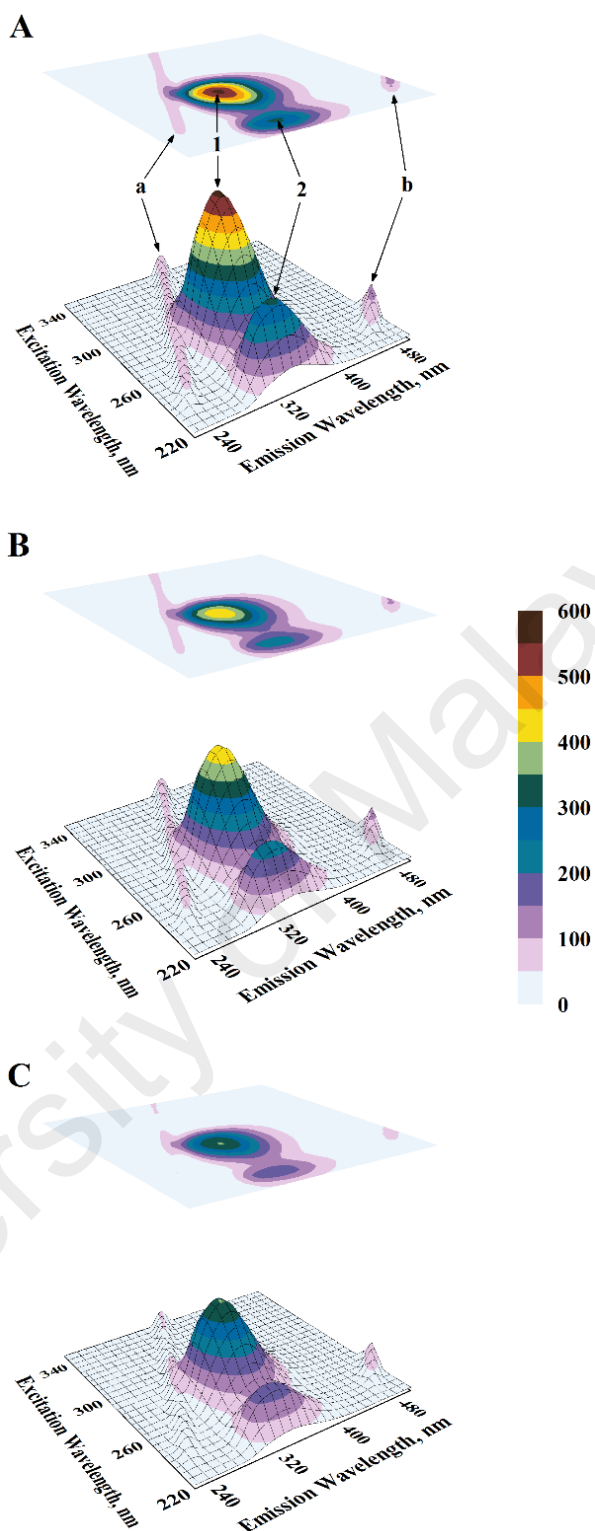


**Figure 3.42.** Three-dimensional fluorescence spectra and corresponding contour maps of (A) HSA (3  $\mu\text{M}$ ), (B) 6S-HSA (2:1) complex and (C) 6S-HSA (4:1) complex, obtained in 10 mM sodium phosphate buffer, pH 7.4 at 25  $^{\circ}\text{C}$ .

**Table 3.11.** Three-dimensional fluorescence spectral characteristics of HSA and 6S–HSA complexes at pH 7.4, 25 °C.

System	Peak	Peak position [ $\lambda_{ex}/\lambda_{em}$ (nm/nm)]	Intensity
HSA	a	230/230 → 350/350	19.18 → 79.06
	b	250/500	125.96
	1	280/336	560.17
	2	235/331	308.49
[6S]:[HSA] = 2:1	a	230/230 → 350/350	17.27 → 70.26
	b	250/500	116.75
	1	280/334	435.59
	2	235/328	230.93
[6S]:[HSA] = 4:1	a	230/230 → 350/350	13.82 → 56.21
	b	250/500	93.40
	1	280/333	348.47
	2	235/325	184.74

reversibility of the denaturation phenomena. As shown in Figure 3.43A, thermal denaturation profiles of HSA as well as its complex with 6S were found to be similar within a temperature range 25–94 °C. However, the denaturation curve of 6S–HSA complex showed a relatively lesser loss in the CD<sub>222 nm</sub> value compared to HSA, demonstrating relatively higher resistance against thermal denaturation. As discussed in the Section 3.1.4, a drastic decrease in the CD<sub>222 nm</sub> value of HSA due to the formation of protein aggregates was observed beyond 94 °C. In contrast, the 6S–HSA complex showed no aggregation beyond 94 °C and significant recovery (58%) in the CD<sub>222 nm</sub> signal was observed upon renaturation at 25 °C. These observations clearly suggested a higher thermal stability of HSA conferred by 6S binding.

In view of the aggregation phenomenon observed at higher temperatures, denaturation experiments were also performed in the temperature range, 25–80 °C (Figure 3.43B). As evident from the figure, HSA showed partial refolding in the cooling experiment, characterized by 50% regain in the CD<sub>222 nm</sub> signal. On the other hand, 71% reversal in the CD<sub>222 nm</sub> value of HSA was achieved in the presence of 6S at 25 °C; thus conclusively demonstrating the stabilizing effect of 6S on the thermal stability of HSA.

### 3.3.5. *Binding site specificity of 6S on HSA*

In order to ascertain the binding site of 6S on HSA, drug displacement experiments were performed using drug markers, PBZ and KTN which bind exclusively to Sudlow's sites I and II, respectively (Kragh-Hansen et al., 2002).

Figure 3.44 shows the effect of increasing PBZ concentrations (0–60 μM) on the fluorescence spectra of 3 μM HSA (A) and 6S–HSA (5:1) complex (B), upon excitation at 295 nm. Values of the fluorescence intensity at 338 nm were transformed into relative fluorescence intensity and plotted against PBZ concentration (Figure 3.45). As evident from the Figure 3.45, addition of PBZ to HSA led to a continuous decrease in the fluorescence intensity at 338 nm, reaching to 73% quenching at 60 μM PBZ. On the other

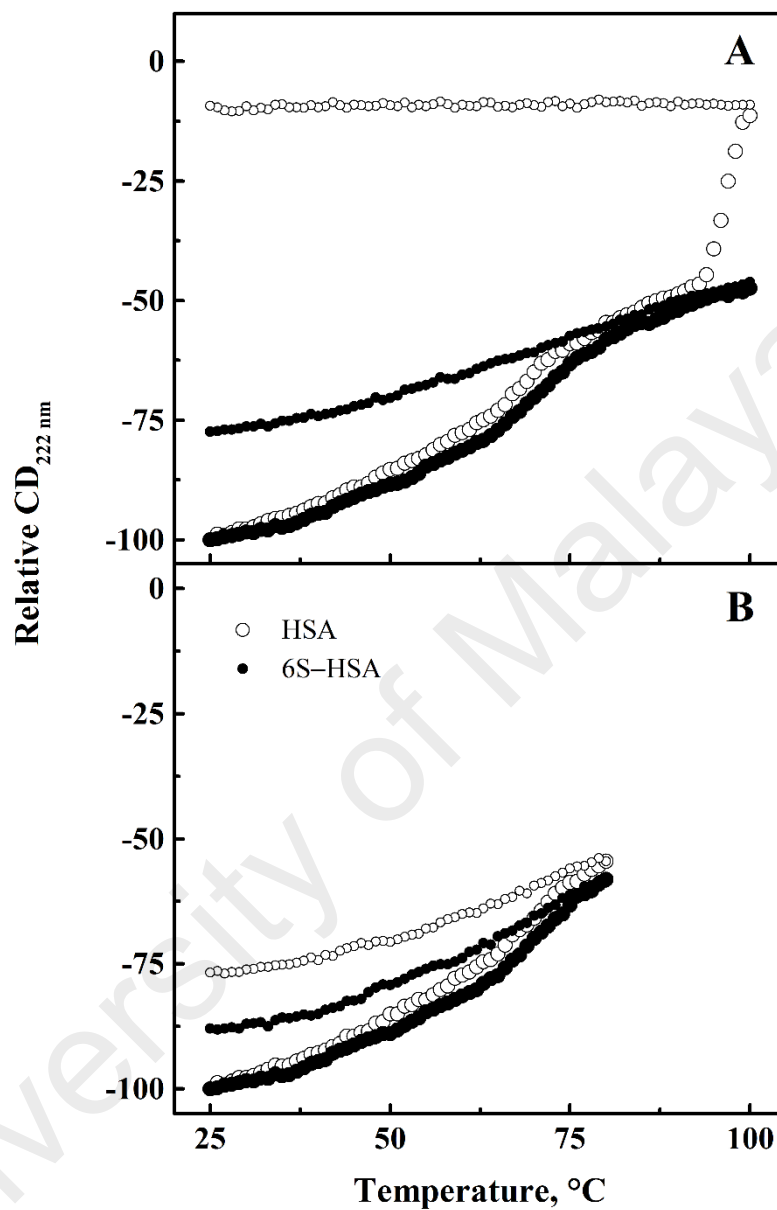


**Figure 3.43.** Thermal denaturation and renaturation curves of HSA (3  $\mu\text{M}$ ) and 6S-HSA (4:1) complex, as studied by  $\text{CD}_{222 \text{ nm}}$  measurements in the temperature range, 25–100 °C (A) and 25–80 °C (B) in 10 mM sodium phosphate buffer, pH 7.4. Renaturation curves are shown with smaller symbols.

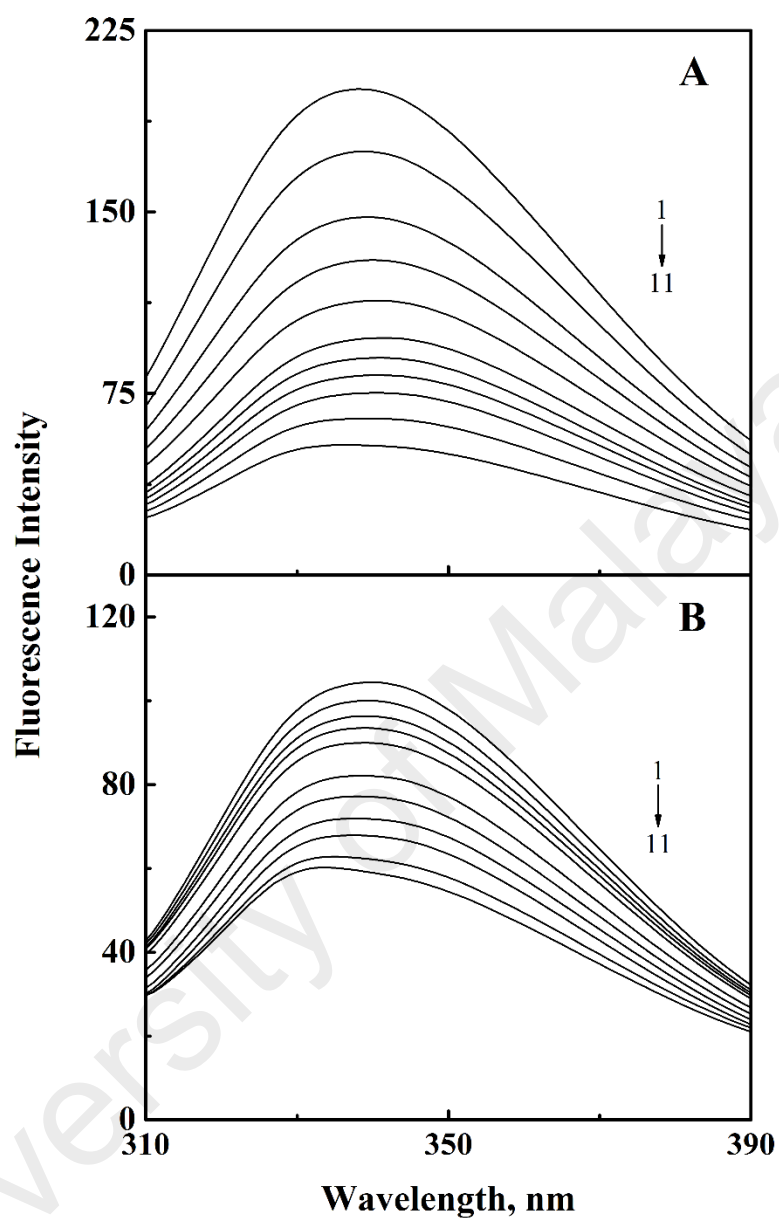


**Figure 3.44.** Fluorescence spectra of (A) HSA (3  $\mu\text{M}$ ) and (B) 6S-HSA (5:1) complex in the absence and the presence of increasing PBZ concentrations, obtained in 10 mM sodium phosphate buffer, pH 7.4 at 25  $^{\circ}\text{C}$  upon excitation at 295 nm. The PBZ concentration was varied (from top to bottom, 1 $\rightarrow$ 11) as 0, 0.75, 1.5, 2.25, 3.0, 9.0, 15.0, 22.5, 30.0, 45.0 and 60.0  $\mu\text{M}$ , respectively.

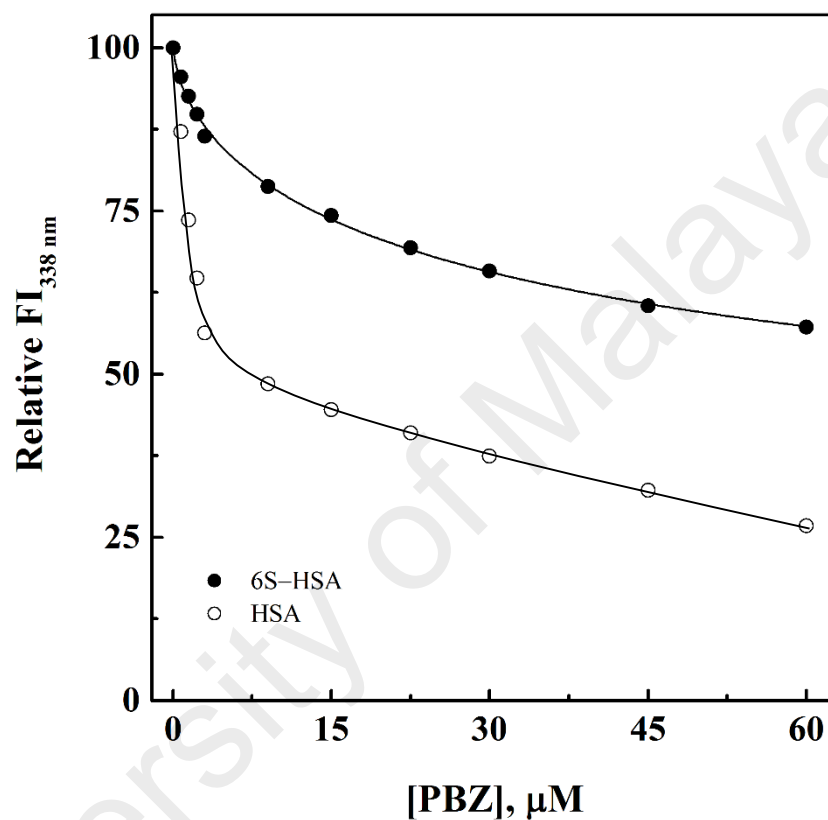


**Figure 3.45.** Plots showing the decrease in the relative fluorescence intensity at 338 nm ( $\text{FI}_{338 \text{ nm}}$ ) of HSA ( $3 \mu\text{M}$ ) and 6S-HSA (5:1) complex with increasing PBZ concentrations. Values of the relative  $\text{FI}_{338 \text{ nm}}$  were obtained from the spectra shown in Figure 3.44.

hand, presence of 6S in the mixture interrupted the quenching phenomena, thus leading to only 43% quenching at 60  $\mu\text{M}$  PBZ. These results indicated interference in PBZ–HSA interaction at site I by 6S, as both ligands seem to compete for the same binding site on the protein. To validate these observations, displacement experiments were also performed with HSA and PBZ–HSA mixture using 6S as the titrant and the fluorescence spectra, thus obtained are shown in Figure 3.46. Whereas a 63% reduction in the fluorescence intensity of HSA was observed at a 6S/protein molar ratio of 10:1, PBZ–HSA (5:1) system showed only 45% quenching (Figure 3.47). These results were similar to those shown in Figure 3.45. In conclusion, these displacement results suggested location of 6S binding site on HSA as site I or its vicinity.

In order to determine the involvement of site II in 6S–HSA interaction, competitive displacement experiments were also repeated using KTN as the marker ligand. As revealed by the displacement results presented in Figures 3.48 and 3.49, a markedly less pronounced difference was noticed between the fluorescence quenching observed with HSA and 6S–HSA (5:1) complex upon titration with KTN (0–22.5  $\mu\text{M}$ ). As can be seen from the Figure 3.49, around 14% difference in the KTN-induced quenching of HSA fluorescence was observed in the absence and the presence of 6S at 22.5  $\mu\text{M}$  KTN concentration. Furthermore, titration of HSA and KTN–HSA (5:1) complex with 6S (Figures 3.50 and 3.51) showed even smaller difference (9%) in the extent of fluorescence quenching observed in the absence and the presence of KTN at 30  $\mu\text{M}$  6S concentration. Although these results also indicated the involvement of site II in 6S–HSA interaction, there was noticeably less interference by KTN to 6S–HSA binding and vice versa. Overall, the drug displacement results pointed toward site I as the primary binding locus of 6S on HSA, with site II having a lower affinity.

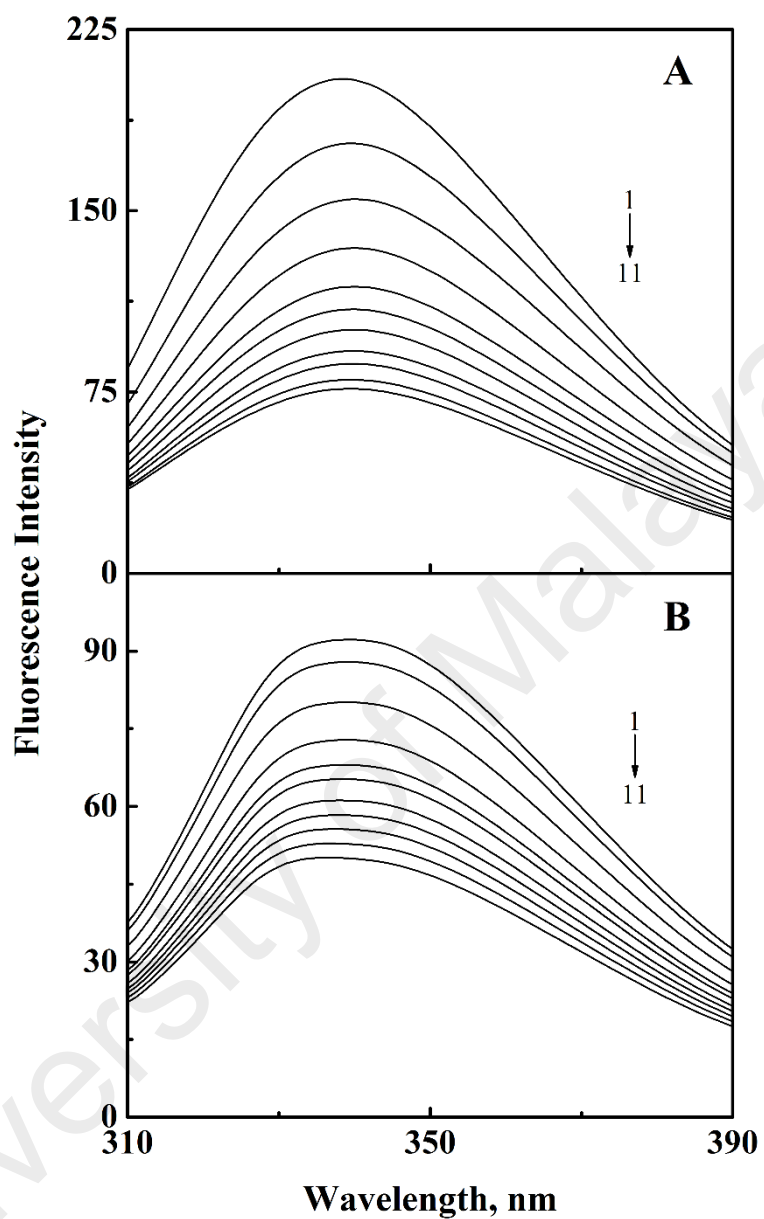


**Figure 3.46.** Fluorescence spectra of (A) HSA ( $3 \mu\text{M}$ ) and (B) PBZ-HSA (5:1) complex in the absence and the presence of increasing 6S concentrations, obtained in 10 mM sodium phosphate buffer, pH 7.4 at  $25 \text{ }^\circ\text{C}$  upon excitation at 295 nm. The 6S concentration was varied (from top to bottom, 1 $\rightarrow$ 11) in the range, 0– $30 \mu\text{M}$  at regular increments of  $3 \mu\text{M}$ .

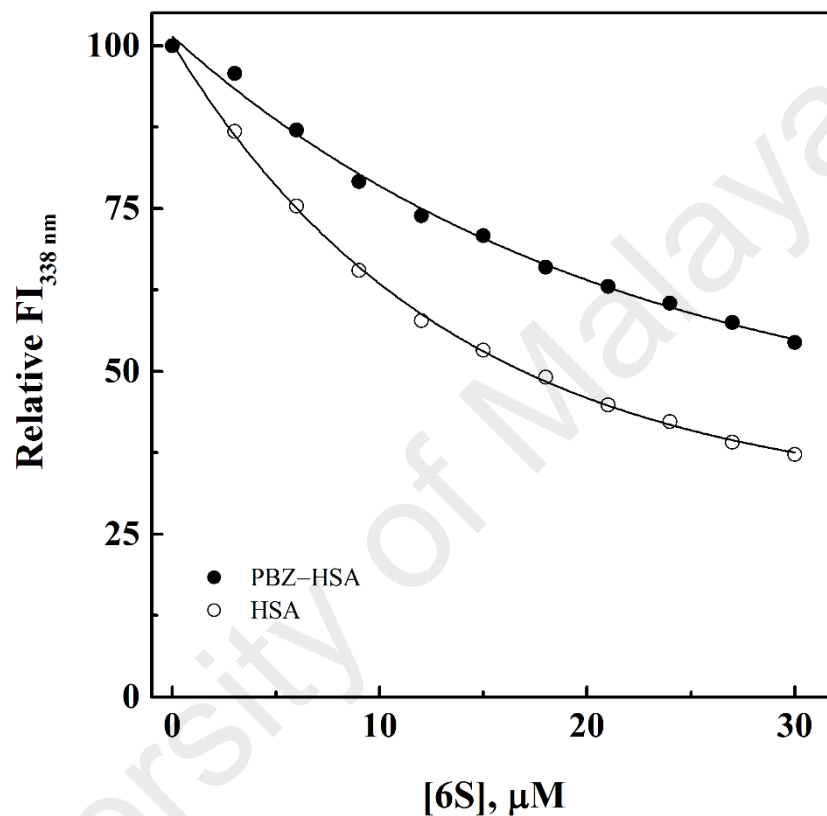


**Figure 3.47.** Plots showing the decrease in the relative fluorescence intensity at 338 nm ( $\text{FI}_{338 \text{ nm}}$ ) of HSA (3  $\mu\text{M}$ ) and PBZ-HSA (5:1) complex with increasing 6S concentrations. Values of the relative  $\text{FI}_{338 \text{ nm}}$  were obtained from the spectra shown in Figure 3.46.

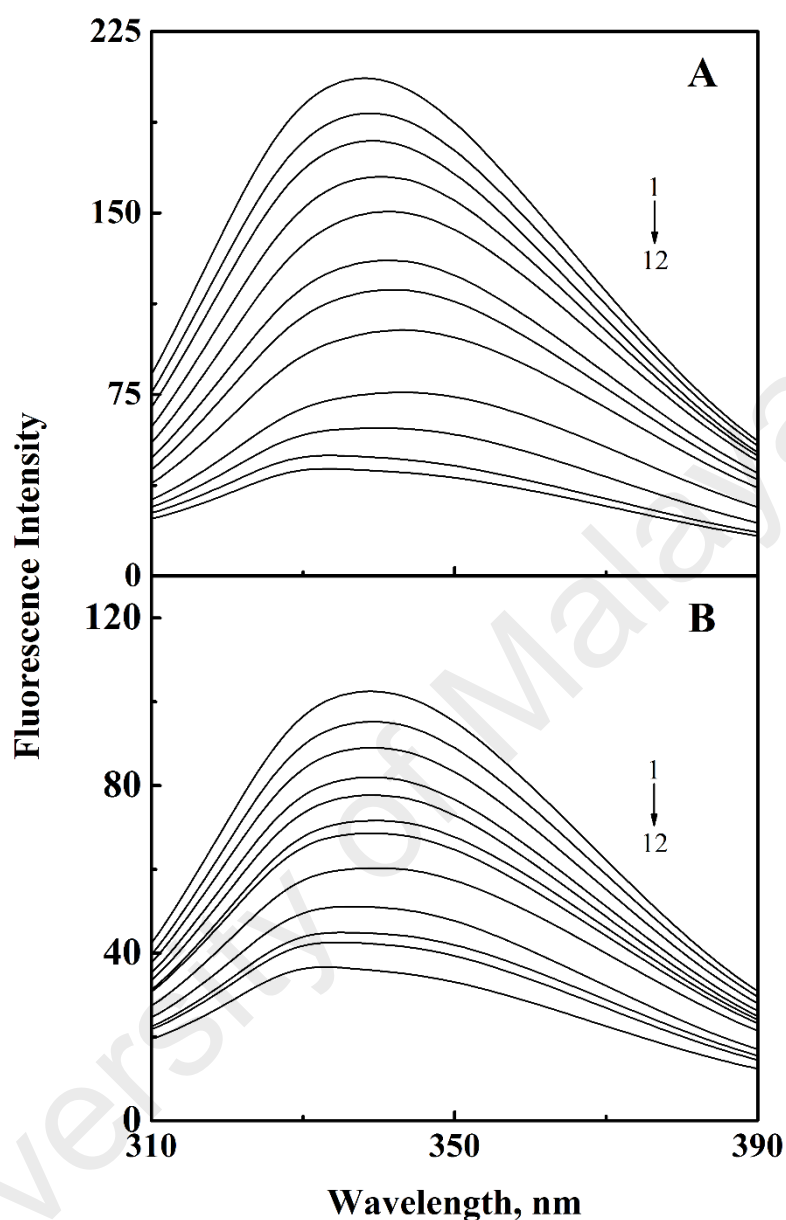


**Figure 3.48.** Fluorescence spectra of (A) HSA (3  $\mu\text{M}$ ) and (B) 6S-HSA (5:1) complex in the absence and the presence of increasing KTN concentrations, obtained in 10 mM sodium phosphate buffer, pH 7.4 at 25  $^{\circ}\text{C}$  upon excitation at 295 nm. The KTN concentration was varied (from top to bottom, 1 $\rightarrow$ 12) as 0, 0.75, 1.5, 2.25, 3.0, 3.75, 4.5, 6.0, 9.0, 12.0, 15.0 and 22.5  $\mu\text{M}$ , respectively.

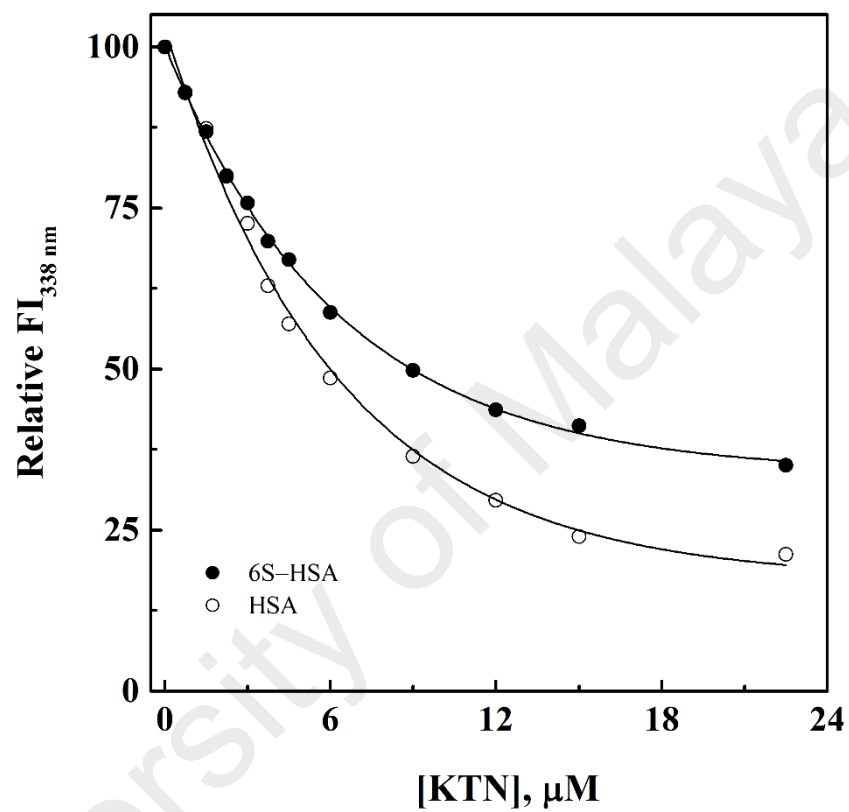


**Figure 3.49.** Plots showing the decrease in the relative fluorescence intensity at 338 nm ( $\text{FI}_{338 \text{ nm}}$ ) of HSA ( $3 \mu\text{M}$ ) and 6S-HSA (5:1) complex with increasing KTN concentrations. Values of the relative  $\text{FI}_{338 \text{ nm}}$  were obtained from the spectra shown in Figure 3.48.

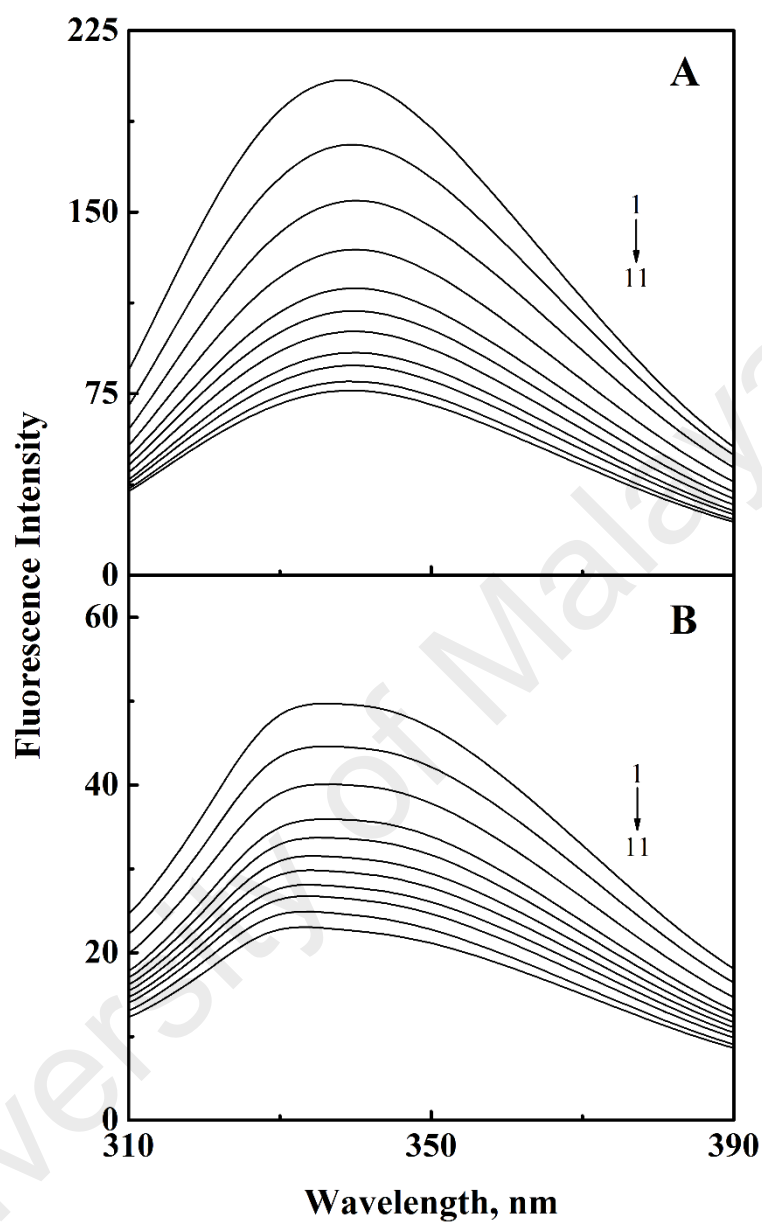


**Figure 3.50.** Fluorescence spectra of (A) HSA ( $3 \mu\text{M}$ ) and (B) KTN-HSA (5:1) complex in the absence and the presence of increasing 6S concentrations, obtained in 10 mM sodium phosphate buffer, pH 7.4 at  $25 \text{ }^\circ\text{C}$  upon excitation at 295 nm. The 6S concentration was varied (from top to bottom, 1 $\rightarrow$ 11) in the range, 0–30  $\mu\text{M}$  at regular increments of 3  $\mu\text{M}$ .

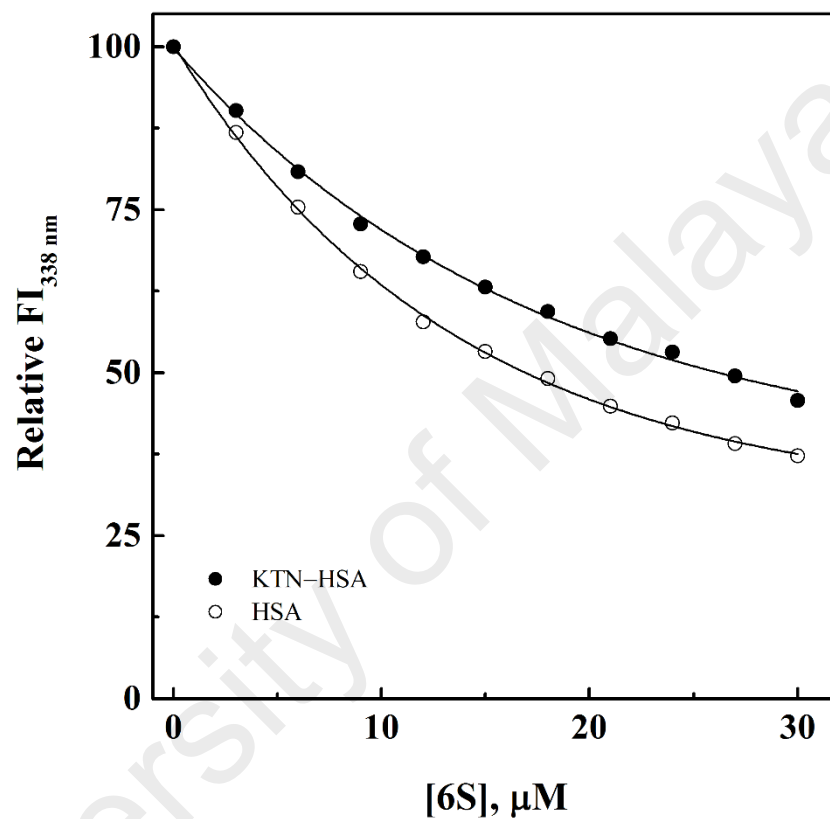


**Figure 3.51.** Plots showing the decrease in the relative fluorescence intensity at 338 nm ( $\text{FI}_{338 \text{ nm}}$ ) of HSA (3  $\mu\text{M}$ ) and KTN-HSA (5:1) complex with increasing 6S concentrations. Values of the relative  $\text{FI}_{338 \text{ nm}}$  were obtained from the spectra shown in Figure 3.50.

### 3.3.6. *Molecular docking*

Docking studies of 6S–HSA interaction were performed to predict the binding of 6S to the two main ligand binding sites of HSA and to validate the drug displacement results. The procedures were carried out in the same way as described in the Section 3.2.6 for PS–HSA system, using three crystal structures of HSA (1BM0, 2BXD and 2BXF) to validate the docking workflow.

The docking analysis of the 6S–1BM0 complex revealed a total of 33 conformation clusters for site I, with the majority of the clusters being single- or double-membered (Figure 3.52A). The highest populated cluster contained 20 out of 100 conformations and was also the most energetically favorable cluster, possessing a mean binding energy of  $-23.27 \text{ kJ mol}^{-1}$ . A similar clustering pattern dominated by single-membered clusters was also observed for site II, where a total of 49 conformation clusters were populated (Figure 3.52B). The two highest populated clusters had the same number of conformations (11 conformations each) and comparable mean binding energies of  $-17.04 \text{ kJ mol}^{-1}$  and  $-16.66 \text{ kJ mol}^{-1}$ . The fewer conformational clusters and lower binding energy associated with docking at site I thus, strongly suggested the preference of 6S to site I and supported the experimental findings, described in the Section 3.3.5.

Clustering analysis of the 6S–2BXD (Figure 3.53) and 6S–2BXF (Figure 3.54) complexes also showed similar results in terms of the binding energy at site I, strengthening our conclusion about site I of HSA as the primary binding site of 6S. However, comparison of the clustering results for site II revealed that the mean binding energy was significantly lower and the number of conformations in the highest populated cluster for site II was also larger than its counterpart for site I, when 6S was docked to 2BXF. In view of these observations, it appears that binding of DZP to HSA might have induced a change in the geometry of site II, which allowed 6S to interact more favorably to HSA at this binding site.

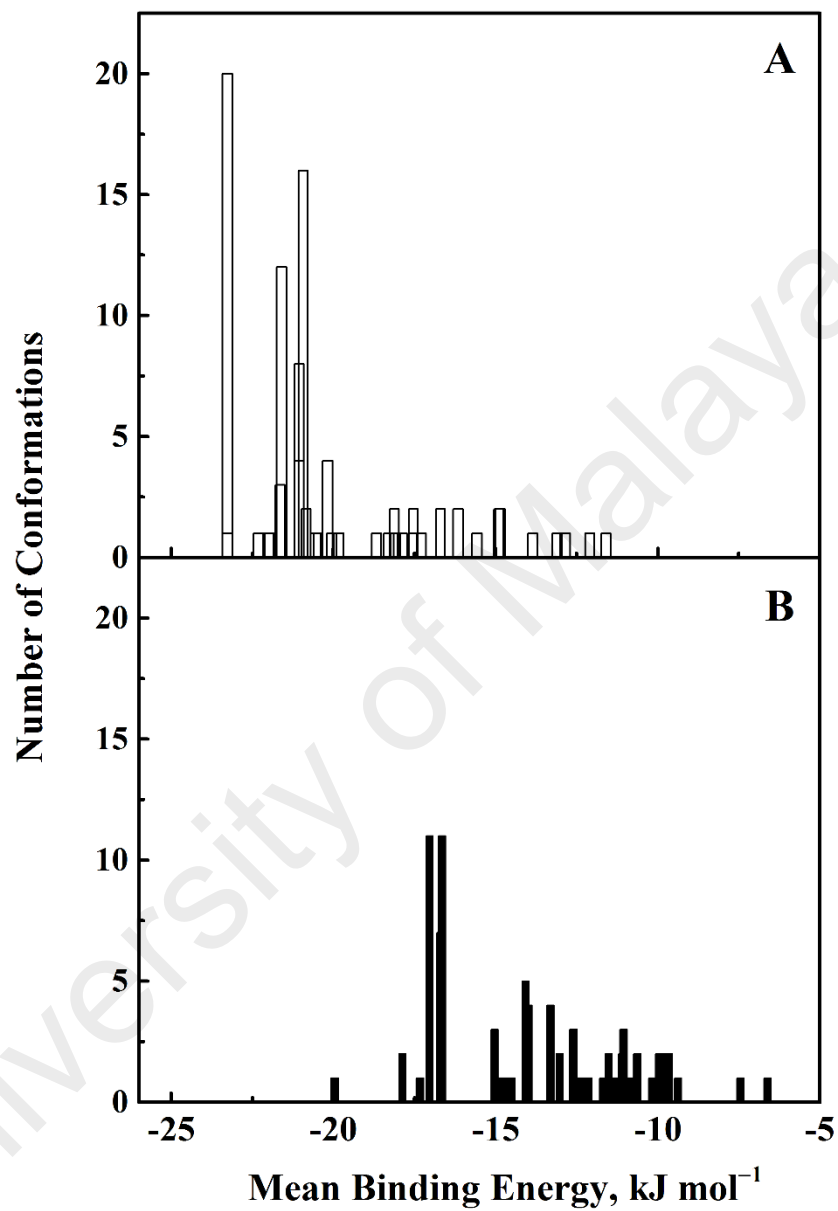


**Figure 3.52.** Cluster analysis of the docking of 6S to Sudlow's sites I (A) and II (B) of HSA crystal structure (1BM0). A total of 100 runs were performed for each binding site.

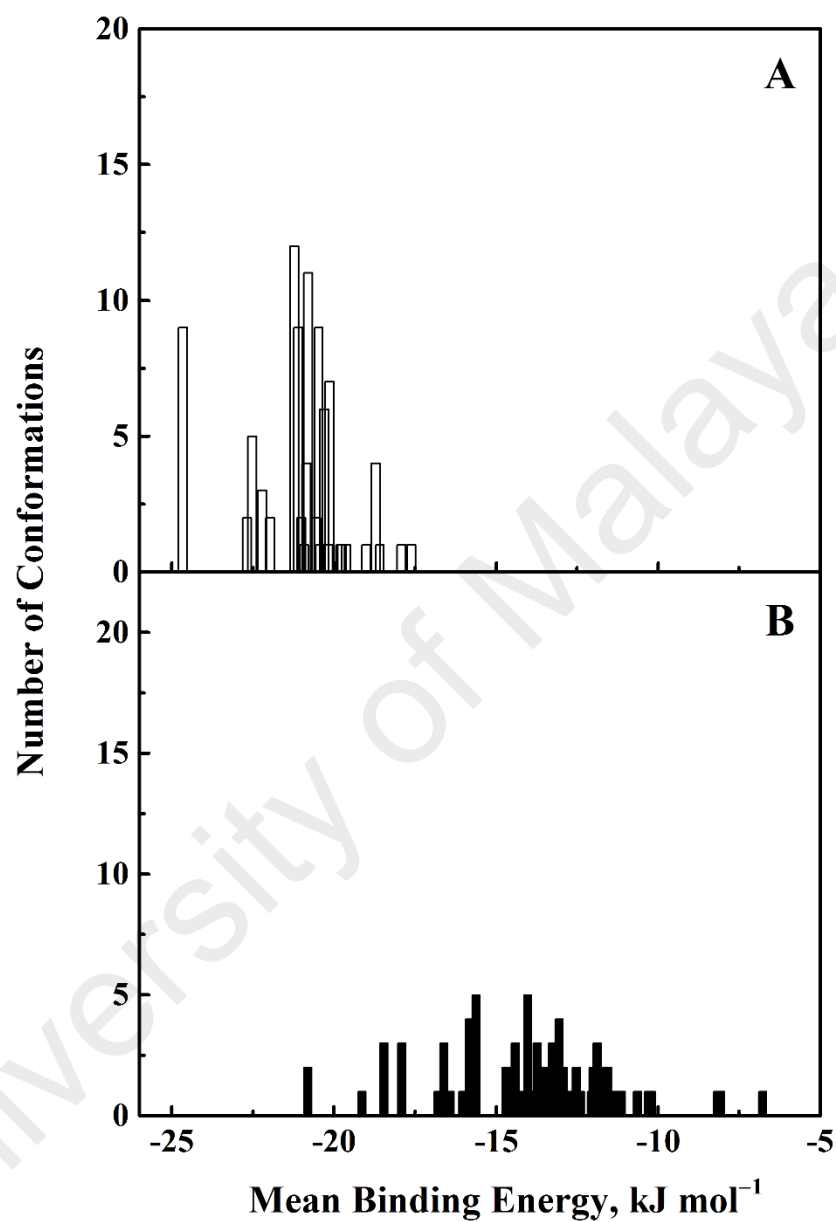


**Figure 3.53.** Cluster analysis of the docking of 6S to Sudlow's sites I (A) and II (B) of HSA crystal structure (2BXD). A total of 100 runs were performed for each binding site.

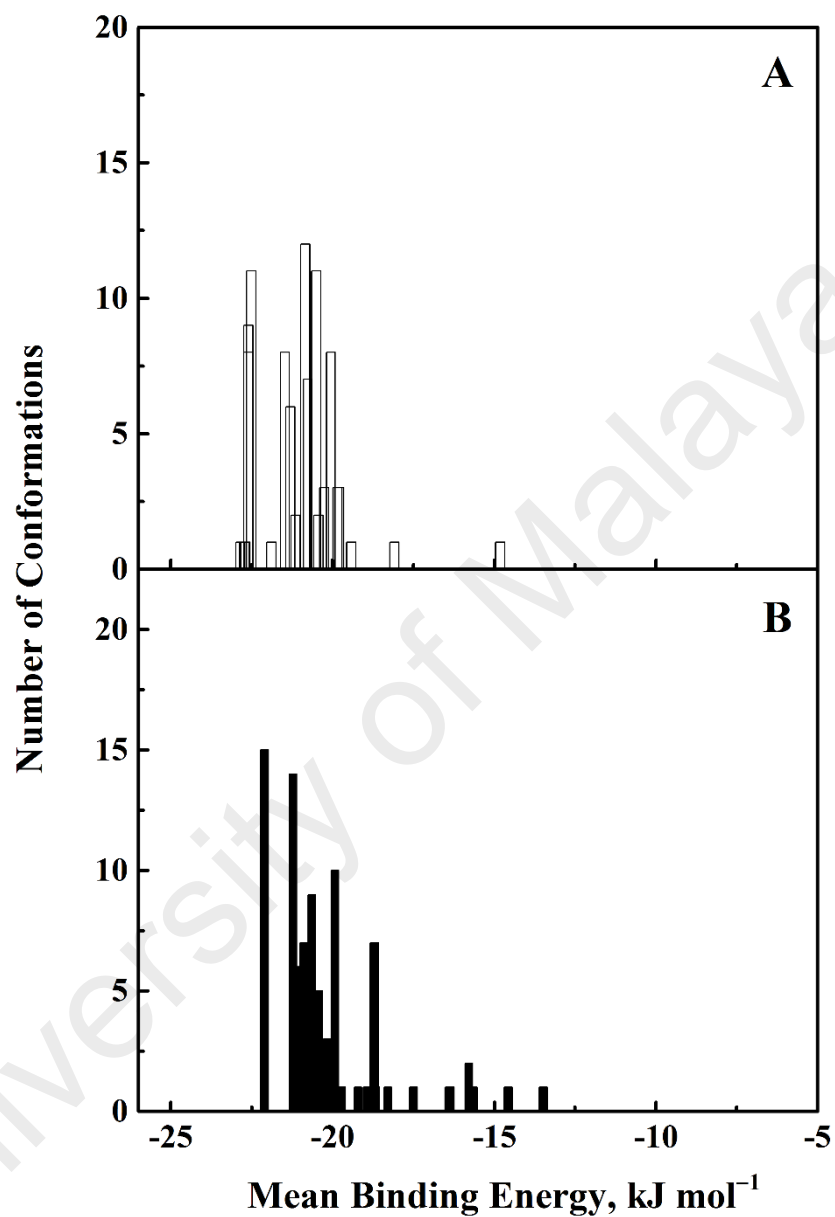


**Figure 3.54.** Cluster analysis of the docking of 6S to Sudlow's sites I (A) and II (B) of HSA crystal structure (2BXF). A total of 100 runs were performed for each binding site.

The predicted binding models showing minimum docking energy for both sites I and II, were then used to analyze the binding orientations. 6S binding site at site I (Figure 3.55) was largely comprised of a hydrophobic cleft, walled by the amino acid residues: Tyr-150, Glu-153, Phe-157, Ala-191, Ser-192, Ser-193, Lys-195, Gln-196, Lys-199, Leu-219, Arg-222, Phe-223, Leu-234, Leu-238, His-242, Arg-257, Leu-260, Ile-264, Ser-287, His-288, Ile-290, Ala-291 and Glu-292. Although hydrophobic interactions between nonpolar amino acid residues and 6S contributed significantly towards the docking stability in the simulation, hydrogen bonding also had a major influence in stabilizing the complex. Three hydrogen bonds were predicted between 6S and HSA at site I, involving Tyr-150, Gln-196 and Arg-257 (details are listed in Table 3.12). On the other hand, at site II (Figure 3.56), the ligand was orientated outward (toward the surface), with its binding pocket bordered by the following residues: Leu-398, Lys-402, Asn-405, Ala-406, Lys-409, Arg-410, Tyr-411, Lys-413, Lys-414, Leu-491, Glu- 492, Val-493, Asp-494, Thr-540, Lys-541 and Lys-545. Furthermore, only a single hydrogen bond was predicted, linking Lys-414 and the hydroxyl oxygen of 6S (Table 3.12).

In summary, the above results provide a detailed description of the interaction of a bioactive ginger constituent, 6S with HSA in terms of binding mode, thermodynamic characteristics, effect on protein thermal stability, as well as binding location. Fluorescence quenching titration experiments revealed the binding of 6S to HSA to be of moderate affinity, while thermodynamic data and molecular docking results suggested the involvement of hydrogen bonds as well as hydrophobic and van der Waals forces in 6S–HSA interaction. The binding reaction also led to a significant increase in HSA thermal stability and 6S was found to interact with both Sudlow’s sites I and II, site I being the preferred site.

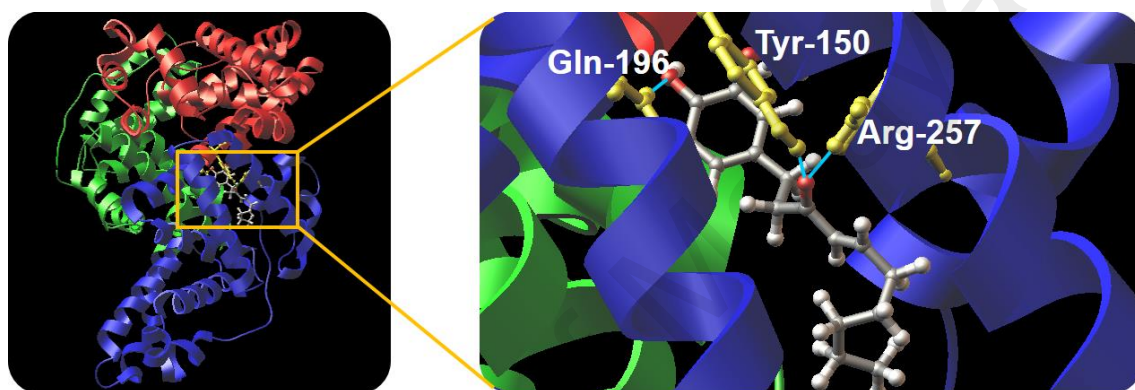


**Figure 3.55.** Binding orientation of the lowest docking energy conformation of 6S (ball and stick rendered) in Sudlow's site I (subdomain IIA) of HSA (1BM0). Domains I, II and III of HSA are represented in red, blue and green, respectively. The zoomed-in view of the binding site shows the hydrogen bonds (turquoise lines) formed between 6S and amino acid side chains of HSA (yellow).

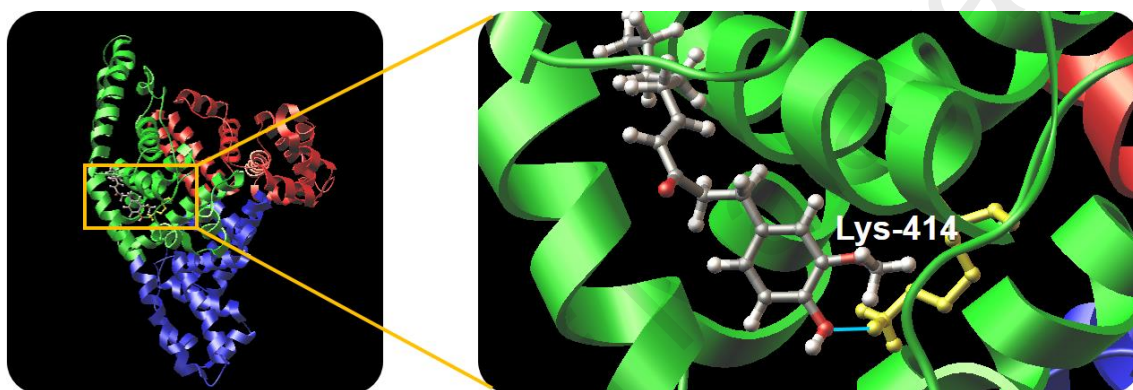


**Figure 3.56.** Binding orientation of the lowest docking energy conformation of 6S (ball and stick rendered) in Sudlow's site II (subdomain IIIA) of HSA (1BM0). Domains I, II and III of HSA are represented in red, blue and green, respectively. The zoomed-in view of the binding site shows the hydrogen bond (turquoise line) formed between 6S and amino acid side chain of HSA (yellow).

**Table 3.12.** Distance of the predicted hydrogen bonds formed between interacting atoms of the amino acid residues of HSA and 6S.

HSA atom	6S atom	Distance (Å)
<i>Site I</i>		
Tyr-150: HH	O (carbonyl)	1.88
Gln-196: HE21	O (hydroxyl)	2.20
Arg-257: HE	O (carbonyl)	1.86
<i>Site II</i>		
Lys-414: HZ2	O (hydroxyl)	1.94



*Chapter 4*

---

# CONCLUSIONS

---



## 4. CONCLUSIONS

In conclusion, the work presented in this thesis provides a comprehensive description of the interactions of three pharmacologically active phytochemicals from the Zingiberaceae family, i.e., FB, PS and 6S with the major transport protein in humans, HSA. Although minor differences in the binding parameters were found, the binding characteristics of these compounds were for the most part similar and comparable to the many other phytochemicals. These ligands displayed moderate affinity towards HSA and their complexation with the protein was stabilized by van der Waals force, hydrophobic interaction and hydrogen bonding. Binding of these compounds to HSA led to significant alteration in the protein fluorophores' microenvironment but increased protein's thermal stability. Whereas FB and PS exhibited a clear binding preference towards site I of HSA, 6S was demonstrated to bind to both sites I and II. Docking results verified the location of binding sites. Investigations on the binding of such therapeutic compounds to HSA are of paramount importance in understanding chemico-biological interactions in clinical research and drug design. These results can be helpful in predicting the pharmacokinetic profiles of FB, PS and 6S, as well as other structurally similar molecules.



*Chapter 5*

---

## REFERENCES

---



## 5. REFERENCES

- Abdelwahab, S. I., Mohan, S., Abdulla, M. A., Sukari, M. A., Abdul, A. B., Taha, M. M. E., Syam, S., Ahmad, S., & Lee, K. -H. (2011). The methanolic extract of *Boesenbergia rotunda* (L.) Mansf. and its major compound pinostrobin induces anti-ulcerogenic property *in vivo*: Possible involvement of indirect antioxidant action. *Journal of Ethnopharmacology*, 137: 963–970.
- Abdollahpour, N., Asoodeh, A., Saberi, M. R., & Chamani, J. (2011). Separate and simultaneous binding effects of aspirin and amlodipine to human serum albumin based on fluorescence spectroscopic and molecular modeling characterizations: A mechanistic insight for determining usage drugs doses. *Journal of Luminescence*, 131: 1885–1899.
- Abou-Zied, O. K., & Al-Shihi, O. I. (2008). Characterization of subdomain IIA binding site of human serum albumin in its native, unfolded, and refolded states using small molecular probes. *Journal of the American Chemical Society*, 130: 10793–10801.
- Albengres, E., Urien, S., Kusmierk, J. & Tillement, J. P. (1982). Benoxaprofen: Plasma binding and binding interactions with some drugs and endogenous compounds. *European Journal of Rheumatology & Inflammation*, 5: 87–97.
- An, J., Gao, Y., Wang, J., Zhu, Q., Ma, Y., Wu, J., Sun, J., & Tang, Y. (2012). Flavokawain B induces apoptosis of non-small cell lung cancer H460 cells via Bax-initiated mitochondrial and JNK pathway. *Biotechnology Letters*, 34: 1781–1788.
- Anraku, M., Tsurusaki, Y., Watanabe, H., Maruyama, T., Kragh-Hansen, U., & Otagiri, M. (2004). Stabilizing mechanisms in commercial albumin preparations: Octanoate and *N*-acetyl-L-tryptophanate protect human serum albumin against heat and oxidative stress. *Biochimica et Biophysica Acta*, 1702: 9–17.
- Bhattacharya, A. A., Curry, S. & Franks, N. P. (2000). Binding of the general anesthetics propofol and halothane to human serum albumin. High resolution crystal structures. *The Journal of Biological Chemistry*, 275: 38731–38738.
- Berman, H. M., Westbrook, J., Feng, Z., Gilliland, G., Bhat, T. N., Weissig, H., Shindyalov, I. N., & Bourne, P. E. (2000). The Protein Data Bank. *Nucleic Acids Research*, 28: 235–242.
- Bertucci, C., Nanni, B., Raffaelli, A., & Salvadori, P. (1998). Chemical modification of human albumin at cys34 by ethacrynic acid: Structural characterisation and binding properties. *Journal of Pharmaceutical and Biomedical Analysis*, 18: 127–136.
- Bertucci, C., & Domenici, E. (2002). Reversible and covalent binding of drugs to human serum albumin: Methodological approaches and physiological relevance. *Current Medicinal Chemistry*, 9: 1463–1481.
- Bhamarapravati, S., Juthapruth, S., Mahachai, W., & Mahady, G. (2006). Antibacterial activity of *Boesenbergia rotunda* (L.) Mansf. and *Myristica fragrans* Houtt.

against *Helicobacter pylori*. *Songklanakarin Journal of Science and Technology*, 28: 157–163.

- Bi, S., Ding, L., Tian, Y., Song, D., Zhou, X., Liu, X., & Zhang, H. (2004). Investigation of the interaction between flavonoids and human serum albumin. *Journal of Molecular Structure*, 703: 37–45.
- Bischer, A., Zia-Amirhosseini, P., Iwaki, M., McDonagh, A. F., & Benet, L. Z. (1995). Stereoselective binding properties of naproxen glucuronide diastereomers to proteins. *Journal of Pharmacokinetics and Biopharmaceutics*, 23: 379–395.
- Bode, A. M., & Dong, Z. (2011). The amazing and mighty ginger. In I. F. F. Benzie & S. Wachtel-Galor (Eds.), *Herbal medicine: Biomolecular and clinical aspects*. (pp. 131–156). Boca Raton: CRC Press.
- Bos, O. J. M., Remijn, J. P. M., Fischer, M. J. E., Wilting, J., & Janssen, L. H. M. (1988a). Location and characterization of the warfarin binding site of human serum albumin: A comparative study of two large fragments. *Biochemical Pharmacology*, 37: 3905–3909.
- Bos, O. J. M., Fischer, M. J. E., Wilting, J., & Janssen, L. H. M. (1988b). Drug-binding and other physicochemical properties of a large tryptic and a large peptic fragment of human serum albumin. *Biochimica et Biophysica Acta*, 953: 37–47.
- Boudinot, F. D., Homon, C. A., Jusko, W. J., Ruelius, H. W. (1985). Protein binding of oxazepam and its glucuronide conjugates to human albumin. *Biochemical Pharmacology*, 34: 2115–2121.
- Boulton, D. W., Walle, U. K., & Walle, T. (1998). Extensive binding of the bioflavonoid quercetin to human plasma proteins. *Journal of Pharmacy and Pharmacology*, 50: 243–249.
- Brandts, J. F., & Lin, L. N. (1990). Study of strong to ultratight protein interactions using differential scanning calorimetry. *Biochemistry*, 29: 6927–6940.
- Bree, F., Urien, S., Nguyen, P., Tillement, J. P., Steiner, A., Vallat-Molliet, C., Testa, B., Visy, J., Simonyi, M. (1993). Human serum albumin conformational changes as induced by tenoxicam and modified by simultaneous diazepam binding. *Journal of Pharmacy and Pharmacology*, 45: 1050–1053.
- Brodersen, R. (1974). Competitive binding of bilirubin and drugs to human serum albumin studied by enzymatic oxidation. *The Journal of Clinical Investigation*, 54: 1353–1364.
- Brodersen, R., & Robertson, A. (1989). Ceftriaxone binding to human serum albumin: Competition with bilirubin. *Molecular Pharmacology*, 36: 478–483.
- Brown, J. R., & Shockley, P. (1982). Serum albumin: Structure and characterization of its ligand binding sites. In P. C. Jost & O. H. Griffith (Eds.), *Lipid-protein interactions* (pp. 25–68). New York: Wiley.
- Butler, M. S. (2005). Natural products to drugs: Natural product derived compounds in clinical trials. *Natural Product Reports*, 22: 162–195.

- Cannistraro, S., & Sacchetti, F. (1986). Rotational and translational dynamics of human albumin. *Physical Review A*, 33: 745–746.
- Carter, D. C., & Ho, J. X. (1994). Structure of serum albumin. *Advances in Protein Chemistry*, 45: 153–203.
- Castiglioni, A. (1985). *A history of medicine*. New York: Jason Aronson.
- Celej, M. S., Dassie, S. A., Gonzalez, M., Bianconi, M. L., & Fidelio, G. D. (2006). Differential scanning calorimetry as a tool to estimate binding parameters in multiligand binding proteins. *Analytical Biochemistry*, 350: 277–284.
- Chan, E. W. C., Ng, V. P., Tan, V. V., & Low, Y. Y. (2011). Antioxidant and antibacterial properties of *Alpinia galanga*, *Curcuma longa*, and *Etilingera elatior* (Zingiberaceae). *Pharmacognosy Journal*, 3: 54–61.
- Chen, I. -N., Chang, C. -C., Ng, C. -C., Wang, C. -Y., Shyu, Y. -T., & Chang, T. -L. (2008). Antioxidant and antimicrobial activity of Zingiberaceae plants in Taiwan. *Plant Foods for Human Nutrition*, 63: 15–20.
- Chi, Z., Liu, R., Yang, H., Shen, H., & Wang, J. (2011). Binding of tetracycline and chlortetracycline to the enzyme trypsin: Spectroscopic and molecular modeling investigations. *PLoS ONE*: 6: e28361.
- Chi, E. Y., Krishnan, S., Randolph, T. W., & Carpenter, J. F. (2003). Physical stability of proteins in aqueous solution: mechanism and driving forces in nonnative protein aggregation. *Pharmaceutical Research*, 20: 1325–1336.
- Chuang, V. T., & Otagiri, M. (2001). Flunitrazepam, a 7-nitro-1,4-benzodiazepine that is unable to bind to the indole-benzodiazepine site of human serum albumin. *Biochimica et Biophysica Acta*, 1546: 337–345.
- Connell, D. W. (1969). The pungent principles of ginger and their importance in certain ginger products. *Food Technology in Australia*, 21: 570–575.
- Cooke, N. E., Willard, H. F., David, E. V., & George, D. L. (1986). Direct regional assignment of the gene for vitamin D binding protein (Gc-globulin) to human chromosome 4q11-q13 and identification of an associated DNA polymorphism. *Human Genetics*, 73: 225–229.
- Curry, S., Mandelkow, H., Brick, P., & Franks, N. (1998). Crystal structure of human serum albumin complexed with fatty acid reveals an asymmetric distribution of binding sites. *Nature Structural & Molecular Biology*, 5: 827–835.
- Curry, S. (2009). Lessons from the crystallographic analysis of small molecule binding to human serum albumin. *Drug Metabolism and Pharmacokinetics*, 24: 342–357.
- Curry, S. (2011). X-ray crystallography of albumin. In M. Otagiri (Ed.), *Human serum albumin - New insights on its structural dynamics, functional impacts and pharmaceutical applications* (pp. 1–29). Kumamoto: Sojo University Publishing Center.

- Damsten, M. C., Commandeur, J. N. M., Fidder, A., Hulst, A. G., Touw, D., Noort, D., & Vermeulen, N. P. E. (2007). Liquid chromatography/tandem mass spectrometry detection of covalent binding of acetaminophen to human serum albumin. *Drug Metabolism & Disposition*, 35: 1408–1417.
- Dev, S. (1999). Ancient-modern concordance in Ayurvedic plants: Some examples. *Environmental Health Perspectives*, 107: 783–789.
- Dewar, M. J. S., Zoebisch, E. G., Healy, E. F., & Stewart, J. J. P. (1985). Development and use of quantum molecular models. 75. Comparative tests of theoretical procedures for studying chemical reactions. *Journal of the American Chemical Society*, 107: 3902–3909.
- Dieter, P., Krause, H., & Schulze-Specking, A. (1990). Arachidonate metabolism in macrophages is affected by albumin. *Eicosanoids*, 3: 45–51.
- Ding, F., Liu, W., Zhang, L., Yin, B., & Sun, Y. (2010). Sulfometuron-methyl binding to human serum albumin: Evidence that sulfometuron-methyl binds at the Sudlow's site I. *Journal of Molecular Structure*, 968: 59–66.
- Dockal, M., Carter, D. C., & Ruker, F. (1999). The three recombinant domains of human serum albumin. Structural characterization and ligand binding properties. *The Journal of Biological Chemistry*, 274: 29303–29310.
- Dubois-Presle, N., Lopicque, F., Maurice, M. H., Fournel-Gigleux, S., Magdalou, J., Abiteboul, M., Siest, G., & Netter, P. (1995). Stereoselective esterase activity of human serum albumin toward ketoprofen glucuronide. *Molecular Pharmacology*, 47: 647–653.
- Dufour, C., & Dangles, O. (2005). Flavonoid–serum albumin complexation: Determination of binding constants and binding sites by fluorescence spectroscopy. *Biochimica et Biophysica Acta*, 1721: 164–173.
- Dugaiczky, A., Law, S. L., & Dennison, O. E. (1982). Nucleotide sequence and the encoded amino acids of human serum albumin mRNA. *Proceedings of the National Academy of Sciences of the United States of America*, 79: 71–75.
- Dugasani, S., Pichika, M. R., Nadarajah, V. D., Balijepalli, M. K., Tandra, S., & Korlakunta, J. N. (2010). Comparative antioxidant and anti-inflammatory effects of [6]-gingerol, [8]-gingerol, [10]-gingerol and [6]-shogaol. *Journal of Ethnopharmacology*, 127: 515–520.
- Eskander, R. N., Randall, L. M., Sakai, T., Guo, Y., Hoang, B., & Zi, X. (2012). Flavokawain B, a novel, naturally occurring chalcone, exhibits robust apoptotic effects and induces G2/M arrest of a uterine leiomyosarcoma cell line. *Journal of Obstetrics and Gynaecology Research*, 38: 1086–1094.
- Evans, T. W. (2002). Albumin as a drug—biological effects of albumin unrelated to oncotic pressure. *Alimentary Pharmacology & Therapeutics*, 16: 6–11.
- Fabricant, D. S., & Farnsworth, N. R. (2001). The value of plants used in traditional medicine for drug discovery. *Environmental Health Perspectives*, 109: 69–75.

- Fahey, J. W., & Stephenson, K. L. (2002). Pinostrobin from honey and Thai ginger (*Boesenbergia pandurata*): A potent flavonoid inducer of mammalian phase 2 chemoprotective and antioxidant enzymes. *Journal of Agricultural and Food Chemistry*, *50*: 7472–7476.
- Faizul, F. M., Kadir, H. A., & Tayyab, S. (2008). Spectroscopic studies on the binding of bromocresol purple to different serum albumins and its bilirubin displacing action. *Journal of Photochemistry and Photobiology B: Biology*, *90*: 1–7.
- Fehske, K. J., Schlafer, U., Wollert, U., & Muller, W. E. (1982). Characterization of an important drug binding area on human serum albumin including the high-affinity binding sites of warfarin and azapropazone. *Molecular Pharmacology*, *21*: 387–393.
- Fenerty, C. A., & Lindup, W. E. (1991). Effect of  $\beta$ -carboline derivatives on the binding of L-tryptophan and diazepam to bovine and human albumin. *Biochemical Pharmacology*, *41*: 1589–1594.
- Figge, J., Rossing, T. H., & Fencle, V. (1991). The role of serum proteins in acid-base equilibria. *The Journal of Laboratory and Clinical Medicine*, *120*: 713–719.
- Freitas, P. G., Barbosa, A. F., Saraiva, L. A., Camps, I., da Silveira, N. J. F., Veloso, M. P., Santos, M. H., & Schneedorf, J. M. (2012). Mangiferin binding to serum albumin is non-saturable and induces conformational changes at high concentrations. *Journal of Luminescence*, *132*: 3027–3034.
- Gao, W., Li, N., Chen, G., Xu, Y., Chen, Y., Hu, S., & Hu, Z. (2011). Binding studies of costunolide and dehydrocostuslactone with HSA by spectroscopy and atomic force microscopy. *Journal of Luminescence*, *131*: 2063–2071.
- Ghuman, J., Zunszain, P. A., Petitpas, I., Bhattacharya, A. A., Otagiri, M., & Curry, S. (2005). Structural basis of the drug-binding specificity of human serum albumin. *Journal of Molecular Biology*, *353*: 38–52.
- Gianazza, E., Frigerio, A., Astrua-Testori, S., & Righetti, P. G. (1984). The behavior of serum albumin upon isoelectric focusing on immobilized pH gradients. *Electrophoresis*, *5*: 310–312.
- Gomez-Betancur, I., Benjumea, D., Patino, A., Jimenez, N., & Osorio, E. (2014). Inhibition of the toxic effects of *Bothrops asper* venom by pinostrobin, a flavanone isolated from *Renalmia alpinia* (Rottb.) MAAS. *Journal of Ethnopharmacology*, *155*: 1609–1615.
- Gonzalez, M., Argarana, C. E., & Fidelio, G. D. (1999). Extremely high thermal stability of streptavidin and avidin upon biotin binding. *Biomolecular Engineering*, *16*: 67–72.
- Goodsell, D. S., Morris, G. M., & Olson, A. J. (1999). Automated docking of flexible ligands: Applications of AutoDock. *Journal of Molecular Recognition*, *9*: 1–5.
- Griggs, B. (1997). *New green pharmacy - The story of western herbal medicine* (3<sup>rd</sup> ed.). London: Vermillion.

- Guo, C. -C., Tang, Y. -H., Hu, H. -H., Yu, L. -S., Jiang, H. -D., & Zeng, S. (2011). Analysis of chiral non-steroidal anti-inflammatory drugs flurbiprofen, ketoprofen and etodolac binding with HSA. *Journal of Pharmaceutical Analysis*, 1: 184–190.
- Guo, J., Wu, H., Du, L., Zhang, W., & Yang, J. (2014). Comparative antioxidant properties of some gingerols and shogaols, and the relationship of their contents with the antioxidant potencies of fresh and dried ginger (*Zingiber officinale* Roscoe). *Journal of Agricultural Science and Technology*, 16: 1063–1072.
- Ha, S. K., Moon, E., Ju, M. S., Kim, D. H., Ryu, J. H., Oh, M. S., & Kim, S. Y. (2012). 6-Shogaol, a ginger product, modulates neuroinflammation: A new approach to neuroprotection. *Neuropharmacology*, 63: 211–223.
- Harper, M. E., & Dugaiczky, A. (1983). Linkage of the evolutionarily-related serum albumin and  $\alpha$ -fetoprotein genes within q11-22 of human chromosome 4. *The American Journal of Human Genetics*, 35: 565–572.
- Hartati, R., Suganda, A. G., & Fidrianny, I. (2014). Botanical, phytochemical and pharmacological properties of *Hedychium* (Zingiberaceae) - A review. *Procedia Chemistry*, 13: 150–163.
- He, X. M., & Carter, D. C. (1992). Atomic structure and chemistry of human serum albumin. *Nature*, 358: 209–215.
- Hein, K. L., Kragh-Hansen, U., Morth, J. P., Jeppesen, M. D., Otzen, D., Møller, J. V., & Nissen, P. (2010). Crystallographic analysis reveals a unique lidocaine binding site on human serum albumin. *Journal of Structural Biology*, 171: 353–360.
- Heller, W. T. (2013). Comparison of the thermal denaturing of human serum albumin in the presence of guanidine hydrochloride and 1-butyl-3-methylimidazolium ionic liquids. *The Journal of Physical Chemistry B*, 117: 2378–2383.
- Ho, J. X., Holowachuk, E. W., Norton, E. J., Twigg, P. D., & Carter, D. C. (1993). X-ray and primary structure of horse serum albumin (*Equus caballus*) at 0.27 nm resolution. *European Journal of Biochemistry*, 215: 205–212.
- Honore, B., & Brodersen, R. (1984). Albumin binding of anti-inflammatory drugs. Utility of a site-oriented versus a stoichiometric analysis. *Molecular Pharmacology*, 25: 137–150.
- Hseu, Y. -C., Lee, M. -S., Wu, C. -R., Cho, H. -J., Lin, K. -Y., Lai, G. -H., Wang, S. -Y., Kuo, Y. -H., Kumar, K. J. S., & Yang, H. -L. (2012). The chalcone flavokawain B induces G2/M cell-cycle arrest and apoptosis in human oral carcinoma HSC-3 cells through the intracellular ROS generation and downregulation of the Akt/p38 MAPK signaling pathway. *Journal of Agricultural and Food Chemistry*, 60: 2385–2397.
- Hsu, Y. -L., Hung, J. -Y., Tsai, Y. -M., Tsai, E. -M., Huang, M. S., Hou, M. -F., & Kuo, P. -L. (2015). 6-shogaol, an active constituent of dietary ginger, impairs cancer development and lung metastasis by inhibiting the secretion of CC-chemokine ligand 2 (CCL2) in tumor-associated dendritic cells. *Journal of Agricultural and Food Chemistry*, 63: 1730–1738.

- Hughes, W. L. (1954). The proteins of blood plasma. In H. Neurath & K. Bailey (Eds.), *The proteins*. (pp. 663–754). New York: Academic Press.
- Hunter, M. J. (1966). A method for the determination of protein partial specific volumes. *The Journal of Physical Chemistry*, 70: 3285–3292.
- Itoh, T., Nakashima, K., Tsuda, Y. & Yamada, H. (1996). Stereoselective binding of carbenicillin epimers to human serum albumin. *Chirality*, 8: 201–206.
- Ivanov, A. I., Christodoulou, J., Parkinson, J. A., Barnham, K. J., Tucker, A., Woodrow, J., & Sadler, P. J. (1998). Cisplatin binding sites on human albumin. *The Journal of Biological Chemistry*, 273: 14721–14730.
- Jacobsen, J., & Wennberg, R. P. (1974). Determination of unbound bilirubin in the serum of newborns. *Clinical Chemistry*, 20: 783–789.
- Ji, H. -F., Li, X. -J., & Zhang, H. -Y. (2009). Natural products and drug discovery. *EMBO Reports*, 10: 194–200.
- Ji, T., Lin, C., Krill, L. S., Eskander, R., Guo, Y., Zi, X., & Hoang, B. H. (2013). Flavokawain B, a kava chalcone, inhibits growth of human osteosarcoma cells through G2/M cell cycle arrest and apoptosis. *Molecular Cancer*, 12: 55.
- Jolad, S. D., Lantz, R. C., Chen, G. J., Bates, R. B., & Timmerman, B. N. (2005). Commercially processed dry ginger (*Zingiber officinale*): Composition and effects on LPS-induced PGE<sub>2</sub> production. *Phytochemistry*, 66: 1614–1635.
- Kalanur, S. S., Seetharamappa, J., & Kalalbandi, V. K. A. (2010). Characterization of interaction and the effect of carbamazepine on the structure of human serum albumin. *Journal of Pharmaceutical and Biomedical Analysis*, 53: 660–666.
- Keire, D. A., Mariappan, S. V. S., Peng, J., & Rabenstein, D. L. (1993). Nuclear magnetic resonance studies of the binding of captopril and penicillamine by serum albumin. *Biochemical Pharmacology*, 46: 1059–1069.
- Kelly, S. M., Jess, T. J., & Price, N. C. (2005). How to study proteins by circular dichroism. *Biochimica et Biophysica Acta*, 1751: 119–139.
- Khan, S. N., Islam, B., Yennamalli, R., Sultan, A., Subbarao, N., & Khan, A. U. (2008). Interaction of mitoxantrone with human serum albumin: Spectroscopic and molecular modeling studies. *European Journal of Pharmaceutical Sciences*, 35: 371–382.
- Khanna, N. C., Tokuda, M., & Waisman, D. M. (1986). Conformational changes induced by binding of divalent cations to calregulin. *The Journal of Biological Chemistry*, 261: 8883–8887.
- Kim, J. S., Lee, S. I., Park, H. W., Yang, J. H., Shin, T. Y., Kim, Y. C., Baek, N. I., Kim, S. H., Choi, S. U., Kwon, B. M., Leem, K. H., Jung, M. Y., & Kim, D. K. (2008). Cytotoxic components from the dried rhizomes of *Zingiber officinale* Roscoe. *Archives of Pharmacal Research*, 31: 415–418.

- Knudsen, A., Pedersen, A. O., & Brodersen, R. (1986). Spectroscopic properties of bilirubin–human serum albumin complexes: A stoichiometric analysis. *Archives of Biochemistry and Biophysics*, 244: 273–284.
- Koehn, F. E., & Carter, G. T. (2005). The evolving role of natural products in drug discovery. *Nature Reviews Drug Discovery*, 4: 206–220.
- Kragh-Hansen, U. (1981). Molecular aspects of ligand binding to serum albumin. *Pharmacological Reviews*, 33: 17–53.
- Kragh-Hansen, U. (1985). Relations between high-affinity binding sites of markers for binding regions on human serum albumin. *Biochemical Journal*, 225: 629–638.
- Kragh-Hansen, U. (1988). Evidence for a large and flexible region of human serum albumin possessing high affinity binding sites for salicylate, warfarin, and other ligands. *Molecular Pharmacology*, 34: 160–171.
- Kragh-Hansen, U. (1991). Octanoate binding to the indole- and benzodiazepine-binding region of human serum albumin. *Biochemical Journal*, 273: 641–644.
- Kragh-Hansen, U., Chuang, V. T. G., & Otagiri, M. (2002). Practical aspects of the ligand-binding and enzymatic properties of human serum albumin. *Biological and Pharmaceutical Bulletin*, 25: 695–704.
- Kremers, P. (2002). In vitro tests for predicting drug-drug interactions: The need for validated procedures. *Pharmacology & Toxicology*, 91: 209–217.
- Kress, W. J., Prince, L. M., & Williams, K. J. (2002). The phylogeny and a new classification of the gingers (Zingiberaceae): Evidence from molecular data. *American Journal of Botany*, 89: 1682–1696.
- Kumar, Y., Tayyab, S., & Muzammil, S. (2004). Molten-globule like partially folded states of human serum albumin induced by fluoro and alkyl alcohols at low pH. *Archives of Biochemistry and Biophysics*, 426: 3–10.
- Kumar, G., Karthik, L., & Rao, K. V. B. (2011). A review on pharmacological and phytochemical properties of *Zingiber officinale* Roscoe (Zingiberaceae). *Journal of Pharmacy Research*, 4: 2963–2966.
- Kuo, Y. -F., Su, Y. -Z., Tseng, Y. -H., Wang, S. -Y., Wang, H. -M., & Chueh, P. J. (2010). Flavokawain B, a novel chalcone from *Alpinia pricei* Hayata with potent apoptotic activity: Involvement of ROS and GADD153 upstream of mitochondria-dependent apoptosis in HCT116 cells. *Free Radical Biology & Medicine*, 49: 214–226.
- Ladokhin, A. S. (2000). Fluorescence spectroscopy in peptide and protein analysis. In R. A. Meyers (Ed.), *Encyclopedia of analytical chemistry* (pp. 5762–5779). Chichester: Wiley.
- Lahlou, M. (2013). The success of natural products in drug discovery. *Pharmacology & Pharmacy*, 4: 17–31.
- Lakowicz, J. R. (2006). *Principles of fluorescence spectroscopy* (3<sup>rd</sup> ed.). New York: Plenum Press.

- Lantz, R. C., Chen, G. J., Sarihan, M., Solyom, A. M., Jolad, S. D., & Timmermann, B. N. (2007). The effect of extracts from ginger rhizome on inflammatory mediator production. *Phytomedicine*, *14*: 123–128.
- Layton, C. J., & Hellinga, H. W. (2010). Thermodynamic analysis of ligand-induced changes in protein thermal unfolding applied to high-throughput determination of ligand affinities with extrinsic fluorescent dyes. *Biochemistry*, *49*: 10831–10841.
- Le Bail, J. -C., Aubourg, L., & Habrioux, G. (2000). Effect of pinostrobin on estrogen metabolism and estrogen receptor transactivation. *Cancer Letters*, *156*: 37–44.
- Li, S., & Li, D. (2011). Investigation on the pH-dependent binding of benzocaine and lysozyme by fluorescence and absorbance. *Spectrochimica Acta Part A: Molecular and Biomolecular Spectroscopy*, *82*: 396–405.
- Li, X., Liu, Z., Xu, X., Blair, C. A., Sun, Z., Xie, J., Lilly, M. B., & Zi, X. (2012). Kava components down-regulate expression of AR and AR splice variants and reduce growth in patient-derived prostate cancer xenografts in mice. *PLoS ONE*, *7*: e31213.
- Li, M., & Hagerman, A. E. (2013). Interactions between plasma proteins and naturally occurring polyphenols. *Current Drug Metabolism*, *14*: 432–445.
- Lin, J. H., & Lu, A. Y. H. (1997). Role of pharmacokinetics and metabolism in drug discovery and development. *Pharmacological Reviews*, *49*: 403–449.
- Lin, C. -T., Kumar, K. J. S., Tseng, Y. -H., Wang, Z. -J., Pan, M. -Y., Xiao, J. -H., Chien, S. -C., & Wang, S. -Y. (2009). Anti-inflammatory activity of flavokawain B from *Alpinia pricei* Hayata. *Journal of Agricultural and Food Chemistry*, *57*: 6060–6065.
- Lin, E., Lin, W. -H., Wang, S. -Y., Chen, C. -S., Liao, J. -W., Chang, H. -W., Chen, S. -C., Lin, K. -Y., Wang, L., Yang, H. -L., & Hseu, Y. -C. (2012). Flavokawain B inhibits growth of human squamous carcinoma cells: Involvement of apoptosis and cell cycle dysregulation *in vitro* and *in vivo*. *The Journal of Nutritional Biochemistry*, *23*: 368–378.
- Lindup, W. E., & Orme, M. C. (1981). Plasma protein binding of drugs. *British Medical Journal*, *282*: 212–214.
- Liu, R., Meng, Q., Xi, J., Yang, J., Ha, C. -E., Bhagavan, N. V., & Eckenhoff, R. G. (2004). Comparative binding character of two general anaesthetics for sites on human serum albumin. *Biochemical Journal*, *380*: 147–152.
- Liu, Q., Peng, Y. -B., Zhou, P., Qi, L. -W., Zhang, M., Gao, N., Liu, E. -H., & Li, P. (2013). 6-Shogaol induces apoptosis in human leukemia cells through a process involving caspase-mediated cleavage of eIF2 $\alpha$ . *Molecular Cancer*, *12*: 135.
- Lohner, K., Sen, A. C., Prankerd, R., Esser, A. R., & Perrin, J. H. (1994). Effects of drug-binding on the thermal denaturation of human serum albumin. *Journal of Pharmaceutical & Biomedical Analysis*, *12*: 1501–1505.

- Lundsgaard-Hansen, P. (1986). Physiology and pathophysiology of colloid osmotic pressure and albumin metabolism. *Current Studies in Hematology and Blood Transfusion*, 53: 1–17.
- Lupidi, G., Scire, A., Camaioni, E., Khalife, K. H., De Sanctis, G., Tanfani, F., & Damiani, E. (2010). Thymoquinone, a potential therapeutic agent of *Nigella sativa*, binds to site I of human serum albumin. *Phytomedicine*, 17: 714–720.
- Malek, S. N. A., Phang, C. W., Ibrahim, H., Wahab, N. A., & Sim, K. S. (2011). Phytochemical and cytotoxic investigations of *Alpinia mutica* rhizomes. *Molecules*, 16: 583–589.
- Maruyama, K., Harada, S., Nishigori, H., & Iwatsuru, M. (1984). Classification of drugs on the basis of bilirubin-displacing effect on human serum albumin. *Chemical and Pharmaceutical Bulletin*, 32: 2414–2420.
- Maruyama, T., Lin, C. C., Yamasaki, K., Miyoshi, T., Imai, T., Yamasaki, M., & Otagiri, M. (1993). Binding of suprofen to human serum albumin. Role of the suprofen carboxyl group. *Biochemical Pharmacology*, 45: 1017–1026.
- Matsushita, Y., Gouda, H., Tsujishita, H., & Hirono, S. (1988). Determination of binding conformations of drugs to human serum albumin by transferred nuclear Overhauser effect measurements and conformational analyses using high-temperature molecular dynamics calculations. *Journal of Pharmaceutical Sciences*, 87: 379–386.
- Meisner, H., & Neet, K. (1978). Competitive binding of long-chain free fatty acids, octanoate, and chlorophenoxyisobutyrate to albumin. *Molecular Pharmacology*, 14: 337–346.
- Merlot, A. M., Kalinowski, D. S., & Richardson, D. R. (2014). Unraveling the mysteries of serum albumin—more than just a serum protein. *Frontiers in Physiology*, 5: 299.
- Mignot, I., Presle, N., Lopicque, F., Monot, C., Dropsy, R., & Netter, P. (1996). Albumin binding sites for etodolac enantiomers. *Chirality*, 8: 271–280.
- Miller, L. L., Bly, C. G., Watson, M. L., & Bale, W. F. (1951). The dominant role of the liver in plasma protein synthesis. *The Journal of Experimental Medicine*, 94: 431–453.
- Miller, J. N. (1979). Recent advances in molecular luminescence analysis. *Proceedings of the Analytical Division of the Chemical Society*, 16: 203–208.
- Minghetti, P. P., Ruffner, D. E., Kuang, W. -J., Dennison, O. E., Hawkins, J. W., Beattie, W. G., & Dugaiczky, A. (1986). Molecular structure of the human albumin gene is revealed by nucleotide sequence within q11-22 of chromosome 4. *The Journal of Biological Chemistry*, 261: 6747–6757.
- Mitra, R. K., Sinha, S. S., & Pal, S. K. (2007). Hydration in protein folding: Thermal unfolding/refolding of human serum albumin. *Langmuir*, 23: 10224–10229.

- Mohamad, H., Abas, F., Permana, D., Lajis, N. H., Ali, A. M., Sukari, M. A., Hin, T. Y. Y., Kikuzaki, H., & Nakatani, N. (2004). DPPH free radical scavenger components from the fruits of *Alpinia rafflesiana* Wall. ex. Bak. (Zingiberaceae). *Zeitschrift für Naturforschung*, 59c: 811–815.
- Mohamad, A. S., Akhtar, M. N., Zakaria, Z. A., Perimal, E. K., Khalid, S., Mohd, P. A., Khalid, M. H., Israf, D. A., Lajis, N. H., & Sulaiman, M. R. (2010). Antinociceptive activity of a synthetic chalcone, flavokawin B on chemical and thermal models of nociception in mice. *European Journal of Pharmacology*, 647: 103–109.
- Mohamad, A. S., Akhtar, M. N., Khalivulla, S. I., Perimal, E. K., Khalid, M. H., Ong, H. M., Zareen, S., Akira, A., Israf, D. A., Lajis, N. H., & Sulaiman, M. R. (2011). Possible participation of nitric oxide/cyclic guanosine monophosphate/protein kinase C/ATP-sensitive K<sup>+</sup> channels pathway in the systemic antinociception of flavokawin B. *Basic & Clinical Pharmacology & Toxicology*, 108: 400–405.
- Monahan, B. P., Ferguson, C. L., Killeavy, E. S., Lloyd, B. K., Troy, J., & Cantilena, L. R. Jr. Torsades de pointes occurring in association with terfenadine use. *JAMA*, 264: 2788–2790.
- Montero, M. T., Pouplana, R., Valls, O., & Garcia, S. (1986). On the binding of cinmetacin and indomethacin to human serum albumin. *Journal of Pharmacy and Pharmacology*, 38: 925–927.
- Mudge G. H., Desbiens, N., & Stibitz, G. R. (1978). Binding of iophenoxate and iopanoate to human serum albumin. *Drug Metabolism & Disposition*, 6: 432–439.
- Murakami, A., Nakamura, Y., Ohto, Y., Tanaka, T., Makita, H., Koshimizu, K., & Ohigashi, H. (2004). Cancer preventive phytochemicals from tropical Zingiberaceae. In J. R. Whitaker, N. F. Haard, C. F. Shoemaker & R. P. Singh (Eds.), *Food for health in the Pacific Rim: 3<sup>rd</sup> International conference of food science and technology* (pp. 125–133). Trumbull: Wiley.
- Muzammil, S., Kumar, Y., & Tayyab, S. (1999). Molten globule-like state of human serum albumin at low pH. *European Journal of Biochemistry*. 266: 26–32.
- Narazaki, R., Hamada, M., Harada, K., & Otagiri, M. (1996). Covalent binding between bucillamine derivatives and human serum albumin. *Pharmaceutical Research*, 13: 1317–1321.
- Narazaki, R., Harada, K., Sugii, A., & Otagiri, M. (1997). Kinetic analysis of the covalent binding of captopril to human serum albumin. *Journal of Pharmaceutical Sciences*, 86: 215–219.
- Newman, D. J., Cragg, G. M., & Snader, K. M. (2000). The influence of natural products upon drug discovery. *Natural Product Reports*, 17: 215–234.
- Newman, D. J. (2008). Natural products as leads to potential drugs: An old process or the new hope for drug discovery? *Journal of Medicinal Chemistry*, 51: 2589–2599.
- Nomura, T., Sakamoto, K., Imai, T., & Otagiri, M. (1992). Study of interaction of pranoprofen with human serum albumin: Binding properties of enantiomers and metabolite. *Journal of Pharmacobio-Dynamics*, 15: 589–596.

- Olson, R. E., & Christ, D. D. (1996). Plasma protein binding of drugs. *Annual Reports in Medicinal Chemistry*, 31: 327–336.
- Olsson, T. S. G., Williams, M. A., Pitt, W. R., & Ladbury, J. E. (2008). The thermodynamics of protein–ligand interaction and solvation: Insights for ligand design. *Journal of Molecular Biology*, 384: 1002–1008.
- Olufemi, O. S., Humes, P., Whittaker, P. G., Read, M. A., Lind, T., & Halliday, D. (1990). Albumin synthetic rate: a comparison of arginine and alpha-ketoisocaproate precursor methods using stable isotope techniques. *European Journal of Clinical Nutrition*, 44: 351–361.
- Oncley, J. L., Scatchard, G., & Brown, A. (1947). Physical-chemical characteristics of certain of the proteins of normal human plasma. *The Journal of Physical Chemistry*, 51: 184–198.
- Otagiri, M., Nakamura, H., Maruyama, T., Imamura, Y., & Takadate, A. (1989a). Characterization of binding sites for sulfadimethoxine and its major metabolite, N4-acetylsulfadimethoxine, on human and rabbit serum albumin. *Chemical and Pharmaceutical Bulletin*, 37: 498–501.
- Otagiri, M., Masuda, K., Imai, T., Imamura, Y., & Yamasaki, M. (1989b). Binding of pirofen to human serum albumin studied by dialysis and spectroscopy techniques. *Biochemical Pharmacology*, 38: 1–7.
- Otagiri, M. (2005). A molecular functional study on the interactions of drugs with plasma proteins. *Drug Metabolism and Pharmacokinetics*, 20: 309–323.
- Pancharoen, O., Prawat, U., & Tuntiwachwuttikul, P. (2000). Phytochemistry of the Zingiberaceae. *Studies in Natural Products Chemistry*, 23: 797–865.
- Paramaguru, G., Kathiravan, A., Selvaraj, S., Venuvanalingam, P., & Renganathan, R. (2010). Interaction of anthraquinone dyes with lysozyme: Evidences from spectroscopic and docking studies. *Journal of Hazardous Materials*, 175: 985–991.
- Pedretti, A., Villa, L., & Vistoli, G. (2002). VEGA: A versatile program to convert, handle and visualize molecular structure on Windows-based PCs. *Journal of Molecular Graphics and Modelling*, 21: 47–49.
- Peters, T. Jr., & Davidson, L. K. (1982). The biosynthesis of rat serum albumin. In vivo studies on the formation of the disulfide bonds. *The Journal of Biological Chemistry*, 257: 8847–8853.
- Peters, T. Jr. (1996). *All about albumin: Biochemistry, genetics and medical applications*. San Diego: Academic Press.
- Petitpas, I., Bhattacharya, A. A., Twine, S., East, M., & Curry, S. (2001). Crystal structure analysis of warfarin binding to human serum albumin: Anatomy of drug site I. *The Journal of Biological Chemistry*, 276: 22804–22809.
- Pico, G. A. (1997). Thermodynamic features of the thermal unfolding of human serum albumin. *International Journal of Biological Macromolecules*, 20: 63–73.

- Poerwono, H., Sasaki S., Hattori, Y., & Higashiyama, K. (2010). Efficient microwave-assisted prenylation of pinostrobin and biological evaluation of its derivatives as antitumor agents. *Bioorganic & Medicinal Chemistry Letters*, *20*: 2086–2089.
- Qin, P., Su, B., & Liu, R. (2012). Probing the binding of two fluoroquinolones to lysozyme: A combined spectroscopic and docking study. *Molecular BioSystems*, *8*: 1222–1229.
- Raffa, R. B. (2003). Experimental approaches to determine the thermodynamics of protein-ligand interactions. In H. J. Böhm & G. Schneider (Eds.), *Protein-ligand interactions: From molecular recognition to drug design* (pp. 51–72). Weinheim: Wiley-VCH Verlag.
- Rahman, M. H., Maruyama, T., Okada, T., Imai, T., & Otagiri, M. (1993a). Study of interaction of carprofen and its enantiomers with human serum albumin--II. Stereoselective site-to-site displacement of carprofen by ibuprofen. *Biochemical Pharmacology*, *46*: 1733–1740.
- Rahman, M. H., Yamasaki, K., Shin, Y. H., Lin, C. C., & Otagiri, M. (1993b). Characterization of high affinity binding sites of non-steroidal anti-inflammatory drugs with respect to site-specific probes on human serum albumin. *Biological and Pharmaceutical Bulletin*, *16*: 1169–1174.
- Rhode, J., Fogoros, S., Zick, S., Wahl, H., Griffith, K. A., Huang, J., & Liu, J. R. (2007). Ginger inhibits cell growth and modulates angiogenic factors in ovarian cancer cells. *BMC Complementary and Alternative Medicine*, *7*: 44.
- Ross, P. D., & Subramanian, S. (1981). Thermodynamics of protein association reactions: Forces contributing to stability. *Biochemistry*, *20*: 3096–3102.
- Ross, P. D., & Rekharsky, M. V. (1996). Thermodynamics of hydrogen bond and hydrophobic interactions in cyclodextrin complexes. *Biophysical Journal*, *71*: 2144–2154.
- Russell, J. H., & Geller, D. M. (1975). The structure of rat proalbumin. *The Journal of Biological Chemistry*, *250*: 3409–3413.
- Russeva, V., Stavreva, N., Rakovska, R., & Michailova, D. (1994). Binding of sulindac to human serum albumin studied by circular dichroism. *Arzneimittel-Forschung*, *44*: 159–162.
- Ryan, A. J., Chung, C. W., & Curry, S. (2011). Crystallographic analysis reveals the structural basis of the high-affinity binding of iophenoxic acid to human serum albumin. *BMC Structural Biology*, *11*: 18.
- Saha, A., Blando, J., Silver, E., Beltran, L., Sessler, J., & DiGiovanni, J. (2014). 6-Shogaol from dried ginger inhibits growth of prostate cancer cells both *in vitro* and *in vivo* through inhibition of STAT3 and NF- $\kappa$ B signaling. *Cancer Prevention Research*, *7*: 627–638.
- Sakai, T., Eskander, R. N., Guo, Y., Kim, K. J., Mefford, J., Hopkins, J., Bhatia, N. N., Zi, X., & Hoang, B. H. (2012). Flavokawain B, a kava chalcone, induces apoptosis in synovial sarcoma cell lines. *Journal of Orthopaedic Research*, *30*: 1045–1050.

- Salvi, A., Carrupt, P. -A., Mayer, J. M., & Testa, B. (1997). Esterase-like activity of human serum albumin toward prodrug esters of nicotinic acid. *Drug Metabolism & Disposition*, 25: 395–398.
- Samari, F., Shamsipur, M., Hemmateenejad, B., Khayamian, T., & Gharaghani, S. (2012). Investigation of the interaction between amodiaquine and human serum albumin by fluorescence spectroscopy and molecular modeling. *European Journal of Medicinal Chemistry*, 54: 255–263.
- Sandhya, B., Hedge, A. H., & Seetharamappa, J. (2013). Elucidation of binding mechanism and identification of binding site for an anti HIV drug, stavudine on human blood proteins. *Molecular Biology Reports*, 40: 3817–3827.
- Sang, S., Hong, J., Wu, H., Liu, J., Yang, C. S., Pan, M. H., Badmaev, V., & Ho, C. T. (2009). Increased growth inhibitory effects on human cancer cells and anti-inflammatory potency of shogaols from *Zingiber officinale* relative to gingerols. *Journal of Agricultural and Food Chemistry*, 57: 10645–10650.
- Sanner, M. F. (1999). Python: A programming language for software integration and development. *Journal of Molecular Graphics and Modelling*, 17: 57–61.
- Sauer, H., & Hänsel, R. (1967). Kawalaktone und flavonoide aus einer endemischen piper - Art Neu Guineas (in German). *Planta Medica*, 15: 443–458.
- Scheider, W., Dintzis, H. M., & Oncley, J. L. (1976). Changes in the electric dipole vector of human serum albumin due to complexing with fatty acids. *Biophysical Journal*, 16: 417–431.
- Schmitz, R. (1985). Friedrich Wilhelm Sertürner and the discovery of morphine. *Pharmacy in History*, 27: 61–74.
- Setoguchi, N., Takamura, N., Fujita, K., Ogata, K., Tokunaga, J., Nishio, T., Chosa, E., Arimori, K., Kawai, K., & Yamamoto, R. (2013). A diclofenac suppository–nabumetone combination therapy for arthritic pain relief and a monitoring method for the diclofenac binding capacity of HSA site II in rheumatoid arthritis. *Biopharmaceutics & Drug Disposition*, 34: 125–136.
- Shanmugaraj, K., Anandakumar, S., & Ilanchelian, M. (2014). Exploring the biophysical aspects and binding mechanism of thionine with bovine hemoglobin by optical spectroscopic and molecular docking methods. *Journal of Photochemistry and Photobiology B: Biology*, 131: 43–52.
- Shrake, A., & Ross, P. D. (1990). Ligand-induced biphasic protein denaturation. *The Journal of Biological Chemistry*, 265: 5055–5059.
- Silva, D., Cortez, C. M., & Louro, S. R. W. (2004). Chlorpromazine interactions to sera albumins: A study by the quenching of fluorescence. *Spectrochimica Acta Part A: Molecular and Biomolecular Spectroscopy*, 60: 1215–1223.
- Smolarz, H. D., Mendyk, E., Bogucka-Kocka, A., & Kocki, J. (2006). Pinostrobin - an anti-leukemic flavonoid from *Polygonum lapathifolium* L. ssp. nodosum (Pers.) Dans. *Zeitschrift für Naturforschung*, 61c: 64–68.

- Stamler, J. S., Jaraki, O., Osborne, J., Simon, D. I., Keaney, J., Vita, J., Singel, D., Valeri, C. R., & Loscalzo, J. (1992). Nitric oxide circulates in mammalian plasma primarily as an S-nitroso adduct of serum albumin. *Proceedings of the National Academy of Sciences of the United States of America*, 89: 7674–7677.
- Sudlow, G., Birkett, D. J., & Wade, D. N. (1975). The characterization of two specific drug binding sites on human serum albumin. *Molecular Pharmacology*, 11: 824–832.
- Sudlow, G., Birkett, D. J., & Wade, D. N. (1976). Further characterization of specific drug binding sites on human serum albumin. *Molecular Pharmacology*, 12: 1052–1061.
- Suekawa, M., Ishige, A., Yuasa, K., Sudo, K., Aburada, M. & Hosoya, E. (1984). Pharmacological studies on ginger. I. Pharmacological actions of pungent constituents, (6)-gingerol and (6)-shogaol. *Journal of Pharmacobio-Dynamics*, 7: 836–848.
- Sueyasu, M., Fujito, K., Shuto, H., Mizokoshi, T., Kataoka, Y., & Oishi, R. (2000). Protein binding and the metabolism of thiamylal enantiomers *in vitro*. *Anesthesia & Analgesia*, 91: 736–740.
- Sugio, S., Kashima, A., Mochizuki, S., Noda, M., & Kobayashi, K. (1999). Crystal structure of human serum albumin at 2.5 Å resolution. *Protein Engineering*, 12: 439–446.
- Takamura, N., Haruta, A., Kodama, H., Tsuruoka, M., Yamasaki, K., Suenaga, A., & Otagiri, M. (1996). Mode of interaction of loop diuretics with human serum albumin and characterization of binding site. *Pharmaceutical Research*, 13: 1015–1019.
- Takamura, N., Maruyama, T., Ahmed, S., Suenaga, A., & Otagiri, M. (1997). Interactions of aldosterone antagonist diuretics with human serum proteins. *Pharmaceutical Research*, 14: 522–526.
- Takamura, N., Shinozawa, S., Maruyama, T., Suenaga, A. & Otagiri, M. (1998). Effects of fatty acids on serum binding between furosemide and valproic acid. *Biological and Pharmaceutical Bulletin*, 21: 174–176.
- Takamura, N., Maruyama, T., Chosa, E., Kawai, K., Tsutsumi, Y., Uryu, Y., Yamasaki, K., Deguchi, T., & Otagiri, M. (2005). Bucolome, a potent binding inhibitor for furosemide, alters the pharmacokinetics and diuretic effect of furosemide: Potential for use of bucolome to restore diuretic response in nephrotic syndrome. *Drug Metabolism & Disposition*, 33: 596–602.
- Tanford, C. (1950). Preparation and properties of serum and plasma proteins. XXIII. Hydrogen ion equilibria in native and modified human serum albumins. *Journal of the American Chemical Society*, 72: 441–451.
- Tang, Y., Li, X., Liu, Z., Simoneau, A. R., Xie, J., & Zi, X. (2010). Flavokawain B, a kava chalcone, exhibits robust apoptotic mechanisms on androgen receptor-negative, hormone-refractory prostate cancer cell lines and reduces tumor growth in a preclinical model. *International Journal of Cancer*, 127: 1758–1768.

- Tetko, I. V., Gasteiger, J., Todeschini, R., Mauri, A., Livingstone, D., Ertl, P., Palyulin, V. A., Radchenko, E. V., Zefirov, N. S., Makarenko, A. S., Tanchuk, V. Y., & Prokopenko, V. V. (2005). Virtual computational chemistry laboratory – design and description. *Journal of Computer-Aided Molecular Design*, 19: 453–463.
- Tokuhara, D., Shimada, T., Asami, A., Takahashi, A., Kobayashi, H., Saimaru, H., & Aburada, M. (2013). Pharmacokinetics of 6-shogaol, a pungent ingredient of *Zingiberis Rhizoma*, and the anti-inflammatory activity of its metabolite, 6-paradol. *Journal of Traditional Medicines*, 30: 199–205.
- Trombley, J. D., Loegel, T. N., Danielson, N. D., & Hagerman, A. E. (2011). Capillary electrophoresis methods for the determination of covalent polyphenol–protein complexes. *Analytical and Bioanalytical Chemistry*, 401: 1523–1529.
- Trynda-Lemiesz, L. (2004). Paclitaxel–HSA interaction. Binding sites on HSA molecule. *Bioorganic & Medicinal Chemistry*, 12: 3269–3275.
- Tsuda, Y., Tsunoi, T., Watanabe, N., Ishida, M., Yamada, H. & Itoh, T. (2001). Stereoselective binding and degradation of sulbenicillin in the presence of human serum albumin. *Chirality*, 13: 236–243.
- Tuchinda, P., Reutrakul, V., Claeson, P., Pongprayoon, U., Sematong, T., Santisuk, T., & Taylor, W. C. (2002). Anti-inflammatory cyclohexenyl chalcone derivatives in *Boesenbergia pandurata*. *Phytochemistry*, 59: 169–173.
- Twine, S. M., Gore, M. G., Morton, P., Fish, B. C., Lee, A. G., & East, J. M. (2003). Mechanism of binding of warfarin enantiomers to recombinant domains of human albumin. *Archives of Biochemistry and Biophysics*, 414: 83–90.
- Urano, Y., Sakai, M., Watanabe, K., & Tamaoki, T. (1984). Tandem arrangement of the albumin and alpha-fetoprotein genes in the human genome. *Gene*, 32: 255–261.
- Vallner, J. J. (1977). Binding of drugs by albumin and plasma protein. *Journal of Pharmaceutical Sciences*, 66: 447–465.
- Varlan, A., & Hillebrand, M. (2010). Bovine and human serum albumin interactions with 3-carboxyphenoxathiin studied by fluorescence and circular dichroism spectroscopy. *Molecules*, 15: 3905–3919.
- Vermeer, A. W. P., & Norde, W. (2000). The thermal stability of immunoglobulin: Unfolding and aggregation of a multi-domain protein. *Biophysical Journal*, 78: 394–404.
- Waldmann, T. A. (1977). Albumin catabolism. In V. M. Rosenoer, M. Oratz & M. A. Rothschild (Eds.), *Albumin: Structure, function and uses* (pp. 255–273). Oxford: Pergamon Press.
- Wallevik, K. (1973). Reversible denaturation of human serum albumin by pH, temperature and guanidine hydrochloride. *The Journal of Biological Chemistry*, 245: 2650–2655.
- Wang, H., Zou, H., & Zhang, Y. (1998). Multi-site binding of fenoprofen to human serum albumin studied by a combined technique of microdialysis with high performance liquid chromatography. *Biomedical Chromatography*, 12: 4–7.

- Wang, T., Xiang, B., Wang, Y., Chen, C., Dong, Y., Fang, H., & Wang, M. (2008). Spectroscopic investigation on the binding of bioactive pyridazinone derivative to human serum albumin and molecular modeling. *Colloids and Surfaces B: Biointerfaces*, 65: 113–119.
- Wang, Y. K., Hong, Y. J., Yao, Y. H., Huang, X. M., Liu, X. B., Zhang, C. Y., Zhang, L., & Xu, X. L. (2013). 6-Shogaol protects against oxidized LDL-induced endothelial injuries by inhibiting oxidized LDL-evoked LOX-1 signaling. *Evidence-Based Complementary and Alternative Medicine*, 2013: ID 503521.
- Wanwimolruk, S., Birkett, D. J., & Brooks, P. M. (1983). Structural requirements for drug binding to site II on human serum albumin. *Molecular Pharmacology*, 24: 458–463.
- Watanabe, H., Tanase, S., Nakajou, K., Maruyama, T., Kragh-Hansen, U., & Otagiri, M. (2000). Role of Arg-410 and Tyr-411 in human serum albumin for ligand binding and esterase-like activity. *Biochemical Journal*, 349: 813–819.
- Wermuth, C. G. (2003). *The practice of medicinal chemistry*. Amsterdam: Academic Press.
- Williams, T. F. (1992). Serum albumin, aging and disease. *Journal of Clinical Epidemiology*, 45: 205–206.
- Wu, D., Nair, M. G., & DeWitt, D. L. (2002). Novel compounds from *Piper methysticum* Forst (kava kava) roots and their effect on cyclooxygenase enzyme. *Journal of Agricultural and Food Chemistry*, 50: 701–705.
- Wu, N., Kong, Y., Zu, Y., Fu, Y., Liu, Z., Meng, R., Liu, X., & Efferth, T. (2011). Activity investigation of pinostrobin towards herpes simplex virus-1 as determined by atomic force microscopy. *Phytomedicine*, 18: 110–118.
- Xian, Y. -F., Ip, S. -P., Lin, Z. -X., Mao, Q. -Q., Su, Z. -R., & Lai, X. -P. (2012). Protective effects of pinostrobin on  $\beta$ -amyloid-induced neurotoxicity in PC12 cells. *Cellular and Molecular Neurobiology*, 32: 1223–1230.
- Yamasaki, K., Maruyama, T., Kragh-Hansen, U., & Otagiri, M. (1996). Characterization of site I on human serum albumin: Concept about the structure of a drug binding site. *Biochimica et Biophysica Acta*, 1295: 147–157.
- Yamasaki, K., Rahman, M. H., Tsutsumi, Y., Maruyama, T., Ahmed, S., Kragh-Hansen, U., & Otagiri, M. (2000). Circular dichroism simulation shows a site-II-to-site-I displacement of human serum albumin-bound diclofenac by ibuprofen. *AAPS PharmSciTech*, 1: article 12.
- Yamasaki, K., Chuang, V. T. G., Maruyama, T., & Otagiri, M. (2013). Albumin–drug interaction and its clinical implication. *Biochimica et Biophysica Acta*, 1830: 5435–5443.
- Yenjai, C., & Wanich, S. (2010). Cytotoxicity against KB and NCI-H187 cell lines of modified flavonoids from *Kaempferia parviflora*. *Bioorganic & Medicinal Chemistry*, 20: 2821–2823.

- Yu, H. Y., & Shen, Y. Z. (1999). Displacement effect of valproate on bilirubin-albumin binding in human plasma. *Journal of the Formosan Medical Association*, 98: 201–204.
- Yue, Y., Zhang, Y., Li, Y., Zhu, J., Qin, J., & Chen, X. (2008). Interaction of nobiletin with human serum albumin studied using optical spectroscopy and molecular modeling methods. *Journal of Luminescence*, 128: 513–520.
- Zatón, A., Martínez, A., & de Gandarias, J. M. (1988). The binding of thioureylene compounds to human serum albumin. *Biochemical Pharmacology*, 37: 3127–3131.
- Zhang, G., Zhao, N., & Wang, L. (2011). Fluorescence spectrometric studies on the binding of puerarin to human serum albumin using warfarin, ibuprofen and digitoxin as site markers with the aid of chemometrics. *Journal of Luminescence*, 131: 2716–2724.
- Zhao, X., Chao, Y. -L., Wan, Q. -B., Chen, X. -M., Su, P., Sun, J., & Tang, Y. (2011). Flavokawain B induces apoptosis of human oral adenoid cystic cancer ACC-2 cells via up-regulation of Bim and down-regulation of Bcl-2 expression. *Canadian Journal of Physiology and Pharmacology*, 89: 875–883.
- Zick, S. M., Djuric, Z., Ruffin, M. T., Litzinger, A. J., Normolle, D. P., Alrawi, S., Feng, M. R., & Brenner, D. E. (2008). Pharmacokinetics of 6-gingerol, 8-gingerol, 10-gingerol, and 6-shogaol and conjugate metabolites in healthy human subjects. *Cancer Epidemiology, Biomarkers & Prevention*, 17: 1930–1936.
- Zunszain, P. A., Ghuman, J., McDonagh, A. F., & Curry, S. (2008). Crystallographic analysis of human serum albumin complexed with 4Z,15E-bilirubin-IX $\alpha$ . *Journal of Molecular Biology*, 381: 394–406.

## LIST OF PUBLICATIONS / PRESENTATIONS

### Publications

1. **Feroz, S. R.**, Mohamad, S. B., Bujang, N., Malek, S. N. A., & Tayyab, S. (2012). Multispectroscopic and molecular modeling approach to investigate the interaction of flavokawain B with human serum albumin. *Journal of Agricultural and Food Chemistry*, 60: 5899–5908.
2. Halim, A. A. A., **Feroz, S. R.**, & Tayyab, S. (2013). Does recovery in the spectral characteristics of GdnHCl-denatured *Bacillus licheniformis*  $\alpha$ -amylase due to added calcium point towards protein stabilization? *Bioscience, Biotechnology and Biochemistry*, 77: 87–96.
3. **Feroz, S. R.**, Mohamad, S. B., Bakri, Z. S. D., Malek, S. N. A., & Tayyab, S. (2013). Probing the interaction of a therapeutic flavonoid, pinostrobin with human serum albumin: Multiple spectroscopic and molecular modeling investigations. *PLoS ONE*, 8: e76067.
4. **Feroz, S. R.**, Sumi, R. A., Malek, S. N. A., & Tayyab, S. (2015). A comparative analysis on the binding characteristics of various mammalian albumins towards a multitherapeutic agent, pinostrobin. *Experimental Animals*, 64: 101–108.
5. **Feroz, S. R.**, Teoh, Y. J., Mohamad, S. B., Hong, S. L., Malek, S. N. A., & Tayyab, S. (2015). Interaction of flavokawain B with lysozyme: A photophysical and molecular simulation study. *Journal of Luminescence*, 160: 101–109.
6. Hamdi, O. A. A., **Feroz, S. R.**, Shilpi, J. A., Anouar, E. H., Mukarram, A. K., Mohamad, S. B., Tayyab, S., & Awang, K. (2015). Spectrofluorometric and molecular docking studies on the binding of curcumenol and curcumenone to human serum albumin. *International Journal of Molecular Sciences*, 16: 5180–5193.

7. **Feroz, S. R.**, Mohamad, S. B., Lee, G. S., Malek, S. N. A., & Tayyab, S. (2015). Supramolecular interaction of 6-shogaol, a therapeutic agent of *Zingiber officinale* with human serum albumin as elucidated by spectroscopic, calorimetric and molecular docking methods. *Phytomedicine*, 22: 621–630.
8. Tayyab, S., Zaroog, M. S., **Feroz, S. R.**, Mohamad, S. B., & Malek, S. N. A. (2015). Exploring the interaction between the antiallergic drug, tranilast and human serum albumin: Insights from calorimetric, spectroscopic and modeling studies. *International Journal of Pharmaceutics*, 491: 352–358.
9. Kabir, M. Z., **Feroz, S. R.**, Mukarram, A. K., Mohamad, S. B., Alias, Z., & Tayyab, S. (2015). Interaction of a tyrosine kinase inhibitor, vandetanib with human serum albumin as studied by fluorescence quenching and molecular docking. *Journal of Biomolecular Structure & Dynamics*, doi: 10.1080/07391102.2015.1089187.
10. Nasruddin, A. N., **Feroz, S. R.**, Mukarram, A. K., Mohamad, S. B., & Tayyab, S. (2015). Fluorometric and molecular docking investigation on the binding characteristics of SB202190 to human serum albumin. *Journal of Luminescence – under revision*.

### **Presentations**

1. **Feroz, S. R.**, Halim, A. A. A., & Tayyab, S. (2012). Does recovery in the spectral characteristics of GdnHCl-denatured *Bacillus licheniformis*  $\alpha$ -amylase (BLA) by added calcium point towards protein stabilization? Proceedings of the 9<sup>th</sup> International Conference on Protein Stability, held in Lisbon, Portugal on May 2–4, 2012. Abstract No. P18, pp. 18.
2. **Feroz, S. R.**, Mohamad, S. B., Bujang, N., Malek, S. N. A., & Tayyab, S. (2012). Characterization of the interaction of a therapeutic flavonoid from *Alpinia mutica*,

flavokawain B with human serum albumin. Proceedings of the 37<sup>th</sup> Annual Conference of the Malaysian Society for Biochemistry and Molecular Biology, held in Kuala Lumpur, Malaysia on July 18–19, 2012. Abstract No. 94, pp. 148.

3. **Feroz, S. R.**, Mohamad, S. B., Malek, S. N. A., & Tayyab, S. (2012). Probing the complexation of a therapeutic flavonoid, pinostrobin with human serum albumin: A molecular study. Proceedings of the 17<sup>th</sup> Biological Sciences Graduate Congress, held in Bangkok, Thailand on December 8–10, 2012. Abstract No. BC-OR 10, pp. 76.
4. **Feroz, S. R.**, Mohamad, S. B., Lee, G. S., Malek, S. N. A., & Tayyab, S. (2014). Calorimetric, spectroscopic and *in silico* investigation of the interaction between 6-shogaol and human serum albumin. Proceedings of the 2014 IUBMB-FAOBMB Young Scientist Program, held in Taichung, Taiwan on October 18–20, 2014. Abstract No. O32, pp. 62. Proceedings of the 15<sup>th</sup> IUBMB-24<sup>th</sup> FAOBMB-TSBMB Conference, held in Taipei, Taiwan on October 21–26, 2014. pp. 341.
5. Tayyab, S., Zarog, M. S., **Feroz, S. R.**, Mohamad, S. B., & Malek, S. N. A. (2014). Studies on the interaction of tranilast, an antiallergic drug with human serum albumin. Calorimetric, spectroscopic and modelling approach. Proceedings of the 15<sup>th</sup> IUBMB-24<sup>th</sup> FAOBMB-TSBMB Conference, held in Taipei, Taiwan on October 21–26, 2014. pp. 216.
6. Kabir, M. Z., **Feroz, S. R.**, Mukarram, A. K., Mohamad, S. B., Alias, Z., & Tayyab, S. (2015). Spectroscopic and molecular docking studies on the interaction of vandetanib, a tyrosine kinase inhibitor with human serum albumin. Proceedings of the 40<sup>th</sup> Annual Conference of the Malaysian Society for Biochemistry and Molecular Biology, held in Sepang, Malaysia on June 10–11, 2015. Abstract No. 15, pp. 55.